UNIVERSITY OF CALIFORNIA,

IRVINE

Multiphoton imaging and phasor approach to identify new biomarkers in Huntington Disease

DISSERTATION

Submitted in partial fulfillment of the requirements

for the degree of

DOCTOR OF PHILOSOPHY

In Biomedical Engineering

by

Sara Sameni

Dissertation Committee:
Assistant Professor Michelle A. Digman, Chair
Professor Enrico Gratton
Associate Professor James P. Brody

2018

DEDICATION

To all Neurodegenerative Disorders Community

TABLE OF CONTENTS

LIST OF FIGURES

ACKNOWLEDGMENTS

I would like to, first of all, acknowledge and express my deepest appreciation to my advisor and committee chair, Dr. Michelle M. Digman who supported me and advised me through my Ph.D. journey. I once heard you are more likely to become like your adviser after your Ph.D.; now, I hope I have learned some of her great attributes: her dedication to all of her students, excitement in research, excellence in teaching, and helping others and community. Without her guidance and commitment, this work would have been impossible.

I would like to also express gratitude to my great committee member, Professor Enrico Gratton who helped me during all the ups and downs of my Ph.D. journey, and sharing his insights, wisdom, and enthusiasm for gaining knowledge. I really admire him in so many ways, but words cannot really encompass his generosity and great attitudes. Grazie mille, Enrico!!I will always remember "not to worry in advance" as you always say.

In addition, special thanks to my other committee member, Dr. James P Brody who helped me even before joining the Ph.D. program and encouraged me to continue my passion for science when I was giving up and helped me to be strong.

I would like to also acknowledge my other collaborators Dr. Larry Marsh, Dr. Adeela Syed and Dr. Gregory Brewer who helped me and trained me on animal experiments on Drosophila and neuronal dissections. In addition, I want to express my appreciation to Doctors: Zhiqun Tan, Joan S. Stephan, Leslie M. Thompson, and Cynthia T. McMurray for great discussions on different aspects of Huntington disease. And also I want to thank Dr. Leonel Malacrida for great discussions, help, and encouragement to move to the world of spectral phasor domain.

Great thank also goes to my magnificent graduate counselor, Dr. Phong Luong who helped me out during difficult times and enlighten my path so I could find myself in this journey. Thank you, Phong!!

And also to Dean Leslie who supported me in so many ways and welcomed me to be part of the minority and women scientists, who made me strong to continue my passion for knowledge and science, and encouraged me to be a pioneer and leader in my field. So thank you, Dean Leslie, you are absolutely incredible!

To my dearest husband and family members who helped me along this path and were so patient and encouraging to me so I could succeed, thank you all! This dissertation would have been impossible without your sacrifices and supports.

To Digman lab and all LFD family, I wanted to say thank you for being part of my exciting journey, for all the great days you filled with joy, and memories and feelings that I will always treasure with my heart. I want to also acknowledge Run Zhang and Xiantong Yang in particular to carrying the torch. Special thanks also go to LFD lab manager Milka Titin who ease the whole experience and helped out the transition to the lab life.

And last but not the least; I would like to acknowledge my funding sources: National Institutes of Health (NIH) grant P41-GM103540 and P50-GM076516, National Science Foundation (NSF) in the Biophotonics across Energy, Space , and Time (BEST) Integrative Graduate Education and Research Traineeship (IGERT) Program, UC Irvine Public Impact fellowship, UC President's Dissertation-Year Fellowship (PDY grant), and UC Regents.

Curriculum Vitae

Sara Sameni

2013-2018 Doctor of Philosophy (Ph.D.) in Biomedical Engineering
University of California Irvine

2009-2012 Master of Science (M.S.) in Biomedical Engineering
University of California Irvine

2004- 2009 Bachelor of Science (B.S.) in Biomedical Engineering
University of California Irvine.
Transferred from West Valley College, Saratoga, Ca

Journal and Conference papers

Publications:

Sara Sameni, Leonel Malacrida, Zhiqun Tan, and Michelle Digman," Alteration in Fluidity of Cell Plasma Membrane in Huntington Disease Revealed by Spectral Phasor Analysis." **Nature**: *Sci. Rep*. 8(1): p. 734 (2018).

Sara Sameni, Adeela Syed, J. Lawrence Marsh, and Michelle A. Digman, "The phasor-FLIM fingerprints reveal shifts from OXPHOS to enhanced glycolysis in Huntington Disease" **Nature**: *Sci. Rep.* **6**, 34755; doi: 10.1038/srep34755 (2016).

John Weidling,† **Sara Sameni**,† Jonathan R. T. Lakey, and Elliot Botvinick, " Method measuring oxygen tension and transport within subcutaneous devices". J. Biomed. Opt. 19(8), 087006 (2014).
† Co-First Author

Sara Sameni, Mark Madou **"**In situ Formation and Dissolution of Hydrogel Plugs for Fluid and Particle Control in Centrifugal Fluidics". Antpac, b4834676. (2012).

Conference Papers

Sara Sameni, Leonel Malacrida, Micelle A. Digman "Laurdan imaging and spectral phasor analysis reveals increased membrane fluidity in Huntington disease.
62nd Annual Meeting of the Biophysical Society. San Francisco, California. February 17–21, 2018.*Biophys J.* 2018; 114(3, Suppl 1): 177a, 891-Pos.

Sara Sameni, Leonel Malacrida, Zhiqun Tan, Enrico Gratton, and Michelle A. Digman. "Leaky plasma membrane in Huntington Disease discovered by LAURDAN Imaging coupled with Spectral Phasor Analysis method."18th Annual UC Systemwide Bioengineering Symposium. UCLA. June 2017.

Sara Sameni, Michelle A. Digman. "Metabolic Shifts in Huntington Disease Revealed by Fluorescence Lifetime Imaging Microscopy."61st Annual Meeting of the Biophysical Society. New Orleans, Louisiana. February 2017.*Biophys J.* 2017; 112(3, Suppl 1): 584a.

Sara Sameni, Michelle A. Digman. "Fluorescence Lifetime Imaging and Phasor Analysis Approach Reveal Deficient Energy Production in Huntington Disease." 14th annual advanced imaging meeting. UC Berkeley. Jan 2017.

Sara Sameni, Adeela Syed**,** Michelle A. Digman, " Phasor fluorescence lifetime imaging approach to understand and analyze cellular mechanism disturbed by Huntington disease**"** Annual Meeting of the American Society for Cell Biology 2015. San Diego, CA, December 2015.*ASCB2015 Abstract Book.* 2015; P47.

Sara Sameni, John Welding, Elliot Botvinick, Jonathan RT Lakey, "Oxygen permeability characterization of clinical UPLVM alginate used for islet cell encapsulation" Annual Meeting of Clinical and Translational Science (ICTS). Irvine CA. 2014.

Selected Awards and Honors

2017-2018	President's Dissertation Year fellowship (PDY) $ 43,404.5
June 2017	Best presentation award. 18th Annual UC Systemwide Bioengineering Symposium. UCLA.
January 2017	First place winner, Student Poster Award. 14th Annual Advanced Imaging Meeting. UC Berkeley.
January 2017	Public Impact Fellow: Nominated and awarded as a public impact fellow which distinguishes researchers with a substantial impact on lives of California and beyond
2015-2017	NSF BEST IGERT Grant**:** Training fellowship and professional biophotonic development funded by the National Science Foundation DGE-1144901 Biophotonics across Energy, Space and Time (NSF BEST) Integrative Graduate Education and Research Traineeship (IGERT)

ABSTRACT OF THE DISSERTATION

Multiphoton imaging and phasor approach to identify new biomarkers in Huntington Disease

By

Sara Sameni

Doctor of Philosophy in Biomedical Engineering

University of California, Irvine, 2018

Assistant Professor Michelle A. Digman, Chair

Neurodegenerative diseases occur when brain cells (neurons) start to deteriorate. Changes in these cells will lead to dysfunction and eventual cell death. This will lead to mild symptoms like problems with coordination, psychiatric disorders, or memory loss; and as more neurons die the symptoms also progressively worsen. World Health Organization (WHO) indicates up to 1 billion people worldwide are affected by various types of neurodegenerative diseases. In this study, I focused on Huntington disease (HD), a model to study neurodegeneration that is caused by a glitch in a single gene called huntingtin gene (HTT). Huntington disease is an autosomal dominant inherited neurodegenerative disease characterized by movement, cognitive and emotional disorders. We all carry HTT; however, the normal length of DNA trinucleotide, CAG, that codes for glutamine are between 10-35. The expanded repeats of above 40 or more will lead to HD. Using advanced functional imaging technique called Two-Photon Fluorescence Lifetime Imaging Microscopy (2P-FLIM), and spectral and temporal phasor approach, spectro-temporal phasor map in living mammalian cells and animal tissue was obtained. Using this sophisticated imaging technique, I have developed new methods and identified novel biomarkers that can help

detect Huntington disease early on. This can also help for evaluating the efficacy of treatment. The novel method established in this work is noninvasive and can be performed at the single cell level. Phasor transformation used here simplifies the FLIM and spectral measurements by providing a graphical global view of the process at each pixel and avoids some of the complexity of the multi-exponential analysis. In this way, using a fit free approach that can be applied to both time and frequency domain measurements, Fluorescence Lifetime and spectral emission can be analyzed. It is hoped that this work shed a light on understanding the mechanism of Huntington disease and for new drug discovery and early diagnosis of the disease. The approach introduced in this work can also be applied as a method for understating similar neurodegenerative diseases. This work is supported in part by NIH grant P41 GM103540, NSF BEST IGERT and UC PDY grant.

CHAPTER 1: OVERVIEW

1.1 INTRODUCTION

Expansion of cytosine, adenine, guanine (CAG) in the gene encoding polyglutamine (PolyQ) protein will result in a family of dominantly inherited neurodegenerative disorders including spinocerebellar ataxia and Huntington disease. When PolyQ homopolymers get extended beyond 40 pairs, normally soluble protein will make cytotoxic protein aggregates [3, 4].

The PolyQ disease belongs to a diverse family of "conformational disease" that is due to a non-native conformation of the protein that leads to aggregations which include Alzheimer disease, prion encephalopathy, Parkinson and etc [5]. In these disorders, a specific protein undergoes conformational changes and rearrangements of aggregate and deposition within tissues or various cellular compartments. It is still unknown how cells respond to this abnormal protein conformation which leads to many unanswered questions.

The focus of this study is on Huntington Disease (HD), as a model to study a diverse family of neurodegenerative disorders. HD is considered as a mitochondrial disorder disease. This fatal progressive autosomal dominant neurodegenerative disorder was first fully described by George Huntington in 1872. HD is mainly characterized by cognitive dysfunction and loss of motor function leading to jerky movements called "chorea" that in Greek means dancelike movements which describe the unwanted movements. Since HD is usually manifest between 30-45 years of age, the majority of patients already have children by then[6].

George Huntington didn't encounter the juvenile form of HD in which the disease onset occurs before the age of 21.The first clear description of the juvenile form of HD goes back to 1888 and

attributed to J. Hoffman. Hoffman used data from three generations of family. In his article, he described a woman who developed chorea at the age of 10 and died in her twenties[7].

The gene for HD was first discovered in 1983 and mapped to chromosome 4 and later cloned in 1993. HD gene codes for a large protein called: Huntingtin(Htt) with the molecular mass of 348kDa. Essentially the unstable CAG repeat resides within the first exon of the huntingtin gene (HTT) is translated into a stretch of polyglutamine in the Huntingtin protein [8]. As it is shown in Figure1, the extended CAG repeats lead to elongated and pathogenic glutamine chain (polyQ).

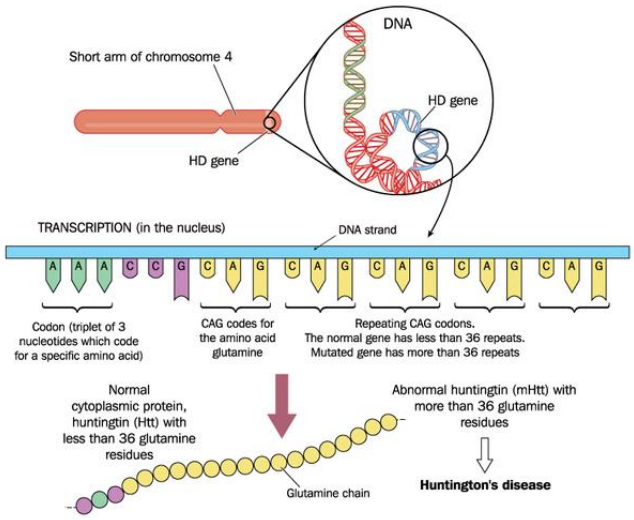

Figure 1: Unstable CAG translation to extended polyQ.
Elongated CAG chain in the 4th chromosome leads to the abnormal length of mutant huntingtin resulting Huntington disease.
Figure adapted based on healthlifemedia.

Despite its gene discovery on decades ago, the normal function of Huntington disease is still not fully understood and incomplete. Some studies show knocked out of the HTT gene is lethal in the mouse early in embryogenesis[9]. Reduction of HTT leveled in knockout embryonic stem cells lead to abnormality in distribution and morphology of different organelles such as endoplasmic reticulum, Golgi, and mitochondria[10]. Moreover, conditional HTT deletion in

forebrain neurons at the late embryonic stage or early neonatal stage has led to progressive neurodegenerative phenotype[11].

Although underlying cellular mechanisms that drive neurodegeneration in Huntington diseases are still not fully understood, dysfunction in energy metabolism, in particular mitochondria dysfunction is a common trend in Huntington pathogenesis studies in human and animal models[12].

It has been shown that mitochondria are the target of oxidative stress in Huntington disease. Under normal condition, mitochondrial and cytosolic antioxidant system control the mitochondrial and cytosolic ROS levels within the safe level; however, if this fails there is a high risk for lipids, protein, and DNA damage[13].

On the other hand, an increased level in ROS including superoxide(O2-)hydrogen peroxide(H2O2), hydroxyl radical(OH-) and reactive nitrogen species like peroxynitrite(ONOO-) as well as impairment of cellular function by degradation of proteins, lipids, and nucleic acid are all associated with oxidative stress. In addition, enhanced oxidative stress in HD leads to increased level of accumulation of lipofuscin, break of DNA strands, and oxidative modification of protein and lipids, that is increased in HD brain and animal model of the disease. Compelling evidence from studies in both HD patients and experimental HD model links oxidative damage and mitochondrial dysfunction to HD pathogenesis[14].

Another recent study indicates that synthetic mitochondria-targeted antioxidant can prevent oxidative damage to mitochondria and also shown to delay the disease progression in the HD in the HdhQ150 knock-in mouse model of HD[15].

Despite ambiguity in the underlying cellular mechanism, changes in the ratio of NAD+ to NADH, mitochondrial function, and level of ATP production are associated with oxidative stress independent of the underlying mechanism. Thus, one can monitor and map up the oxidative stress of the cell at different stages of disease progression in order to better understand the stages of the disease. Using coenzyme such as NADH, FAD as a natural biomarker, oxidative stress of the cell can be monitored non-invasively[16] and can be used to predict metabolism dysfunction in the cells.

As mentioned, aggregates are the hallmark of many neurodegenerative diseases including HD. Yet, the role of these aggregates in pathogenesis and how it affects the cells is not clear. There have been many attempts to correlate the presence of aggregate with the onset of phenotype, but this is very difficult and complicated as detecting and quantifying small aggregates form of PolyQ is not easy. While some researchers believe aggregates are protective, W. Yang argues the role of these aggregates and shows that polyQ aggregates are highly toxic when directed to the cell nucleus[17].

Many other papers indicated that the role of aggregation in the disease is not as obvious and simple. Some researchers indicate the large insoluble inclusion bodied seen via microscope may actually be helpful to support the cell with the disease [18-21]. Other studies specify that pathogenesis might depend instead on small oligomers or micro-aggregates that are formed as a possible byproduct of aggregation process [21-23]. While these studies all agree and suggest the presence of mutant protein inclusion, it is not fully understood whether these inclusions are highly toxic, benign or actually cytoprotective as stated by some studies.

As described, HD is a progressive neurodegenerative disease. It occurs usually in midlife, and thus there is a lag phase that can be an indication of possible transfer of mutant proteins. On the other hand, Htt aggregates may have a role in neuropathology in such genetic neurodegeneration.

This lag phase also is a great target for identifying biomarkers, an indication of the disease prior to major symptoms which can assess the treatment and possibly benefit the prevention of the disease.

1.2. M.G LETTER

Before getting to the specific objectives of this thesis, here I have included part of the letter that I received from one of the students I was training during the minority Undergraduate Student Initiative for Biomedical Research (USIBR) program who was also diagnosed with a mitochondrial disorder similar to HD.

" Dear Sara,

Thank you so much for allowing me to work in your lab and for taking the time to give me a foundation in fluorescence imaging.

Back in 2004 I was accepted to UCI as a biology major, but could not attend due to a sudden diagnosis of mitochondrial disease. At the time, doctors had really no concrete clue what that entailed and just sent me one my way. Three years later, I had a son, then two years after that, a daughter. I never got genetic counseling and never thought twice about passing my genes to my children. My son began showing severe symptoms at three years old, but it took me two years to find a doctor who heard of the mitochondrial disease. Just after his 5th birthday, he passed away in his sleep from what I now know was a prolonged tonic-clonic seizure. Today, my daughter is

7 years old and was just diagnosed with epilepsy and confirmed that she also carries the mitochondrial DNA mutation in 100% of her blood.

Early detection could have saved my son. This is why when I first heard about the work you were doing, I knew I wanted to be a part of it. What you are doing is an incredibly selfless and incredible. I admire you on so many levels for doing this. There is no doubt in my mind that you will find something great. I look forward to keeping updated with your research. This is all so very exciting!

Best wishes,

M.G"

Her letter really touched my heart and further emphasize the need for early detection and identification of new biomarkers as a new screening method and also hopefully to treat such disorders.

1.3. OBJECTIVES

The main objective of this study was to establish new assays and to identify new biomarkers that can be used in the diagnosis of Huntington disease. In addition, such biomarkers can help screen the progression of the disease, use as a targeted treatment, and also test the efficacy of the new treatments. For this purpose, using phasor approach of two-photon microscopy, the initial aim was to develop the technique and method to characterize metabolic alteration in HD using NADH FLIM. Phasor method is a graphical representation of FLIM analysis in which the fluorescent decay at each pixel is transformed into polar coordinates (i.e phasor plot).The

analysis was done in live HEK293 cell lines *in vitro* as our model for non-neuronal cells and further confirmed in live tissue of transgenic Drosophila expressing expanded and unexpanded polyQ HTT ex1 in the eye disc. Here, we measured the changes between free and bound fractions of NADH which is an indirect measure of metabolic alteration in living cells. Using Phasor-FLIM, pixel maps of the metabolic index in HEK293 cell lines and in transgenic Drosophila expressing expanded and unexpanded polyQ HTT ex1 in the eye disc was developed. We found a significant shift towards increased free NADH, indicating an increased glycolytic state for cells and tissues expressing the expanded polyQ compared to unexpanded control. In the nucleus, a further lifetime shift occurs towards higher free NADH indicating synergism between metabolic dysfunction and transcriptional regulation. Our results indicate that metabolic dysfunction in HD shifts to increased glycolysis which can lead to oxidative stress and cell death.

The proceeding goal of this study was to analyze the effect of HD on the mammalian cells plasma membrane as a cell structure. In fact, many diseases are rooted in an imbalance of important lipids. For example, there is an excess of lipids in heart disease, or there is lack of certain lipids in autism or schizophrenia. In the case of Huntington disease, altered lipid metabolism is linked to dysfunction in HD. Some researchers indicate the disturbance of biogenesis of cholesterol and other fatty acids. Other recent literature also suggests rather the disturbance in trafficking of the lipids due to the interaction of Htt with Cav-1, a vesicle transporting cholesterol through the membrane. In normal cases, sphingolipids and cholesterol trafficking are synthesized in the endoplasmic reticulum and transported to the Golgi and then to the plasma membrane by passing through the endosomal compartment. However, when trafficking is disturbed, cholesterol and sphingolipids are accumulated in late endosomes and lysosomes.

Although lipids are an essential part of the cell plasma membrane our understanding on the role Htt and the disruption of lipid homeostasis and its effect on the cell plasma membrane is very limited. And thus another aim of this study was to clarify if Htt can affect cell membrane fluidity. For this purpose spectral phasor analysis coupled with LAURDAN was used to characterize the plasma membrane fluidity. Spectral phasor analysis is similar to phasor-FLIM analysis. However, in this case, using the Fourier transformation, the emission spectra at each pixel will be obtained in the spectral phasor plot. We have also further validated our result using secondary fluorescent probe Nile red that is sensitive to the polarity of the lipid environment. Our results indicate a shift in the position of the phasor indicating changes in the emission spectra. We have also developed the triangular combination method that defines the linear combination of fluorescent probe and the fluorescent protein. In this case, if there is a third fluorescent component within the same pixel along with the LAURDAN, the trajectory lies between the two spectra of LAURDAN connecting to the third components(lies along the hypothetical triangle connecting two poles of the spectra of LAURDAN to the third fluorescent). Altogether, our results indicate increased in membrane fluidity of the mammalian cells expressing expanded polyQ homopolymer. Here we have identified another biomarker. Changes in the membrane fluidity in the expanded polyQ can be used as a biomarker to screen the progression of the disease and also to analyze the effect of new treatments.

Lastly, having developed the first two aims, the final goal of this study was to look into the clinical relevance and to characterize the propagation of Htt via transport of polyQ inclusions within the infected cells as well as uninfected cells. For this purpose, we looked at the inclusions translocation between cells via lipid nanotubes and axon in mammalian cells using natural and synthetic inclusion. Using algorithm developed using the Icy program we characterized the

inclusions using their brightness and intensity characterization and were able to detect the transfer. In addition, we have characterized the passive transport of inclusions by characterizing the uptake of the inclusions from the infected medium. Our investigations indicate that mammalian cells are capable of uptaking synthetic polyQ. In addition, inclusions can be transported actively via cell to cell contract and through microtubes/ axons. Moreover, we have also shown normal cells can also get transfected by infected cell medium. This study further clarifies the understanding of how the disease is propagated between the cells, and to get a better sense of the interaction of normal and infected cells, as well as understating how normal cells can be transfected even without a direct cell to cell contact. Altogether the results clarify further the transport of the inclusions and infection to the uninfected cells.

Here I have developed novel biomarkers that can be used to screen the HD severity. The proceeding research should focus on whether we can stop the aggregations process or stop the transfer and if so how significant that is at the single cell level. This has been further discussed as a future work of this study on the final chapter.

1.4. BACKGROUND INFORMATION

Huntington disease is a great model for identification of biomarkers that contribute to the pathogenesis of disease condition as it is resulted by a single mutation in HD gene. Unfortunately available medications are only to relieve some psychiatric problem combined with some speech and physical therapy, and there is no cure for this fatal neurodegenerative disease[24].

One of the early signs of HD before the occurrence of any other symptoms is an energetic impairment that is correlated with the severity of the disease. Such impairment is signified by the profound weight loss despite the adequate food intake. In the past, most of the focus has been on

the central nervous system and solely on the neuronal cells; however, recent studies are indicative of the HD affecting peripheral tissues and non-neuronal cells as well[25, 26]. Many studies indicate that these peripheral features in HD including weight loss or skeletal muscle wasting are affected directly by expression of mutant Htt and is independent of neurological defects[27].In fact, Htt is not only expressed in the brain, it is also presented in many tissues and organs in mammals[28-30].

Although the precise function of huntingtin is still not clear, Htt is involved in many cellular functions including transcription, cellular trafficking, and other vesicular transport[31].In addition, the dysfunction in peripheral cells has been observed even on the isolated condition which indicates that genesis of these abnormalities is the results of mutant huntingtin expression rather than a secondary consequence of brain dysfunction[32, 33]. It is also observed that when Htt was expressed in the cardiomyocyte of wild-type mice, it leas to heart failure [34]. In another study, decreased concentration of testosterone in HD patient has been shown that is not correlated with the decreased luteinizing hormone, a hormone secreted by the pituitary gland which stimulated the synthesis of androgen in males[35].

More fundamentally, studies show abnormality in metabolism and mitochondrial function[33, 36], and also cholesterol defect[37, 38] that resembles the abnormality in the brain which can bring valuable insight for the disease mechanism upon further investigations.

Essentially, mitochondria are the powerhouse of the cell with a key function in providing essential energy demands for all cellular process. Mitochondria play a vital role in programmed cell death or apoptosis, aging (free radical generation and oxidative stress), as a biomolecular sensor of glucose, oxygen, and nitric oxide. Thus, it is not surprising that mitochondria

dysfunction has been linked to a range of disease and health problems like cancer and neurodegenerative diseases[16].Early detection of mitochondria anomalies and metabolic dysfunction is a key step toward effective diagnosis and proceeding treatment.

Beside abnormality in mitochondrial function, lipid homeostasis is also disturbed in Huntington disease. Many studies have shown the decreased biosynthesis of cholesterol and other fatty acids in HD [37-39]. However, other studies indicate the accumulation of cholesterol in neurons due to abnormalities in lipid transport mechanism [40, 41].

Clearly, lipids are vital for brain function and any changes to the lipid level either due to impaired biogenesis or abnormality in its trafficking can ultimately lead to neurodegeneration. Lipis is also vital structural components of cell plasma membrane which directly influences membrane solubility and fluidity. Any damage to the cell plasma membrane can lead to the cell injury as a result of toxic enzyme leakage or trigger of apoptosis[42].However, it is not well understood how changes in the homeostasis in lipid either due to the cholesterol biosynthesis or abnormality of its trafficking influences the cell structure, plasma membrane. And thus a possible single cell assay that can elucidate the alteration in cell membrane fluidity can be a huge benefit for targeting the pathogenies of HD.

Noninvasive imaging technique:

There are various medical imaging modalities that are becoming popular due to their nature of non-invasiveness to study neurodegenerative disorders. Many efforts have been put into the development of advanced imaging protocols leading to the possible identification of imaging-related biomarkers that can be used as a diagnosis and prediction of the course of the disease for

HD and similar neurodegenerative disorders. In this section, we will discuss some of the commonly used technique as well as the imaging and the method used in this work.

fMRI imaging:

One of the cores clinical imaging that is well established is magnetic resonance imaging (MRI) with the potential to be used as an important tool in neuroimaging. Using a technique called nuclear magnetic resonance(NMR), nucleus of hydrogen behave like a magnet and generate a signal that can be mapped and turned into an image[1](Fig.2).

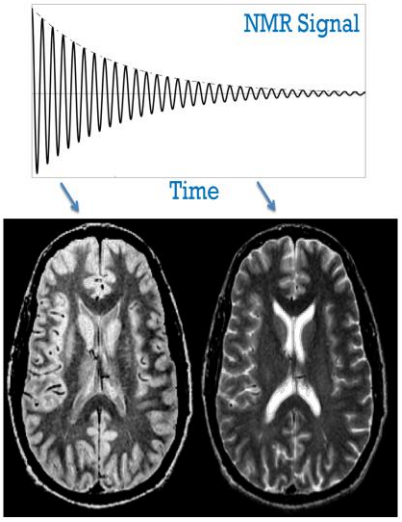

Figure 2: Generating MRI images from NMR signal [1]

MRI relies on the emission of radio frequency (RF) signal, Echo, arise from the relaxation of the magnetic dipole that is disturbed using a pulsed magnetic field from aligned state and relaxed back to equilibrium and received by the receiver coil.

MRI is a well-established imaging technique that with an excellent soft tissue contrasts. However, the *in vivo* study often suffers from low signal to noise ratio (SNR). Data analysis relies on fitting multiexponential decays that is sensitive to SNR to perform such multi-component analysis. Besides, the signal from each pixel can arise from various unknown components and often demand previous information regarding this sub-pixel composition.

Functional magnetic resonance imaging, fMRI, has been used and shown to be correlated with neuronal activity[43]. In fMRI, the blood oxygen level contrast (BOLD) is utilized. In an active

level, neurons utilized increased oxidative metabolic rate and thus increase their demand for higher oxygenated hemoglobin and also the amount of deoxygenated hemoglobin will be decreased[44].

In Huntington disease study, Cerebral Blood Volume (CBV) was measured via fMRI. Results in an R6/2 mouse model of HD indicates that affected area in striatum and neocortex has abnormally high CBV[45]. Since CBV is high, the affected area should have a greater access to glucose than other reasons. And so it can be inferred from the results that there are an inherit differences in metabolism of glucose in HD.

PET imaging:

Positron emission tomography, PET is another molecular imaging technique that probes a radioactive substance called tracer that is a target like a receptor, an enzyme or a transporter to look for the disease in the body[46]. In this imaging modality, $[^{15}O]H_2O$ and $[^{18}F]$FDG that is the marker for cerebral blood flow and glucose metabolism are being typically used.

In FDG-PET scan, the $[^{18}F]$fluorodeoxyglucose (FDG) which is analog to glucose is being traced.In this case, FDG-PET allows the measurements of glucose consumption. Similar to glucose, FDG is transferred from blood to different brain regions. FDG is then phosphorylated to FDG-6-PO_4.At this step, glucose gets phosphorylated and continue along the metabolic pathway; however, since phosphorylated FDG is not the substrate for metabolism it thus gets trapped in tissue and cannot get further processed[47].

Since glucose is the only energy source in the brain then tracking it reflect the neuronal activity and underlying pathology in the brain. $[^{15}O]H_2O$ is also the measurement of blood flow that

indicates the local cerebral metabolic rate of oxygen, as well as cerebral blood flow that is usually increased during neuronal activities and is all shown to be diminished in HD models when supposed to be activated by some tasks [48].

In general whole organ PET can provide a powerful means to determine glucose uptake, however, these measurement doesn't show how glucose is being processed in distinct brain regions. In addition, there are some contradictory results in the field. A study by Gouarné group reveals early defects in glycolysis in striatum using PET imaging[49].However contradictory to other studies Nambron et al. reported that their analysis reveals no abnormalities in lipid, protein or carbohydrate metabolism markers and no significant changes in HD patients compared to controls[50].This contraction can be in part due to sample preparations, the sensitivity of the measurements and bulk measurements. In addition, metabolites are in constant flux and leave the regain of interest multiple times which makes it difficult to do region specific measurements. And effort should continue to explore more diverse new target classes in this imaging. And also there is a need for more powerful and sensitive technique to resolve fundamentally the specific pathways that are being affected and also to provide proven biomarkers that enable the monitoring of the progression of the disease.

FLIM:

Fluorescence lifetime imaging (FLIM) is a method to measure fluorophore lifetime using advance microscopic approach. In past few decades, there has been a huge focus on the use of fluorescence intensity in biological sciences including DNA sequencing and genetic analysis, environmental and chemical monitoring and sorting cells. The issue with such measurement is that intensity-based technique is limited due to the fact that it suffers from variation in

concentration, photobleaching, and other artifacts like detector gain setting or optical loss. In such, FLIM which describes how rapidly an excited state fluorophore decays can be helpful as intrinsic excited state lifetime is unchanged due to such variations. In addition, FLIM can be used to characterize microenvironments such as temperature, pH, polarity, oxygen concentration and etc, and thus can be used to provide a way to probe local environment as well [51]. There are different ways to measure flourcent life time of a fluorophore: time domain (TD) and Frequency domain (FD).

Time domain (TD) FLIM is ideal for large temporal range system and specifically for long lifetime measurements.TD typically involves pulsed excitation and reconstruction of decay over time. This can be accomplished using various techniques, among which time-correlated single photon counting(TCSPC) is the most common one. The reference for timing here corresponds to excitation pulse. The " start" here provided by laser pulse while "stop" signal is generated by detection with a sensitive detector(eg. Photon avalanche diodes). In this technique, a photomultiplier tube (PMT) is used as a vacuum tube to multiply electrons and detect signal.

Frequency domain (FD) FLIM used any continuous wave light source that is suitable for short lifetime measurements. A sinusoidally modulated light is used to excite the desired fluorophore. The resulting emission is modulated and phase shifted. In this case, demodulation is measured with M and phase delay with phi(φ).Plotting phase delay and demodulation over a range of frequency provides a frequency response of the samples[52].

NADH-FLIM imaging:

Reduced nicotinamide adenine dinucleotide (NADH) has been extensively used as an endogenous fluorescent biomarker in the cell. NADH is the principal electron acceptor in

glycolysis and electron donor in oxidative phosphorylation[53]. Intracellular NADH can be found in a form of free and bound to many dehydrogenases and exists in dynamic equilibrium in the cell. It has been shown that NADH binds to dehydrogenase function in energy metabolism and thus the ratio of these two forms can indicate the metabolic state of the cell.

Despite the fact that the redox state of the cell is measured based on the measurement of NADH and NAD+ since NAD+ does not fluoresce, research has been focused on measuring the fraction of intercellular free and bound NADH[54]. High metabolic demand increases the respiration rate leading to decrease in NADH/NAD+ ratio[55]. In addition, NADH can bind to the dehydrogenase Complex I, a mitochondrial membrane protein mediating electron transfer from NADH to oxygen. This transfer causes hydrogen protons to be pumped into the intermembrane space of the mitochondria from the matrix creating an electric potential [56]. Thus, ATP is generated from the activation of ATP-synthase through adenosine diphosphate (ADP) phosphorylation via this electron potential change [57].

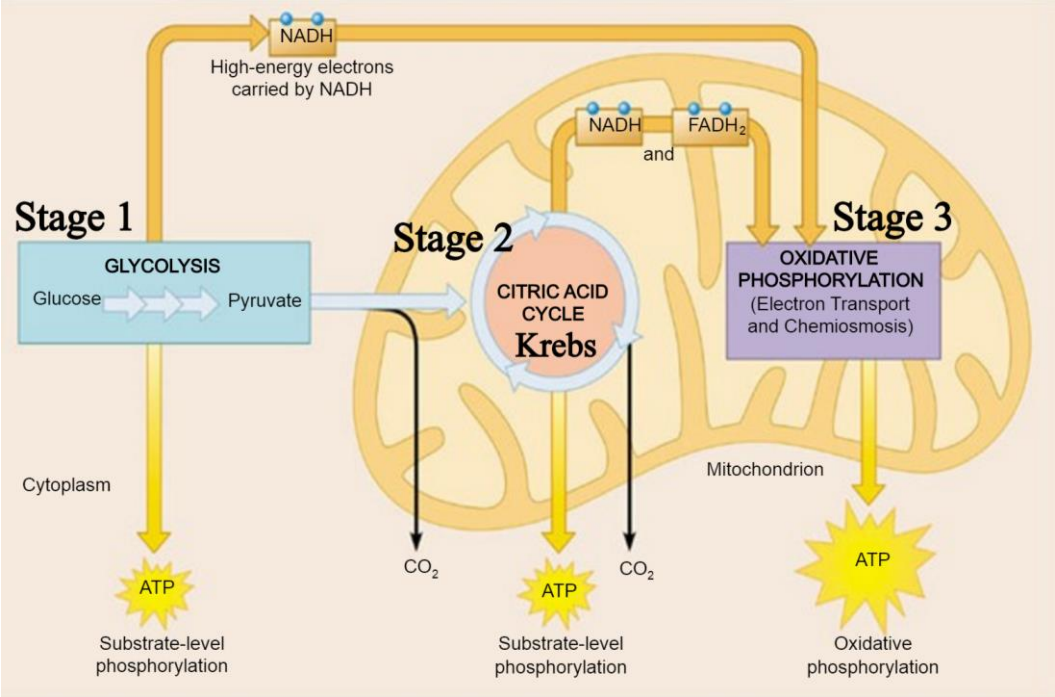

Figure 3: Glycolysis and oxidative phosphorylation pathways[58]

Consequently, the bound form of NADH serves as a biomarker of energy generation and relative ratios between the free and bound form can be used as an index of metabolic states [59].Figure 3 summarizes the cellular respiration pathway.

Following the pioneering work of Britton Chance et al., NADH fluorescence level imaging and relative amounts of reduced and oxidized NADH has been extensively monitored for changes in metabolism [60]. NADH is characterized by long lifetime when it is bound to protein and short lifetime when it is free. The shorter lifetime of Free State NADH is due to the dynamic quenching by adenine moiety (Fig.4).

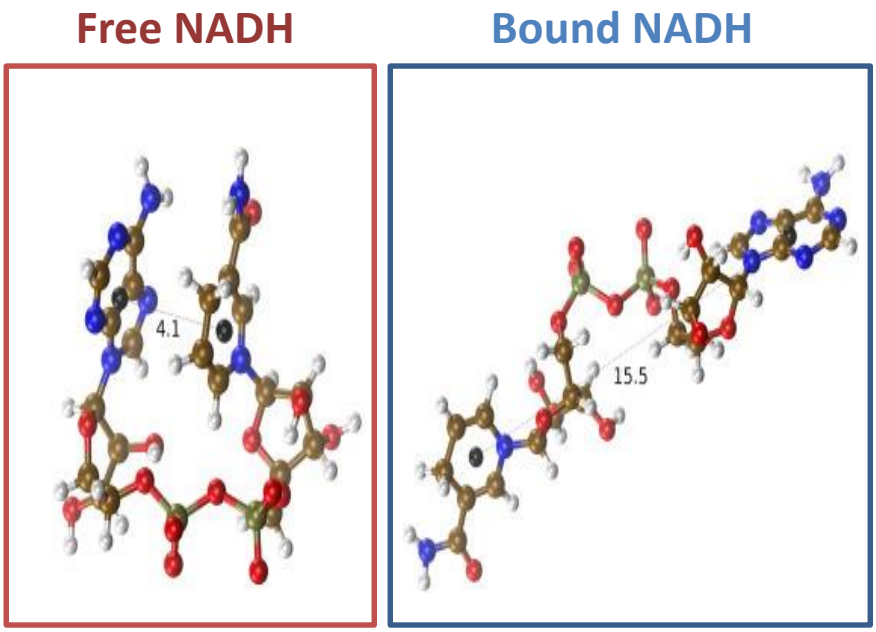

Figure 4: Two conformation of NADH are shown here.

The folded form is when NADH is free that leads to shorter lifetime. The other confirmation is extended or open that is shown in the right blue box with a longer lifetime. The black dot shows the adenine and nicotinamide center of mass and the distance between them is shown with dotted line. This figure is adapted based on Formoso et al[61].

Bird et al, in 2005, showed the changes in the ratio of free to bound NADH is associated with NADH/NAD+ in breast cancer cells[62].

Stringari et al. in 2012 also found the ratio of free to bound NADH correlated with differentiation state of the cells and their role in the fate commitment. Based on their analysis, they have shown undifferentiated NPSCs to be highly glycolytic characterized by the higher ratio of free to bound NADH while differentiated neurons have oxidative phosphorylation phenotype characterized by the lower ratio of free to bound NADH[53].

Despite all the benefit of FLIM imaging, analysis of fluorescence lifetime imaging can be difficult as it composes of multi-exponential decays coming from different molecular species or

even different conformation of the same molecule[51, 63]. Analysis of fluorescence decay using fluorescence lifetime imaging microscopy(FLIM) can be performed in various ways: time-correlated single photon counting(TCSPC)[64], the frequency domain, and the time domain approach[65-67]. For analysis of FLIM data using time domain approach, the decay at each pixel is fitted using one or two exponentials and then decay times and amplitudes are found.

The issue with this approach is that many of the fluorescent protein display a complex decay behavior[68]. In addition, there is a correlation between the amplitude and characteristics exponential time. More than that, such analysis(~10^5 pixel in an image) requires expertise to correctly extract the information regarding the number and abundance of the molecular species[69, 70]. Here, in this work, using phasor FLIM imaging approach cellular metabolism that is affected by Huntington disease has been measured and analyzed.

Phasor method:

Phasor transformation used here simplifies the FLIM analysis by providing a graphical global view of the process at each pixel and avoids some of the multi-complexity of exponential analysis. In this way, using a fit free approach that can be applied to both time and frequency domain measurements, fluoresce lifetime can be analyzed.

Fig.5 shows the phasor transformation. Here for each pixel in an image, a phasor lifetime is plotted in a graph using Fourier transformation (equation set (1)).

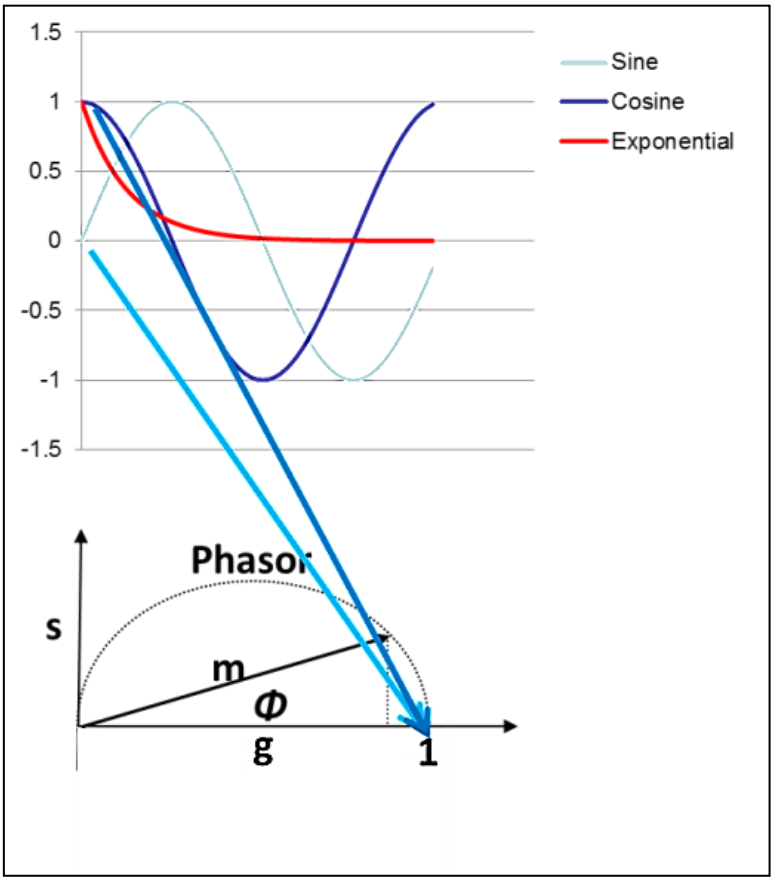

Figure 5: phasor transformation using sine and cosine function

$$g_{i,j}(\omega) = \frac{\int_0^\infty I_{i,j}(t)\cos(\omega t)dt}{\int_0^\infty I_{i,j}(t)dt},$$
$$s_{i,j}(\omega) = \frac{\int_0^\infty I_{i,j}(t)\sin(\omega t)dt}{\int_0^\infty I_{i,j}(t)dt},$$

Equation 1: G and S representation in phasor plot equations

We then use a cursor to highlight the cluster of points that correspond to the lifetime in that range (Fig. 6).

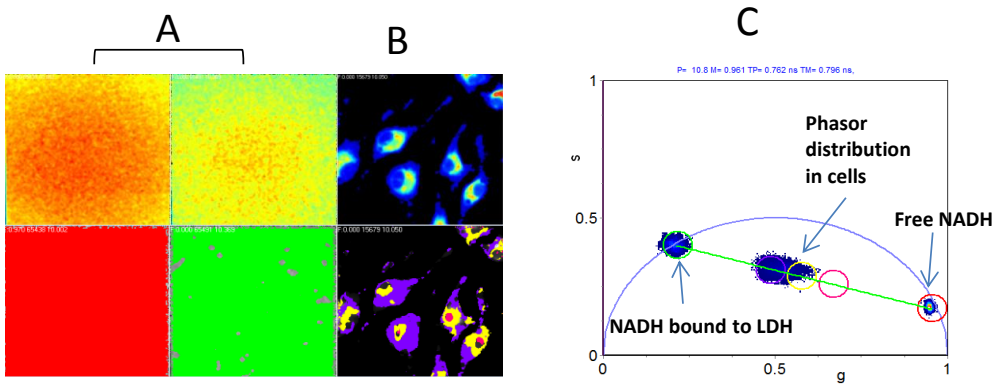

Figure 6: NADH Phasor plot.

Panel A shows NADH intensity of free NADH, NADH bound to LDH with corresponding lifetime color map underneath. Panel B also shows the intensity and color map of the NADH autofluorescence in the cells. Panel C is the phasor transformation with colored cursors corresponding to the figure A and B color map.

Spectral phasor:

Similarly, we have used spectral phasor transformation as a way to characterize the impact of the changes in the homeostasis of the lipid in HD and the effect this could have in the membrane fluidity. Similar to what was explained in FLIM-phasor analysis; spectral phasor analysis calculates the sine and cosine of Fourier components, but now from spectrum profile (shown in equation set 2). For each component, g and s are obtained and represented in a polar plot.

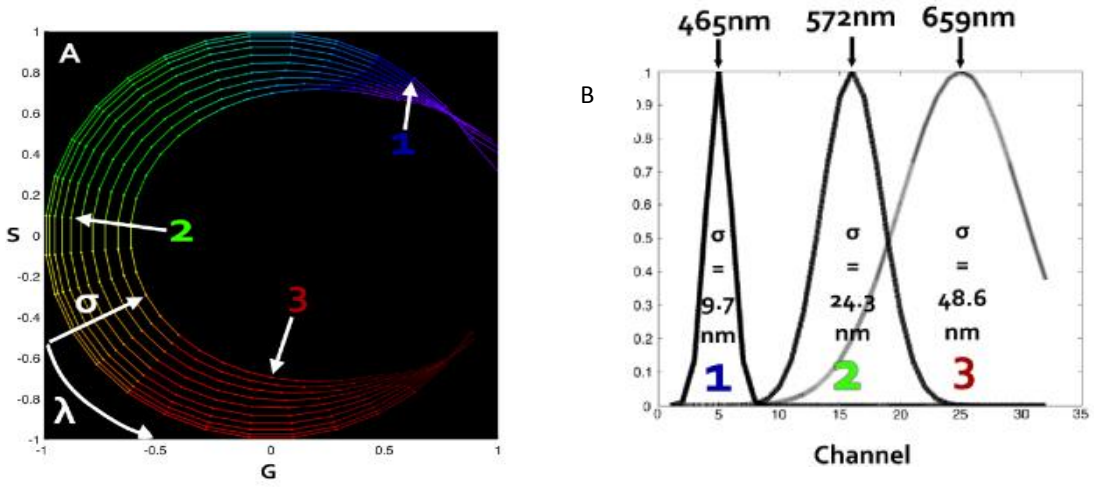

Figure 7: Spectral phasor graph.

Spectral phasor are depicted in A.B shows three of the simulated spectra to calculate phasor A. Figure adapted based on Cutrale et al. [2]

In this case, “L” is the total wavelength range of our spectrometer. The angular position, in this case, is proportional to the average of the spectrum and the spectral width is represented in terms of the distance from the origin as it is depicted in Fig 7.

$$G = \frac{\sum_\lambda I(\lambda) \cos(\frac{2\pi n\lambda}{L})}{\sum_\lambda I(\lambda)} \qquad \text{eq. A}$$

$$S = \frac{\sum_\lambda I(\lambda) \sin(\frac{2\pi n\lambda}{L})}{\sum_\lambda I(\lambda)} \qquad \text{eq. B}$$

Equation 2: Spectral phasor equations for G and S calculation.

1.5. ORGANIZATION OF THE DISSERTATION

In this study, I focused on identifying new peripheral biomarkers using phasor-FLIM imaging. During my extensive study, I was able to develop new assays/methods that can be potentially used to monitor the progression of the disease and evaluate the efficacy of the treatment benefits.

In chapter 2, I will discuss the metabolism and FLIM imaging of free/bound NADH that I used for in vitro and in an animal model of HD. Using FLIM imaging I was able to get a deeper understanding of how metabolism is affected in HD and also was able to identify a new potential biomarker that can be used for the disease screening. In addition, the method I have developed in this study can be applied in a piece of tissue and pixel map of cellular metabolism that is affected can be obtained.

In chapter 3, I have focused on understanding if the changes in lipid homeostasis in HD that has been previously reported have any influences in the cell structure. I have studied the plasma membrane structure at the single cell level using spectral phasor analysis. This study led to a novel discovery that shows cell membrane of the mammalian cells affected by HD can be the target of the disease. My results indicate increased fluidity in the cell plasma membrane

compared to the control. This can also have implication in the propagation of the HD inclusions and pathogenesis of the disease to the normal cells. In addition, it will affect the normal cell function and eventually can lead to the apoptosis.

In chapter 4, I have focused on clinical relevance and further explored the transfer of both synthetic and natural polyQ inclusions. I was able to confirm that mammalian cells can uptake synthetic inclusions. In addition, using a co-culture study in mammalian cells, I was also able to track the transfer of inclusion and the propagation of the inclusions to the normal cells by means of different mechanism like cell uptake or active mechanism via microtubes/axon. The time-lapse imaging also shows the interaction of the cells and the dynamic of the polyQ inclusions transfer.

Finally, in chapter 5, I have further elaborated on the outcome of this study and its implications in HD and similar neurodegenerative disease. In addition, I have further discussed the future perspective of this work.

CHAPTER 2: NADH AS A BIOMARKER IN HD

THE PHASOR-FLIM FINGERPRINTS REVEAL SHIFTS FROM OXPHOS TO ENHANCED GLYCOLYSIS IN HUNTINGTON DISEASE[1]

2.1. ABSTRACT:

Huntington disease (HD) is an autosomal neurodegenerative disorder caused by the expansion of Polyglutamine (polyQ) in exon 1 of the Huntingtin protein. Glutamine repeats below 36 are considered normal while repeats above 40 lead to HD. Impairment in energy metabolism is a common trend in Huntington pathogenesis studies; however, this effect is not fully understood. Here, we used phasor approach and Fluorescence Lifetime Imaging Microscopy (FLIM) to measure changes between free and bound fractions of NADH which is an indirect measure of metabolic alteration in living cells. Using Phasor-FLIM, pixel maps of metabolic alteration in HEK293 cell lines and in transgenic Drosophila expressing expanded and unexpanded polyQ HTT exon1 in the eye disc was developed. We found a significant shift towards increased free NADH, indicating an increased glycolytic state for cells and tissues expressing the expanded polyQ compared to unexpanded control. In the nucleus, a further lifetime shift occurs towards higher free NADH indicating synergism between metabolic dysfunction and transcriptional regulation. Our results clearly indicate that metabolic dysfunction in HD shifts to increased glycolysis leading to oxidative stress and cell death. This powerful label-free method can be used to screen native HD tissue samples and for potential drug screening.

2.2 INTRODUCTION

[1] A version of this chapter was also published in nature scientific report [Sameni S, Syed A, Marsh JL, Digman MA.The phasor-FLIM fingerprints reveal shifts from OXPHOS to enhanced glycolysis in Huntington Disease. *Sci Rep.* 2016; 6: 34755. PMCID: PMC5054433]

The mechanisms underlying neurodegeneration in Huntington Disease(HD) are unknown, but compelling evidence suggests that mitochondrial defects may play a central role[14]. Mitochondria dysfunction has been linked to a range of disease and health problems such as cancer and neurodegenerative diseases[16]. Thus early detection of mitochondria anomalies and metabolic dysfunction is a key step toward effective diagnosis and proceeding treatment.

Previous studies showed that HD onset can be identified from disturbed glucose metabolism. Glucose metabolism in asymptomatic HD carriers reveals significant hypometabolism and a 2-3% reduction in caudate glucose metabolism per year. This implies that there would be a significant reduction of glucose metabolism occurring on the onset of the disease, and the measurement of striatal metabolism receptor binding would be a good marker for the diagnostic of the progression of the disease[71, 72]. Yet other studies on the opposite front, report that lactate produced by glucose uptake is enhanced in HD brain tissue of in transgenic and in 3-nitropropionic acid-treated mouse models for HD[73]. Olah and coworkers measured a high glycolytic flux in the posterior region of HD brains by measuring mitochondrial complex activities, NADH absorption, pyruvate formation and lactate production.[73] In their experiment-based mathematical model, the authors calculated the increased flux through the glycolytic pathway where they revealed that the increased energy metabolism enhances the rate of glycolytic flux in comparison to the control. However, the hypothesis that the ATP production through oxidative phosphorylation (OXPHOS) shifts metabolism to glycolysis in HD is not yet clear[74]. Here using the phasor-FLIM fingerprinting approach we aim to help elucidate this pathway. electron donor in oxidative phosphorylation [53]. While NADH fluoresces, its oxidized form (NAD+) does not, and research has been focused on measuring the fraction of intracellular free and bound form (to enzymes) of NADH [54]. Given that the fluorescence lifetime of NADH

shifts in the bound versus free state, NADH autofluorescence has been used as a biomarker for oxidative stress in alpha-synuclein aggregation, metabolic changes in Wnt signaling in colon cancer was characterized using NADH-FLIM, [75-77]. Since FLIM is independent of concentration, the free and bound forms of NADH lifetimes are unbiased from endogenous levels produced in living cells. Also, the lifetime of free NADH is shorter (~0.4ns), indicating more glycolysis, compared to the fully bound form (3.2ns-3.4 ns), indicating more oxidative phosphorylation. Thus their fractional contributions can be a measure of oxidative stress or cellular homeostasis [16, 75, 78].

In this work, we have used the phasor approach to FLIM to measure the fraction of free to bound NADH as a way to map the metabolic alteration in cells transfected with expanded and unexpanded polyQ HTT exon 1. Image segmentation to isolate the cytoplasm was also done and further characterized lifetime shift towards the free fractional component of NADH in the cell nucleus. In addition, we have validated our data in the late third instar Drosophila eye disk which is model of Huntington disease [79]. During this stage (approximately 3- 4.5 days post fertilization) eye imaginal complete their development and photoreceptor neurons are born [80, 81].

Our results indicate that in the presence of the expanded Huntingtin repeat nuclear fingerprints of the phasor distributions shifts towards an increased free NADH lifetime. It has been shown that NADH interaction with regulatory protein such as CtBP influences the transcriptional activity [82, 83]. Moreover, while NAD(P)H shown to enhance heterodimerization and DNA binding to

Chance et al., in the 1950s, pioneered the measurement and quantification of tissue and cellular metabolic states, and since then many studies followed [84-86]. These investigations were based

on fluorescence emission of reduced nicotinamide adenine dinucleotide (NADH) as an endogenous fluorescent biomarker. NADH is the principal electron acceptor in glycolysis and

transcription factors, its oxidized form, NAD(P), inhibits such activities[83]. Thus we hypothesize that such an increase in nuclear NADH leads to transcriptional dysregulation. Further, we observed an increase in the ratio free/bound NADH (shift toward anaerobic glycolysis) in the cytosolic region in the presence of the expanded Huntingtin repeat.This is in correlation with previous studies that showed hypoxic conditions by a shortening of NADH fluorescence lifetime (i.e. more free NADH) in cells [87], tissue [88] and organs *in vitro* [89] and *in vivo* [90].

2.3. RESULTS:

HEK 293 cell lines:

Using the transiently transfected cell lines HEK 293 (EGFP expanded versus the unexpanded polyQ from exon 1 of the Huntingtin protein) we show that the relative ratio of free to bound NADH increases as an average. This increase in the free/bound ratio indicates that cells expressing the expanded Htt repeat show a shift of ATP production from OXPHOS to glycolytic state. We have used the phasor approach to FLIM in which the fluorescence decay at each pixel is transformed into a single point in the phasor plot, defined in material and method section and supplemental figure A1. In the phasor plot, the s(ω) and g(ω) coordinates for every pixel of the image, Fourier sine vs. the Fourier cosine, are plotted on the y and x-axis where the x coordinate spans from 0 to 1 and the Y spans from 0 to 0.5. Thus the g coordinate is more sensitive to the ratio of free to bound NADH as shown in supplemental (figure A2)[91, 92].

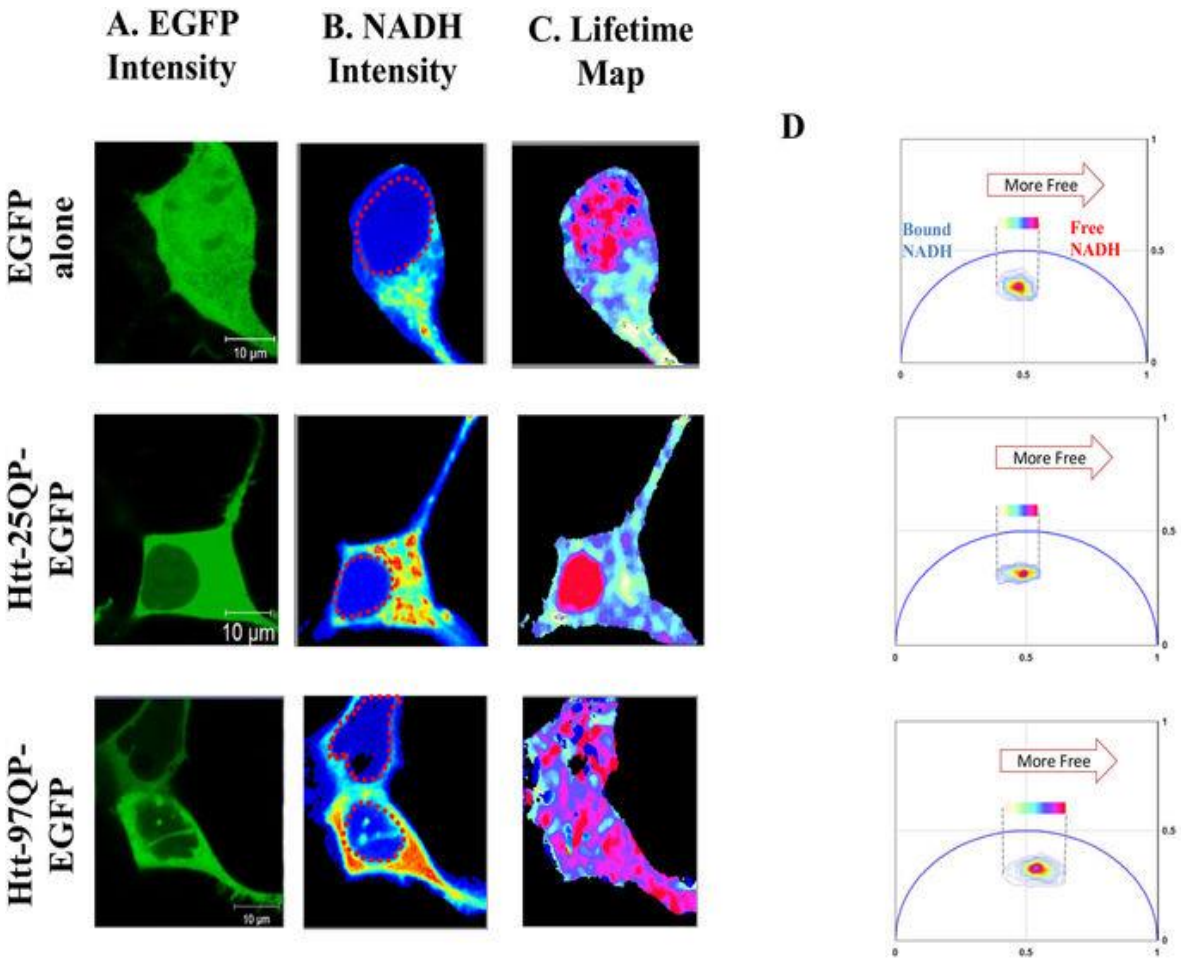

Figure 8: HEK293 NADH FLIM Map.

Panel A shows confocal images obtained using the 488 nm laser to excite EGFP directly. In panel B NADH emission was obtained with 740 nm two-photon excitation. NADH is detected with a blue filter (442/46nm) in one channel and EGFP emission with a green filter (520/35nm). Nuclei of the cells are shown with dashed red circle. Panel C represents lifetime maps of NADH colored according to the color scale in the phasor plot in panels D. When cells express the expanded Htt 97Qp, there is a significant shift toward the shorter lifetime indicating a higher glycolytic state. Panel D also shows the phasor plot for each representative cell. The phasor histogram of the cell transfected with 97Q is shifted to the direction of free NADH. Scale bar on the image is 10µm.

The color of the lifetime maps (Fig. 8.C) corresponds to the fluorescence lifetime distribution along the phasor plot shown in panel D for each of the 3 conditions. We applied to image segmentation to isolate the nuclear compartment from the cytoplasmic pool as it shown in

supplement A3 to further quantify the average phasor coordinates corresponding to the g and s axis on the phasor plot.

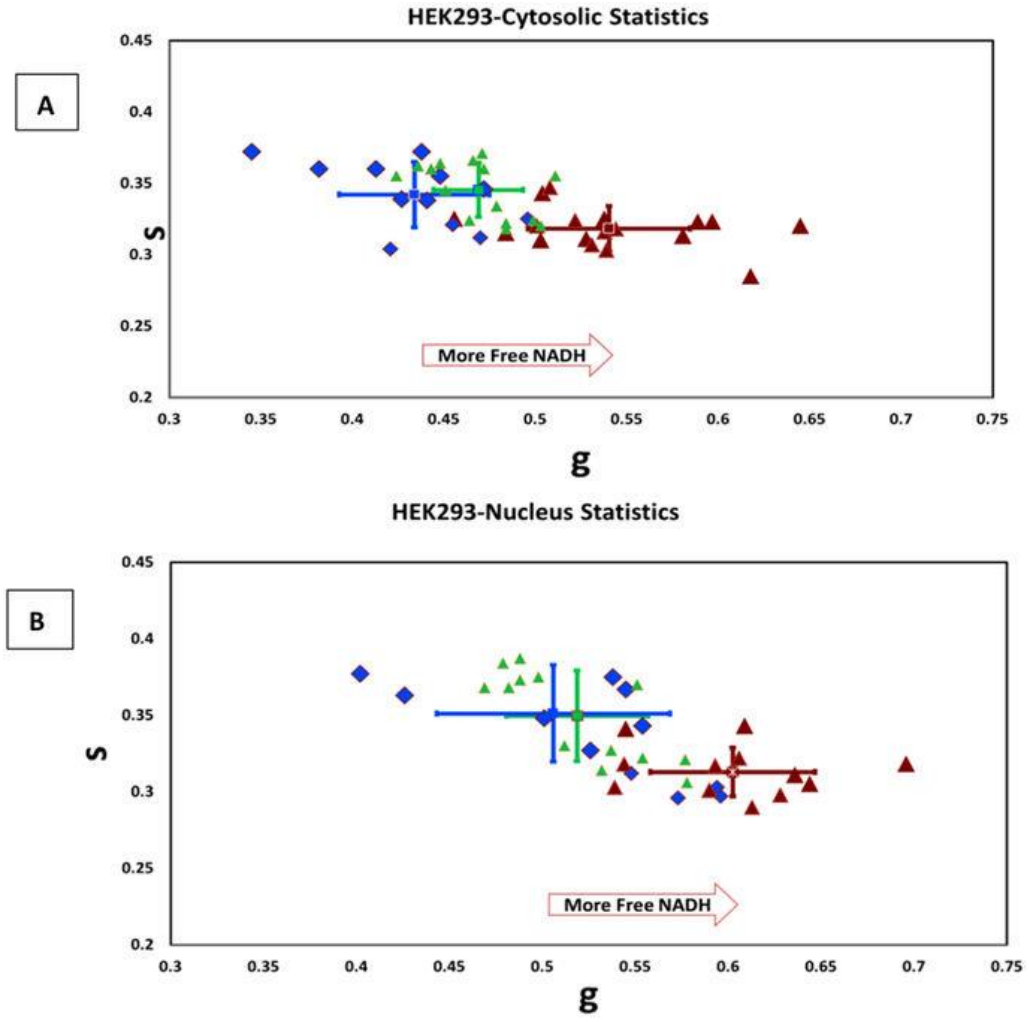

Figure 9: A. Scatter plot of NADH cell phasor FLIM

Plot shows in the cytoplasmic pool of the Httex1p25Q (N=12, in blue) expressing cells compared to the Httex1p97Q cells in red (N=18), EGFP control is plotted in green triangle (N=15). Each point represents the average lifetime plotted in the phasor coordinates. Using image segmentation the cytoplasmic region for each cell is selected. Expanded cells (97Q) shows higher free to bound NADH ratio (shifted toward right). B. Similar plot was obtained for individual cell nuclei of the Httex1p25Q cells compared to Httex1p97Q cells. Cells transfected with 97Q are further shifted towards the right side of the plot indicating an increase of free NADH in the nucleus.

Our results

indicate a significant shift in NADH lifetime, indicating a transition from the NADH bound to free form, in cells expressing the expanded Httex1p97Q-EGFP protein compared to the Httex1p25Q expressing cells as shown in Figure 9 A ($P= 1.02x10^{-6}$).

We identified two distinct populations (Fig. 9) in the nuclear and cytoplasmic phasors corresponding to the Httex1p25Q-EGFP and Httex1p97Q-EGFP variants in HEK 293 cells. To further confirm our data and to ensure that changing the fluorescent protein does not perturb NADH readings we have performed an experiment in 15 more animals (total of 66 ROIs) tagged with Kaede (Figure A4). The applied image segmentation for the nuclear compartment shows a decreased nuclear activity in cells expressing the expanded form of the Htt protein. In both expanded and unexpanded HTT protein expressing cells, the nucleus is characterized by high amount of free NADH. This is consistent with the results published by Wright et al [75] which shows reduced nuclear activity characterized by shorter lifetime (more free NADH) for undifferentiated or early differentiating cells and more bound NADH due to increased nuclear activity in differentiating cells. In the expanded Htt expressing cells, there is a significantly increased fraction of free NADH indicating a lower nuclear activity ($p= 0.0024$) (Fig.9 B). No differences were observed for the control experiments of the cell cytoplasm and nucleus in the EGFP expressing cells compared to the wild-type, Httex1p25Q-EGFP with p-value higher than 0.05 ($p=0.206$ and $p=0.209$ accordingly).

Transgenic Drosophila results:

To further validate our results *in vivo*, we have used the transgenic Drosophila eye disk model. Drosophila is an excellent source for modeling neurodegenerative disease as it contains fully

functional nervous system with separate specialized functions including vision, olfaction, learning, and memory[93]. The most common method for generating restricted transgene expression in Drosophila is based on the yeast GAL4 protein and its target upstream activating upstream sequence (UAS) system[94].

The eye develops from the eye-antennal disk. The disk arises from about 20 cells of the optic primordium in the embryonic blastoderm. By the third instar larva disk forms approximately 2000 cells [95]. Barbaro et al. earlier showed temporal gradients of neurons expressing Htt transgenes in Drosophila eye disk. Cells begin to differentiate into neurons in the eye disk as a wave of differentiation derived from the morphogenetic furrow. The wave moves from the posterior toward the anterior in an array of cells ordered in rows. Each row of cells from the leading edge of the furrow toward the posterior expresses the Htt transgene 2 h longer than the rows in front of it [96]. We have selected to analyze the posterior part of the eye disk where cells are fully differentiated into neuron expressing different concentrations of the 120Q, 96Q compared with the 25Q and control (no transfection).

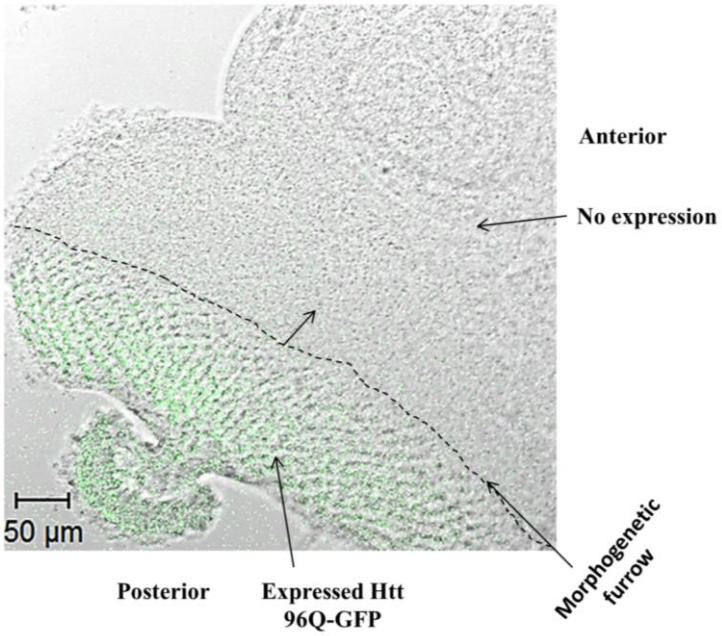

Figure 10: Tiled images of ELAV-GAL4 X UASQ96-GFP Drosophila eye disk.

Bright field image merged with FITC shown here (Scale bar on the image is 50 um).

Figure 10 shows a tiled image of expanded $90^{ex1\ 96Q\text{-}GFP}$. The Drosophila eye disk excited at 488nm in respect to the whole eye disk (bright field image merged with FITC) is depicted here. The posterior region expressing the Htt 96Q-GFP was selected and the distributions of lifetimes were mapped on the phasor plot and a scatter graph was obtained (Fig.12). Similar to what we have observed in the HEK 293 cells, a shift toward shorter lifetime in expressed Htt 96Q-GFP of the live eye disc was detected. To ensure that the expression of GFP did not perturb the metabolism in this model, we tested the unexpanded versus the expanded Htt with no fluorophore tag (Unexpanded $90^{ex1\ 25Q}$ vs. expanded $90^{ex1\ 120Q}$ expressing flies). The images here are obtained from the most posterior part of each animal eye disk that is associated with either 25Q or 120Q expressions. As shown in Figure 11, the three representative tissue ROI of the 25Q populations are characterized with longer lifetime associated with decreased ratios of free to bound NADH similar to what was observed in the HEK 293 cell line (white/aqua color) with

unexpanded transfection; while the expanded models (i.e. 120 Q) are shifted towards the shorter lifetime with increased ratio of free to bound NADH (pink/red color).

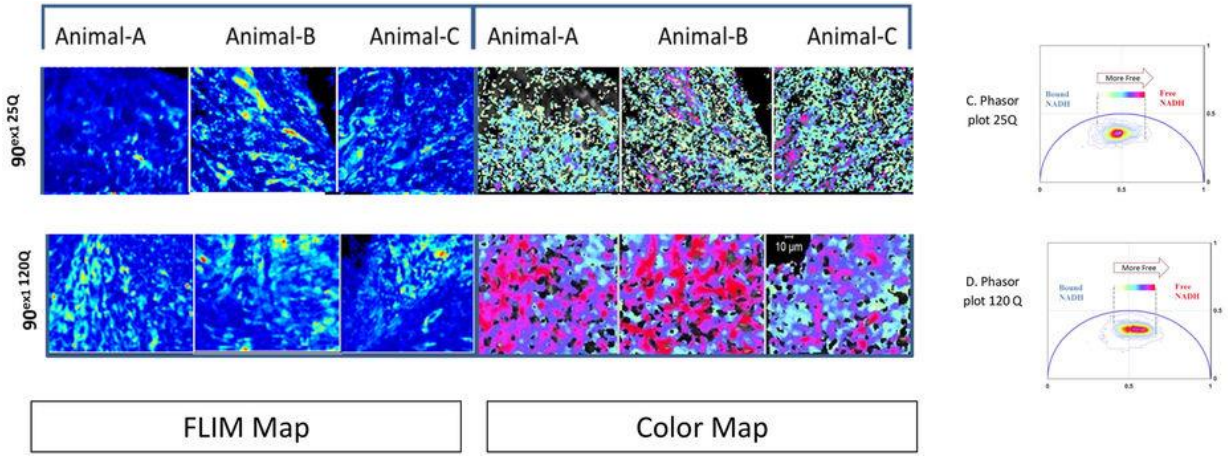

Figure 11: Unexpanded ELAV-GAL4 X UASQ25 vs. expanded ELAV-GAL4 X UASQ120 expressing flies results are depicted here.

NADH emission obtained with 740 nm two-photon excitation is shown under intensity map. Lifetime color map of NADH is depicted on the right (color map). Shorter lifetime is color coded with red here while longer lifetime on the phasor plot is associated with cyan. As it is shown here Htt 120Q cells are characterized by a distinct population shifted toward shorter lifetime (red) that has a higher ratio of free to bound NADH. Panels C&D show phasor plot for 25Q and 120 Q respectively. The phasor histogram is shifted toward the direction of free NADH (glycolysis) in the expanded form 120Q compared to unexpanded 25Q.Scale bar is 10 um.

Figure 12 shows the scatter plot of phasor lifetimes averages for the eye discs expressing the unlabeled unexpanded (blue) and expanded Htt protein (red). The analysis of the phasor distribution, in this case, is performed by cluster identification as described in [97].

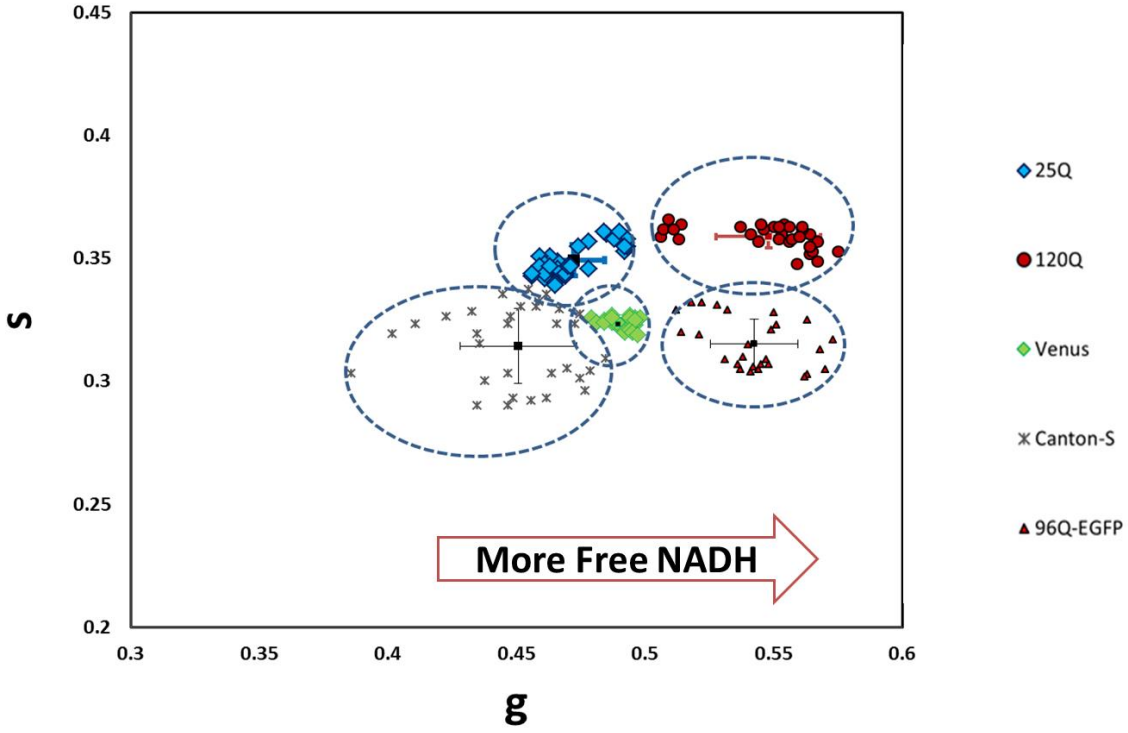

Figure 12: Scatter plot of the NADH phasor FLIM showing average g and s phasor values for each animal eye disk

ROI for total of 15 animals and 149 ROI measurements. The blue diamond refers to 25Q (N=30), green diamond Venus control (N=28), gray asterisk wildtype with no Htt (canton-S, N=32).Tissue with expanded expression 120Q (N=32, in red circle) and 96Q-EGFP (N=27,in red triangles) indicates shortening of the lifetime towards the glycolytic state, shifted to the right.

The clusters refer to all the pixels selected in the ROI and are the average coordinates lifetime for each ROI of the three eye discs.

The Student t-test was done to compare the 25Q population and 120Q population in terms of g values. Our result indicates that these two populations are statistically significant different (p-value of 0.034). In addition, 25Q group shows significantly longer lifetime compared to 96Q group (p-value 0.023).

No difference was observed in control group (Venus with no *Htt*) compared to 25Q with the p-value >0.05(P=0.14) (Fig.13).

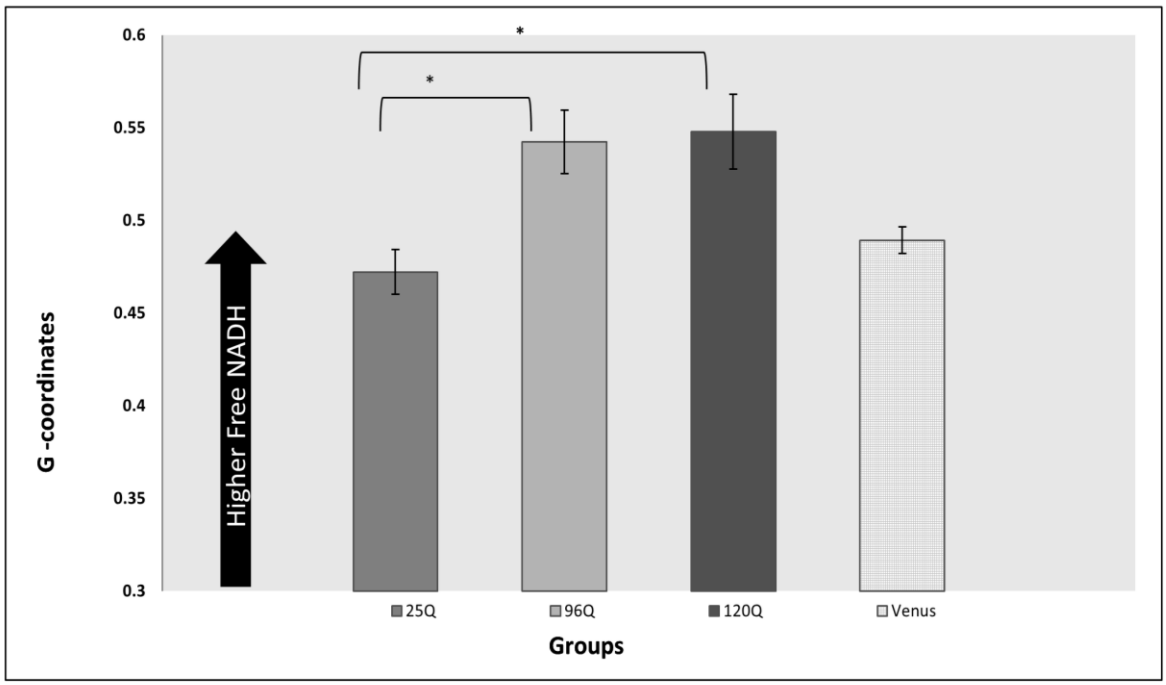

Figure 13: Summary of the data analysis for live tissue of drosophila eye disk

(expanded 96Q (N=27), 120Q (N=32), unexpanded 25Q (N=30), and control (Venus, N=28) are depicted here. Arrow bar shows the direction of Free NADH. Expanded Htt (both 96Q and 120Q) are characterized with significant increased ratio of free to bound NADH(more Glycolytic) compared to unexpanded Htt (25Q**).**

2.4. DISCUSSION:

Energy production deficiency contributes to the progression of the HD brain is observed by weight loss in HD patients[98]. The dysfunction in energy metabolism, in particular, mitochondrial perturbations, is a common trend in Huntington pathogenesis studies in human and animal models [12]. It has been postulated that Htt perturbs the activation of SIRT 3 leading to a decrease in concentration of NAD and PGC-1α (a transcriptional coactivator controlling mitochondrial biogenesis and function). Given that SIRT 3 acetylates the flavoprotein (Fp) subunit of complex II, the loss of SIRT 3 activity in HD leads to a reduced binding of complex II with the Fpp thereby dysregulating mitochondrial function[99].

Alterations of metabolism have recently gained traction in identifying the mechanism by which this pathway is affected. Insight into a metabolic requirement in distinct populations of a striatal versus cortical neuron is provided by Gorarne and co-workers [49]. They showed that early glycolysis subtle defects were found in striatal neurons using PET in living patients. However, contradicting results were recently reported by Nambron at al. that revealed metabolic carbohydrate, lipid and protein metabolites as wells as hormones related to energy metabolism screening in HD patients resulted in no significant changes compared to the control subjects[50]. These conflicting results can be due to the sensitivity of sample preparation as well as average population or bulk measurements. Thus pursuing the quest to understand and learn about metabolic dysfunctions in a non-invasive manner and at the single cell level will elucidate the role of impaired metabolic pathways that can leads to transcriptional dysregulation in the disease.

Previous studies in animal models and HD patients reported perturbation of metabolism in HD in an animal study and HD patients. Several studies associate HD with Diabetes mellitus as significant numbers of R6/2 mice develop diabetes gradually[72, 100]. Other studies also reported that glucose metabolism can be an indicator of HD onset[101, 102].

Our present study, using 2P-FLIM, indicates a decreased in fluoresce lifetime of NADH that is correlated with increased in free to the bound ratio of NADH in HD. These changes indicate ATP production shifts from oxidative phosphorylation to glycolysis that can lead to increase in oxidative stress and eventual cell death. Given that the lifetimes of NADH and Nicotinamide Adenine Dinucleotide Phosphate (NAD(P)H) are virtually indistinguishable, alternations of free to bound NAD(P)H could also reflect these changes. Our results are consistent with the earlier

report by Valencia et al group showing elevated NADPH oxidase activity leading to overproduction of ROS and cell death in HD mice[103].

Here for the first time, we were able to examine changes in fluorescence lifetime of NADH to increased glycolytic state in HD using Phasor FLIM approach. Earlier, Nicoletta Plotegher et al. showed shifts of NADH to a shorter lifetime in the presence of alpha-synuclein aggregates in Parkinson disease(in HEK293-aS)[77].Similar results were also reported recently using 2P-FLIM by Sandeep *et al*. in pc12 model of Parkinson disease[104]. In more recent advancement, in a pilot study, Jentsch used FLIM based technology in ophthalmoscopy based setting to examine the alteration in the retina of Alzheimer disease patients. In this study, the dependence of fluorescence lifetime imaging parameter on the severity of Alzheimer's disease is reported[105].

The real advantage of the powerful method that we have proposed here is that it can be applied in tissue and pixel map of cellular alteration can be obtained. We foresee that such precise measurements using phasor-FLIM fingerprinting approach can help address some of the current issues in the literature.

2.5.CONCLUSIONS:

The underlying mechanism that affects neurodegeneration in Huntington disease is still under investigation. Compelling evidence indicates that mitochondria may play an essential role that affects neurodegeneration in Huntington disease. In this work, we have measured metabolic perturbations of the cells transfected with various glutamine repeats (expanded vs unexpanded) as well as in the transgenic Drosophila eye disk using FLIM coupled with phasor analysis. We used the autofluorescence lifetime of NADH as an intrinsic biomarker for such measurements. Results obtained here indicate a shift toward larger free/bound NADH ratio in the presence of the

expanded Huntington repeat both *in vitro* in Human Embryonic Kidney (HEK 293) cells as well as in the Drosophila eye disk model of Huntington disease. Such shift in the expanded model may indicate depletion of ATP production and an increase in oxidative stress that can eventually lead to cell death. In addition, nuclear FLIM analysis on expanded polyQ HTT exon1 cells indicates increased free NADH which influences CtBP activity, a phosphoprotein and transcriptional corepressor in the nucleus. We propose that such a shift toward increased free NADH in the nucleus indicates transcriptional dysregulation which is crucial in Huntington pathogenies.

This report fingerprints metabolic shifts from OXPHOS to glycolysis in HD cells. In addition, it leads to transcriptional dysregulation in the nucleus which is important to understand in HD pathogenies studies and also for similar neurodegenerative diseases such as Alzheimer, Parkinson, ALS, and etc. Further investigations need be done to understand if different stages of inclusion formation or inclusions themselves uniquely alter redox state of the cells.

2.6. MATERIAL AND METHODS:

Cell cultures and transfection:

Human Embryonic Kidney cell 293(HEK293) plated on 3ug/ml fibronectin were plated with ~70% confluency and transfected overnight with Httex1p containing pcDNA with varying length of polyglutamine fused at C-terminus to EGFP(Httex1p 97Q-EGFP, Httex1p25Q -EGFP, and EGFP alone).

Confocal Imaging:

The EGFP tagged cells were visualized via confocal microscopy Zeiss LSM 710 confocal microscope (Carl Zeiss, Jena, Germany). Images are obtained with a 488nm argon-ion laser and imaged using the internal detectors using a filter 500-550nm. Using laser scanning confocal microscope, the fluorophore of the entire specimen was acquired and assigned a pseudo-color. Images are acquired using 63x oil objective.

FLIM set up :

Fluorescence lifetime imaging was acquired using the same Zeiss LSM 710 confocal microscope equipped with a Ti-Sapphire laser(Mai Tai Spectra-Physics, Newport, CA), using external detectors (H7422P-40, Hamamatsu Corporation, Bridgewater, New Jersey) and an ISS A320 FastFLIM (ISS, Champaign, IL) acquisition card.NADH fluorescence lifetime was measured at 2–photon excitation at 740 nm. A 495 nm long-pass filter used to separates the blue and the green fluorescence channel. The pure signal of NADH is detected with a blue filter (442/46nm) in one channel and EGFP emission with a green filter (520/35nm).

Images were acquired using 63X oil objective. Images were collected with 256x256 pixels with a minimum of 100 counts per pixel which requires at least integrating 30 frames with the pixel dwell time of 25.6 us/ pixel.The temperature was set at 37℃ throughout the experiment with 5% CO_2.

Data analysis:

The phasor analysis was performed using the method explained by Digman et al. [106] and analyzed with the SimFCS software available at (www.lfd.uci.edu). Briefly, for each pixel in an image, a phasor lifetime is plotted in a graph using Fourier transformation, we then use a cursor to highlight the cluster of points that corresponded to the lifetime in that range. Figure A1 in supplemental material schematically shows the transformation process to a single point in a 2D phasor plot. Phasor plot coordinates are G and S (x and y).

Statistical analysis:

We have used student's t-test with critical p-value set at 0.05 for our analysis. Total of 45 cells has been tested for in vitro study of HD. For the animal study, we have used a total of 15 animals and analyzed 149 ROI (N=30 for 25Q, N=32 for 120Q, N=27 for 96Q-EGFP, N=28 for Venus, N=32 for wildtype Canton-s).

Animal Study:

ELAV-GAL4 is used for constitutive expression of UAS transgene. Fly stock was cultured on cornmeal medium at 25 degrees (room temperature). Larvae in the late 3rd instar, instar refers to larvae stage, were selected and transferred into a petri dish with dissection buffer. Using forceps, the mouth hooks were pulled away from the rest of the body. The eye discs were dissected away from the rest of the tissue and immediately placed on a coverslip for imaging. In this experiment, we have used Unexpanded $90^{ex1\ 25Q}$, expanded $90^{ex1\ 96Q\text{-}EGFP}$ (a kind gift of T. Littleton), expanded $90^{ex1\ 120Q}$, and wild-type, Canton-S, with no HTT transfection and Venus as controls. In addition, we have verified our analysis by co-expressing Kaede expanded vs. unexpanded HTT($90^{ex1\ 25Q\text{-}Kaede}$ vs. $90^{ex1\ 120Q\text{-}Kaede}$) to further verify the NADH FLIM readings.

CHAPTER 3: LIPID ORDER AND MEMBRANE FLUIDITY

ALTERATION IN FLUIDITY OF CELL PLASMA MEMBRANE IN HUNTINGTON DISEASE REVEALED BY SPECTRAL PHASOR ANALYSIS[2]

3.1. ABSTRACT

Huntington disease (HD) is a late-onset genetic neurodegenerative disorder caused by expansion of cytosine-adenine-guanine (CAG) trinucleotide in the exon 1 of the gene encoding the polyglutamine (polyQ). It has been shown that protein degradation and lipid metabolism is altered in HD. In many neurodegenerative disorders, impaired lipid homeostasis is one of the early events in the disease onset. Yet, little is known about how mutant huntingtin may affect phospholipids membrane fluidity. Here, we investigated how membrane fluidity in the living cells (differentiated PC12 and HEK293 cell lines) are affected using a hyperspectral imaging of widely used probes, LAURDAN. Using phasor approach, we characterized the fluorescence of LAURDAN that is sensitive to the polarity of the immediate environment. LAURDAN is affected by the physical order of phospholipids (lipid order) and reports the membrane fluidity. We also validated our results using a different fluorescent membrane probe, Nile Red (NR). The plasma membrane in the cells expressing expanded polyQ shows a shift toward increased membrane fluidity revealed by both LAURDAN and NR spectral phasors. This finding brings a new perspective in the understanding of the early stages of HD that can be used as a target for drug screening.

[2] A version of this chapter was also published in nature scientific report [Sameni S, Malacrida L, Tan Z, Digman MA.
Alteration in fluidity of cell plasma membrane in Huntington disease revealed by spectral phasor Analysis.
Sci Rep. 2018; 8(1): 734. PMCID: PMC5768877]

3.2. INTRODUCTION

One of the common characteristics of neurodegenerative diseases is the aggregation of specific proteins that lead to deposits in tissue or subcellular compartments. This is commonly known as protein misfolding or conformational disorder in Alzheimer's disease (AD), Parkinson's disease (PD), Huntington disease (HD) and other neurodegenerative disorders [107]. HD is a progressive genetic neurodegenerative disorder with complex pathogenies including protein aggregation and dysregulation of lipid homeostasis. The key event in such pathologies is the conversion of protein to an abnormal conformation that may lead to the formation of toxic aggregates. In the case of HD, polyglutamine (PolyQ) aggregation is the hallmark of the disease. In the last decades, there has been an intense research effort to determine the toxicity of the aggregate species as protein aggregation progresses from monomeric to oligomeric and finally a mature inclusion[18, 108]. This understanding is relevant since there are currently no effective measures or treatments of HD. Recent research shows that metabolism is also affected as a result of HD and indicates disturbed OXPHOS pathway and a shift of the metabolism toward more free NADH as the disease progresses that implies a disruption of glucose uptake in HD cells compared to normal[109].

Besides glucose, lipid metabolism is also shown to be affected in HD and other neurodegenerative disorders[110-113]. Lipid and cholesterol are important cell plasma membrane components as they control normal cell function. In Alzheimer disease (AD), impaired lipid homeostasis is one of the early events in the disease [114]. The alteration in lipid composition can lead to instability in the membrane and synaptic loss in AD [113]. Furthermore, rising evidence indicates that altered lipid metabolism is linked to dysfunction in HD [110]. In particular, research in animal and human indicates that cholesterol metabolism is disturbed in

HD [37]. However, the specific alteration remains controversial. In normal condition, sterol regulatory element binding protein, SREBPs, regulate lipid homeostasis by sensing the level of cholesterol in the cell and provides negative feedback in synthesizing more cholesterol. Upon activation, SREBP acts as a transcriptional factor and stimulates expression of enzymes that regulate the fatty acid biosynthesis pathway [115]. Some evidence indicates up to 50% reduction in active SREBP in both HD cells and mouse brain tissue [37]. This can be implicated in HD pathogenesis by reduced biosynthesis of cholesterol and fatty acids. Other evidence also shows the slower growth of skin fibroblasts of HD patients compared to normal when they are treated with lipid deprived medium [110]. However, other studies suggest an accumulation of cholesterol as a result of dysfunction in the transport of cholesterol due to mutant huntingtin interaction with Caveolin-1(vesicles transporting cholesterol through membranes)[40].

Given that there is a perturbation in the biosynthesis of fatty acid or disruption of transport mechanisms of lipid in HD, in this paper we aim to address how membrane fluidity is affected in HD. For this characterization, we used two distinct fluorescent probes: LAURDAN and Nile Red. Both dyes are commonly used for membrane phase characterizations[116, 117]. These probes are sensitive to the polarity of the environment since their emission and lifetimes shift toward shorter wavelength and longer lifetime with decreasing solvent polarity [118-120].On the other hand, in the apolar solvents, the emission of these probes are blue shifted. LAURDAN, 6-dodecanyl-2-dimethylamino naphthalene, was first developed by Gregorio Weber [121]. It is a common dye used to study membrane fluidity defined as changes in the lipid order as it senses the water penetration into the membrane [122, 123]. Nile red (NR), 9-diethylamino-5H-benzo[alpha]phenoxazine-5-one, is another lipophilic stain that has been successfully used to label lipid droplets [124, 125], to characterize total lipid content [126], and also to study

membrane organization [127, 128]. NR is an uncharged red phenoxazine dye and its fluorescence emission is altered based on the immediate environmental properties and a change in the dipole moment upon excitation [129, 130].

We used aforementioned dyes and a powerful fit-free approach based on spectral shifts analyzed with the spectral phasor approach to mapping membrane fluidity in living cells as opposed to the traditional method using normalized ratio-metric assay known as generalized polarization, GP[131-133]. The method and technique presented here has the advantage of analyzing the fluorescently tagged cells and can detect the contribution of multi-components emissions compared to the GP approach. This method was used in two different cell lines, HEK 293 and differentiated PC12, where expanded polyQ HTT exon 1 was tagged with different fluorescent proteins (EGFP and mRuby). We detected membrane fluidity changes by the combining spectral phasor analysis and solvatochromic dyes related to liquid disordered (Ld) and liquid ordered (Lo) phases. Our analysis indicates increased membrane fluidity and shifts toward Ld phase when expanded polyQ was expressed. This approach can open up new frontiers to evaluate the efficacy of treatments in HD or other similar neurodegenerative disorders.

3.3. MATERIALS AND METHODS

Spectral image acquisition was achieved using the 32 channel QUASAR multispectral scanning module on the Zeiss LSM710 laser scanning microscope (Carl Zeiss, Jena, Germany) equipped with Ti: Sapphire laser (Spectra-Physics Mai Tai, Newport Beach, CA) and 63x NA 1.4 oil objective. For each experiment, cells were first visualized using either 488nm or 561nm excitation, with respective bandpass filters, to excite either green fluorescent protein (EGFP) or mRuby with the single channel PMT detector. For LAURDAN experiment, we used a 405nm

and 561 nm laser lines to excite LAURDAN and mRuby, respectively. Figure B1 shows a cartoon representation of LAURDAN in the membrane. Nile red was then used separately as a sensor to characterize membrane fluidity in the cells with EGFP labeled HTT protein stained with Nile Red (NR). We employed 2-photon (2-PE) excitation microscopy by setting the excitation wavelength to 950 nm to co-excite NR and EGFP. For all experiments, spectral images were acquired using the lambda mode 32 channels from 416 nm to 728 nm and a bandwidth of 9.78 nm. The frame resolution was set to 256x256 pixels and with a pixel dwell time of 12.61μs/pixel. All data were analyzed using SimFCS software available at (www.lfd.uci.edu). All cells were maintained at 37^{o}C and 5% CO_2 during imaging.

Spectral Phasor Plot and Linear Combination Rule:

Here we employed an elegant way to separate fluorescently tagged protein signal from LAURDAN signal in living cells using a fit-free spectral phasor analysis (Fig. 14).

Spectral phasor analysis is based on the Fourier transformation (shown in equation.1 and 2) of the fluorescence emission spectra (in this case wavelength range is 416 nm to 728 nm) obtained from at each pixel in the hyperspectral image using the 32 channels detector of the Zeiss LSM 710 [116, 120]. In the equations 1 and 2, I (λ) represents intensity at each spectral step, n is the harmonic number (1 for the data shown in this paper), L is the spectrum range (λ_{max}-λ_{min}):

$$G = \frac{\sum_\lambda I(\lambda) \cos(\frac{2\pi n\lambda}{L})}{\sum_\lambda I(\lambda)} \qquad \text{eq. 1}$$

$$S = \frac{\sum_\lambda I(\lambda) \sin(\frac{2\pi n\lambda}{L})}{\sum_\lambda I(\lambda)} \qquad \text{eq. 2}$$

By applying the spectral phasor transformation, we produce a polar plot with a single spot for each pixel. In this case, the emission spectra at each pixel are transformed into two parameters called G and S (a real and imaginary component of the Fourier transformation, see equation 1 and 2), and then plotted in a four-quadrant polar plot, called spectral phasor plot, as it shown in Fig.14B.

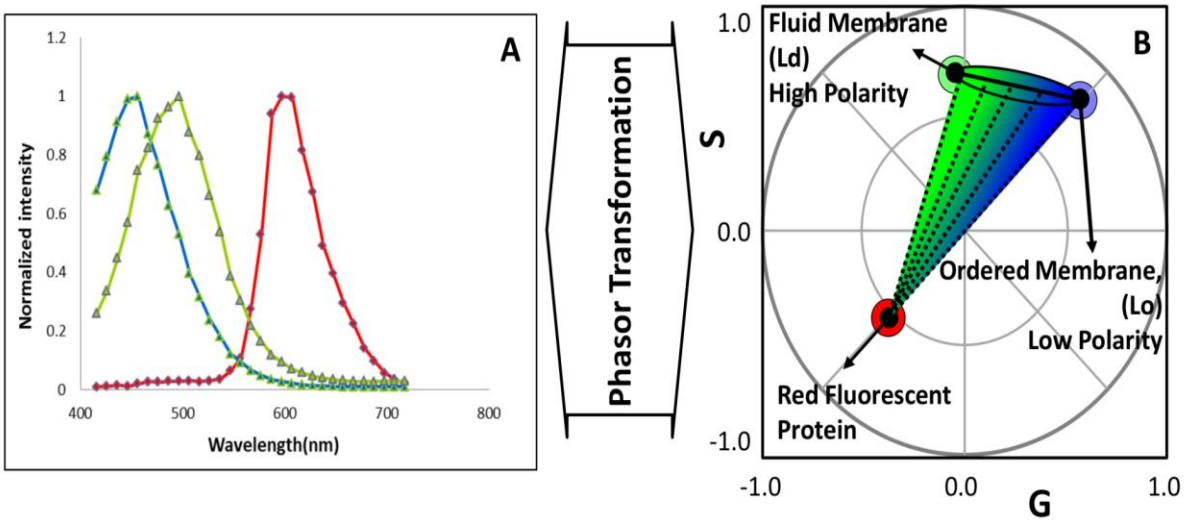

Figure 14: Spectral phasor transformation and the three-component analysis.

A) Three spectra for LAURDAN (in a low or high polarity environment, blue and green spectra respectively) and for a red fluorescence protein (RFP). B) The Phasor polar plot with the transformed spectral emissions and a single spot for the emission of LAURDAN in ordered membrane (Lo), fluid membrane (Ld) and a red fluorescent protein (RFP) (blue, green and red dots, respectively). The spectral longer wavelength shift is represented by a counterclockwise shift in the phasor plot from the coordinate (1,0).The spectra of the LAURDAN are shown in an ellipsoid in 1B which is colored in a gradient from green (high polarity environment) to blue (low polarity environment). If LAURDAN is coexisting with a RFP in the same pixel, then the pixels should fall in a dotted line shown in the picture connecting RFP to LAURDAN trajectory.

Using the phasor approach, we can resolve small spectral shifts on LAURDAN labeled cells that are induced due to changes in the membrane microenvironment even in the presence of fluorescent proteins. The phasor is calculated over a finite wavelength range. The position of the phasor coordinates will change if the emission spectra are truncated as shown in the emission spectral for (Lo and Ld) LAURDAN (Figure 14A). In the calculations of the Fourier transformation, we used spectra data of a specified wavelength range (416-728nm). Since all the data has the same wavelength emission range, the comparison between all the experiments is valid. However, if the wavelength emission range is changed the data are no longer comparable. More importantly, the rule of the linear combination of the phasors is not affected by the truncation

As it is depicted in Fig.14 B the LAURDAN spectral phasors are shown in an ellipsoid with color changing from blue to green that indicates a low or high polarity environment respectively. In cells stained with LAURDAN, if there is a third fluorescent component in the same pixel indicated by the red dot in figure 14B, the position of the phasor at that pixel should fall on the dashed lines that joins the LAURDAN trajectory and the fluorescent protein (in this case mRuby) which defines the linear combination. Using linear combination rule, we can resolve complex combinations and characterize membrane fluidity independent of the spectral contamination due to the other fluorescent labels or fluorescent proteins. In this case, blue indicates liquid-ordered membrane (Lo) with highly packed phospholipids, and a shift toward green indicates loosely packed liquid disordered (Ld) phase. The penetration of water molecules in the membrane directs the dipolar relaxation of the LAURDAN. Due to the complex deexcitation mechanism of LAURDAN, the spectral phasor analysis provides a better interpretation of fluorescence emission of LAURDAN at the membrane interface compared to

classical GP analysis. Note that the LAURDAN spectrum cannot be determined due to the dipolar relaxation effect so that spectral demixing methods cannot be applied in this situation. However, the phasor approach can separate the LAURDAN spectral position from the contribution of the fluorescent proteins by a simple graphical construction.

Sample Preparation:

The stabilized inducible cell model of HD previously established Htt14A2.6 PC12 cells, as well as newly generated PC12 cells that inducibly express HTT exon 1 containing either 25Q or 97Q repeat fused at C-terminus to EGFP or mRuby were propagated as previously described [134, 135]. For differentiation process, cells were supplemented with reduced levels of fetal bovine serum (FBS, 4% or lower) and plated on poly-L-lysine coated glass bottom dish. Neuronal differentiation was induced using 50 ng/ml NGF (Harlan Bioproducts for Science, Inc., Madison, WI) for 7-10 days. Cells were induced with 5 μM ponasterone A (PA) to induce expression of HTT exon fusion proteins 48 hours prior to the imaging.

HEK 293 (ATCC® CRL-1573™) cells were plated on 35mm glass bottom dish (MatTek, Ashland, MA) that was previously coated with 3ug/ml fibronectin. Cells were transfected overnight using Lipofectamine 2000 (Invitrogen, Carlsbad, CA) and according to manufacturer's protocol. Transfection was performed with Httex1p 97Q-EGFP, Httex1p25Q-EGFP (kindly provided by Thompson L.M., UC Irvine) or EGFP alone. Cells were then stained with 1 μM NR and incubated at 37 degrees for 5 to 10 min followed by imaging.

LAURDAN and NR were used at final concentration of 1.0 μM in the medium for the cell staining.

For cholesterol depletion study, first cells were grown to 70% confluency. Cholesterol was depleted by Methyl-beta-cyclodextrin (MβCD) extracts (Sigma). Cells medium were aspirated, and cells were treated with Opti-MEM™ I (ThermoFisher) Reduced-Serum Medium buffered with HEPES and total final concentration 10 mM of MβCD. Spectral images were then followed immediately by the treatments (every 2-5 min) for 45 min.

GUV preparation:

Giant unilamellar vesicles (GUVs) were prepared following the electroformation protocol described by Angelova et al [136]. Briefly, dioleylphosphatidycholine (DOPC) or dipalmitoilphosphatidylcholine: cholesterol (1:1 molar, DPPC:Chol) was prepared at a final concentration of 0.3 mM in chloroform. LAURDAN at 0.5 % molar was added to the lipid mixture in chloroform. Then, 4 μL of the organic mixture was applied to each platinum wire and dried under vacuum overnight. The electroformation chamber was filled with 300 μL of sucrose 200 mM at 50°C. To keep the temperature constant we used a circulation bath at 50°C. For the GUV growth, we applied a sinusoidal potential of 2 volts and 10 Hz during 1.5 hours. To detach the GUV from the wire, the frequency of the sinusoidal potential was reduced to 1 Hz for 10 min, and then the function generator and circulating bath were turned off. For the measurements, 50 ml of the GUVs dispersion were transferred to 8-wells bottom-glass imaging chamber containing 300μl of a 200 mM glucose solution. The imaging chamber was coated with 1 mg/ml bovine serum albumin (BSA) solution.

3.4. RESULTS:

LAURDAN Fluorescence

Figure 15 shows the range of LAURDAN fluorescence in DOPC representing Ld phase in the membrane (green vesicle) and DPPC: Cholesterol, 1:1 molar (blue vesicle) representing Lo phase in the membrane combined with RFP forming a theoretical triangle with the area of the green triangle indicating all possible linear combinations.

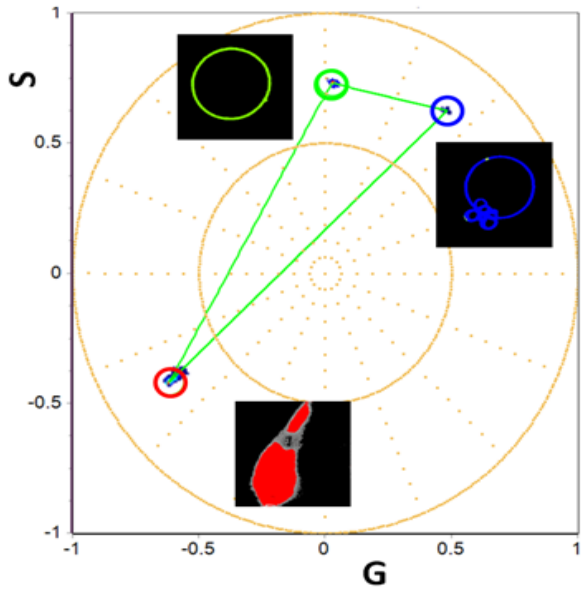

Figure 15: Three component analysis depicting LAURDAN fluorescence emission in Ld/Lo in GUVs and mRuby expressing cells (differentiated 97QmRuby).

The framework for the three-component analysis is done by defining the emission of LAURDAN in the liquid disorder (Ld, DOPC, green GUV) or liquid ordered (Lo, DPPC: Cholesterol, 1:1 molar, blue GUV) membranes, and cells expressing the 97Q-mRuby (cell colored by red cursor).

First, we identified the spectral phasor position for differentiated PC12 cells expressing 97Q-mRuby. Figure 16 A shows a zoomed in the region in the phasor plot selecting all the pixels, color-coded in pink, corresponding to the phasor position of a cell expressing mRuby. Next, we characterized membrane fluidity using the spectral phasor plot in differentiated PC12 cells stained with LAURDAN (Figure 16C; the average intensity of LAURDAN is shown in the inset image). In this case, we used blue and green cursors to identify low to high polar environments sensed by LAURDAN. Then we imaged differentiated PC12 cells expressing 97Q-mRuby

(Figure 16 D) to show the phasor position of LAURDAN emission in the presence of 97Q-mRuby. The position along the Lo to Ld phases are shown as a normalized histogram along the blue to the green trajectory (Figure 16 E & F). A hypothetical triangle is drawn to depict the combination of the possible lipid phase emissions of LAURDAN with the emission of mRuby.

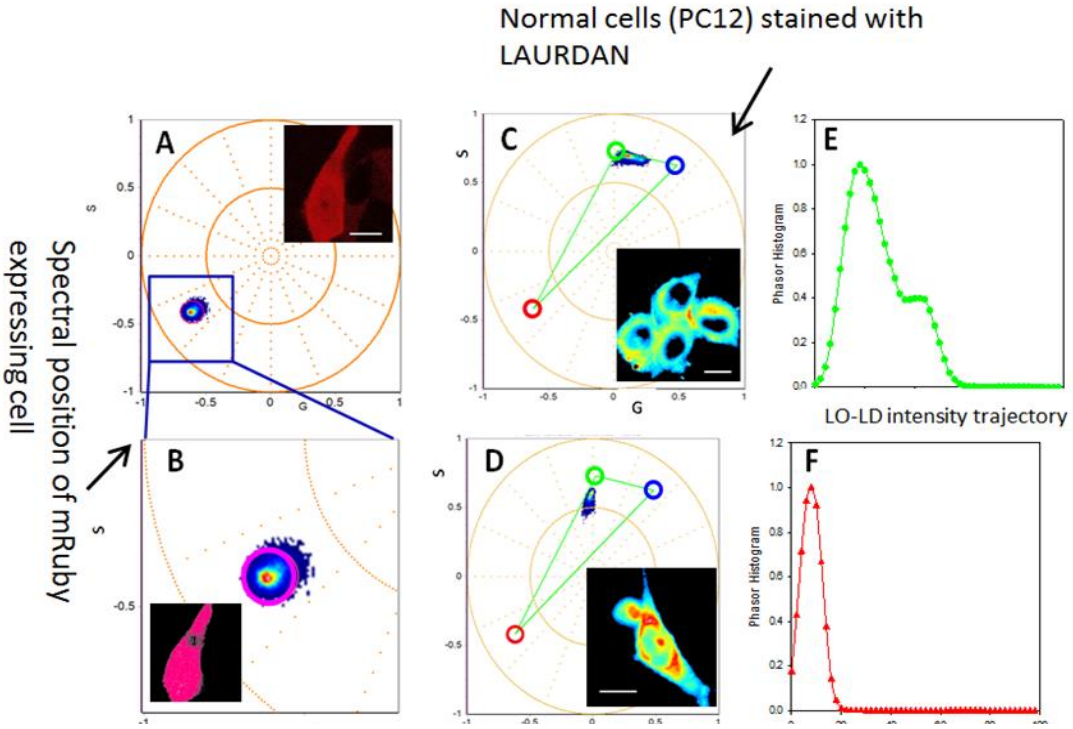

Figure 16: Phasor plot signature for PC12 cell stained with or without LAURDAN.

A) Zoomed region from the phasor plot in (B) showing a pink cursor highlighting the spectral emission of mRuby of a differentiated PC12 cells expressing 97Q-mRuby in the absence of LAURDAN. Using a pink cursor at the phasor plot we can color code the pixels at the spectral image (see pseudo color image on the top figure). C) Differentiated PC 12 cells stained with LAURDAN in the absence of mRuby with its correspondings fluidity fraction histogram shown in E. The histograms (E&F) indicate the position along the green/ trajectory that identifies the fluidity fraction. Here, green cursors means high and blue means low fluidity. D) Differentiated PC12 cells expressing 97Q-mRuby stained with LAURDAN. A trajectory representing all the linear combinations between LAURDAN and the 97Q-mRuby can be seen on the phasor plot. The spectra intensity image is provided on the right side of the spectral graph with the corresponding fluidity histogram shown on F. All Scale bars have a length of 10μm.

To characterize the cell plasma membrane fluidity, we either applied a threshold or cell mask to separate cell plasma membrane and background as it is shown in the supplemental material (Figure B2). Figure 17 shows the spectral phasors of differentiated PC12 cells stained with (A) LAURDAN alone, (B) expressing mRuby alone, (D) 97Q-mRuby stained with LAURDAN and (E) expressing mRuby stained with LAURDAN. On the corresponding phasor plot (Figure 17 C), the light green cursor identifies the liquid disorder (Ld) phase and the dark blue cursor highlights the liquid order (Lo) phase, both connecting to the red cursor (mRuby) to make the theoretical triangle, in gray, that encompasses all possible emission species.

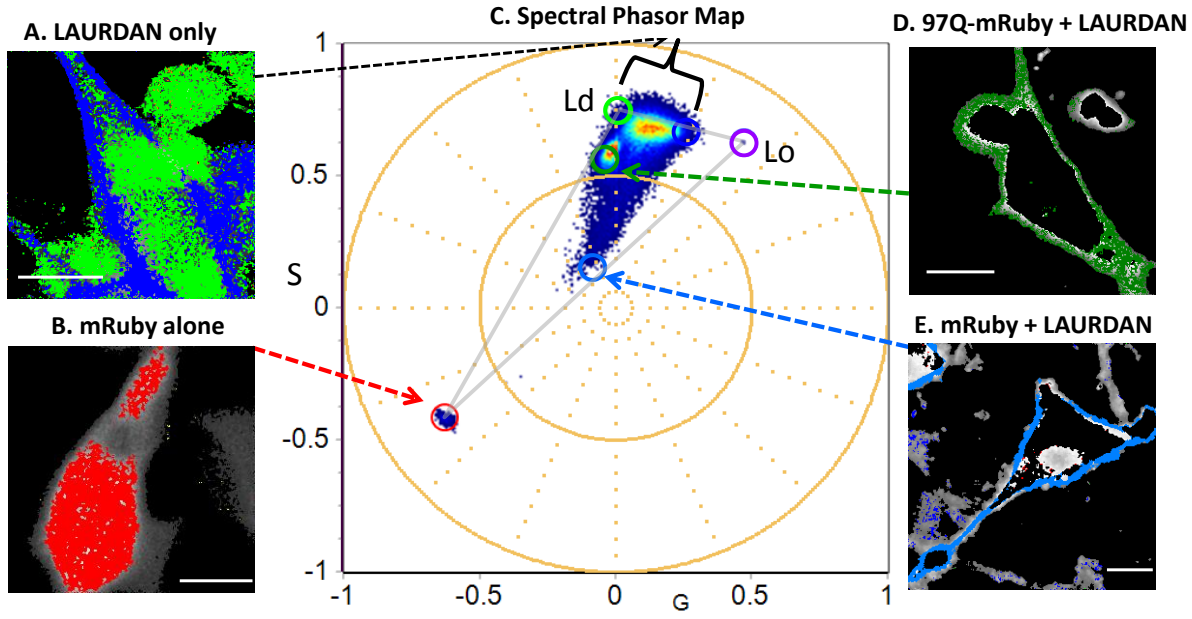

Figure 17: Mapping the emission spectra of LAURDAN and mRuby using spectral Phasor plot in differentiated PC12 cells.

A) Differentiated PC12 cells stained with LAURDAN alone are highlighted by the light green and dark blue cursors corresponding to the Ld and Lo phases, respectively. The Ld and Lo spectral emission coordinates were plotted from DOPC and DPPC GUVs (light green and purple cursors; respectively). B) Shows the red pseudo-color image of mRuby alone. C) Corresponding Spectral phasor plot is depicted here in which the light green (Ld) phase and the purple (Lo) phase are connected to the red cursor (mRuby) to make the theoretical triangle of the three pure emission peaks, in gray. As it is shown in D, 97Q-mRuby is characterized with increased fluidity in the membrane (shift to Ld phase, highlighted in dark green) compared to the controls (LAURDAN alone and mRuby+ LAURDAN, blue color, Lo phase). Scale bar in images is 10μm.

Figure 17A shows the pseudo-colored highlighted image of the PC12 cells stained with LAURDAN where the dark blue cursor in the spectral phasor plot highlights the pixels identifying the Lo phase and light green cursor highlights the Ld phase. Note that the cell membranes of PC12 cells are highly ordered (dark blue pixels) compared to the inner cellular compartment (light green pixels). As it is shown in Figure 17D, when we have 97Q-mRuby stained with LAURDAN, we observed a shift towards the liquid disorder phase (Ld) phase (highlighted with dark green pixels) compared to the controls (Fig. 17A&E). When we have both mRuby and LAURDAN presents, the spectral phasor coordinates are aligned in the triangle connecting the fractional contribution of LAURDAN with mRuby.

To further characterize the membrane stained with LAURDAN, we plotted the normalized histograms of the solid to fluid fractions in PC12 cell membranes along the line between green to the blue cursor (Figure 18).

When the phasor position of mRuby is presented together with LAURDAN, the mixture of the possible components will fall inside the theoretical triangle that connects the green/blue cursors and the red cursor. We defined the position along the green (Ld) and blue (Lo) trajectory as a fluidity fraction. Supplemental Figure B3 and B4 show the histogram of the fraction of solid to fluid phases on the membrane obtained in the differentiated PC12 cells(control line) and in differentiated PC12 cells expressing 97Q-mRuby, respectively.

Figure 18 summarizes the results obtained with LAURDAN. As it is depicted in this summary graph, the 97Q-mRuby histogram is shifted toward increased fluidity in the membrane (Ld phase) compared to the cells with LAURDAN alone and LAURDAN-mRuby (controls).

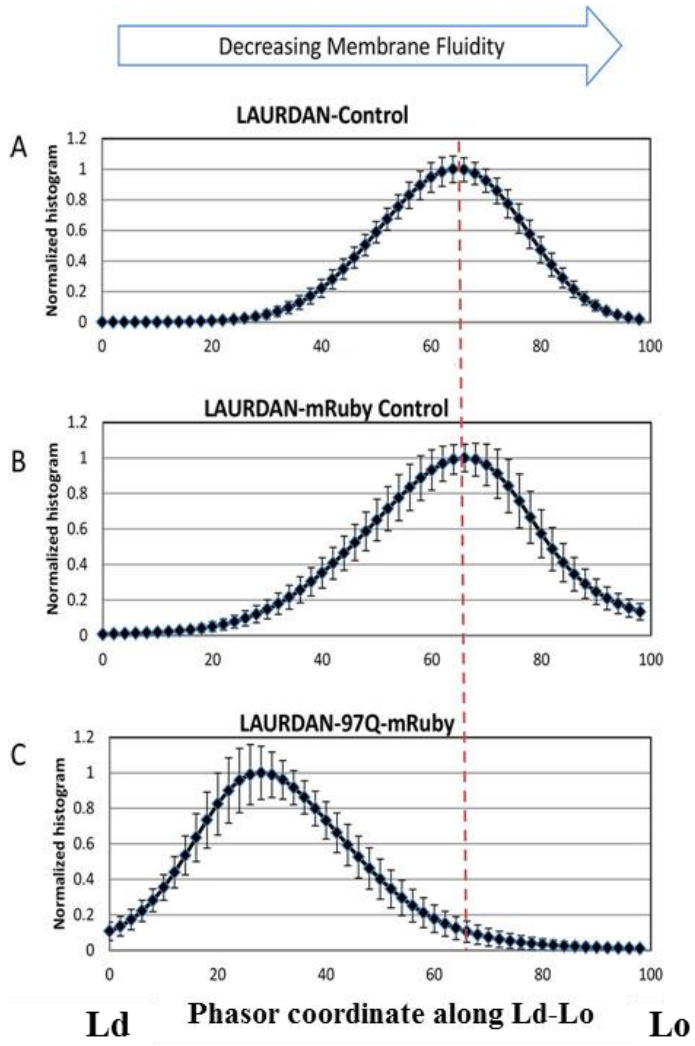

Figure 18: Normalized histograms of the solid to fluid fractions in PC12 cell membranes.

(A) Cells were stained with LAURDAN only. (B) PC12 cells expressing mRuby stained with LAURDAN. (C) Histogram of the solid to fluid fraction in cells expressing 97Q-mRuby stained with LAURDAN showing a shift toward increased membrane fluidity (Ld phase) compared to control lines(top two curves, A&B). Data are averaged for N=25 for LAURDAN-Control, N=19 for LAURDAN-mRuby-CTR, and N=16 for 97QmRuby, N= number of the cells, standard deviation are represented by error bars.

We have also further characterized the histograms shown in Figure 18 by analyzing the shift in the center of mass, termed it as fluidity index, where 0 corresponds to the extreme red spectrum (fluid) and 100 corresponds to the extreme blue emission (rigid). The axis is divided linearly according to the linear combination between the Lo and Ld phasor coordinates. Figure 19 shows

an increasing shift in membrane fluidity index for the membrane of PC12 cells expressing 97QmRuby.

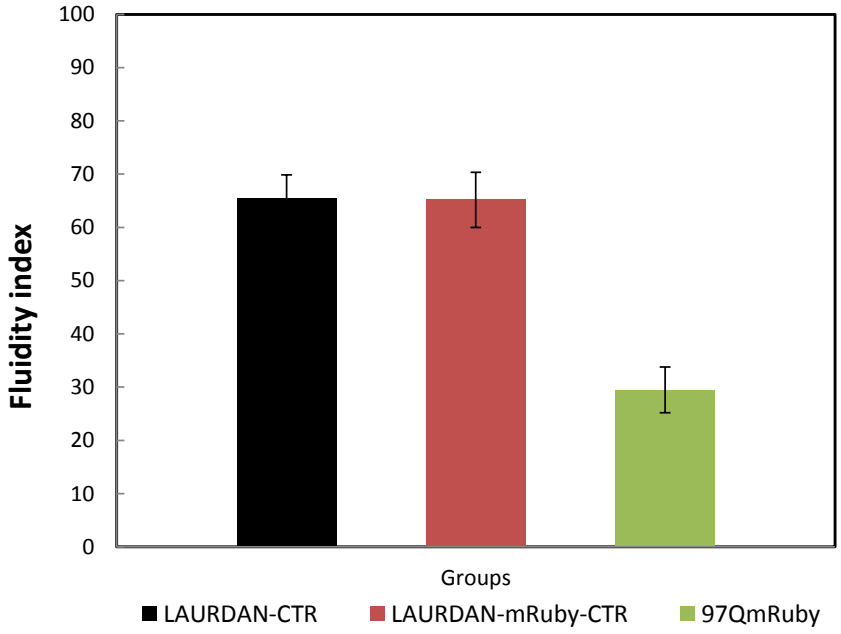

Figure 19: Fluidity index bar graph.

Cells expressing 97Q-mRuby have a decrease in membrane fluidity index indicating increased membrane fluidity compared to controls.

Nile Red Fluorescence:

To confirm if the expression of the 97Q was sufficient to cause a spectral shift in the plasma membrane, we expressed 97Q with EGFP and used another fluorescent probe, Nile Red, which has also shown to be sensitive to the polarity of the lipid environment. NR has an emission peak at 633nm in Phosphatidylcholine (PC) vesicles and emission spectra at 621nm in (1:1) PC: Cholesterol vesicles[125]. For the spectral analysis, we determined the fractional contribution of liquid-ordered (Lo) versus liquid disordered phases (Ld). The emission distribution in each pixel

in the image is color-coded with two different pseudo-colors within the phasor plot: yellow corresponding to low fluidity and blue corresponds to high fluidity in the membrane.

Similar to the experiment with LAURDAN, we applied linear combination properties of the phasor plot to characterize membrane fluidity. Supplemental Figures B5 and B6 display the condition when a green fluorescent protein with or without HTT is expressed in HEK293 cell (Fig. B5) and differentiated PC12 cells (Fig. B6). NR was used to stain the cell and characterize lipid order. In this situation, we identified the location of EGFP tagged protein in the spectral phasor, recognized by the cursor shown in green. Then, we calculated the fraction of the contributing pixels in the lines connecting the protein (green cursor) to the high/low polarity environment for the NR probe (cursors shown in blue and yellow, shown in Fig. B6). Supplemental Figure B5, confirm that HEK293 cells expressing 97Q-GFP are shifted toward blue in the yellow/blue trajectory that indicates increased membrane fluidity (Ld phase).

Similar results indicate a shift toward higher polarity sensed by NR in 97Q-GFP indicating fluid membrane in PC12 cells expressing 97Q-GFP compared to 25Q-GFP (control) (Supplemental Figure B6). Supplemental Figure B7 summarizes the results shown in a bar graph as a normalized fraction of color contribution obtained in this section. As it is shown in the bar graphs, control cells have a higher fraction of yellow color (Lo phase) indicating highly packed membrane. However, in the case of 97Q-GFP, we have a higher fraction of blue color (Ld phase) indicating the shift toward higher polarity and increased membrane fluidity.

Acute Cholesterol Depletion Influences Cell Membrane Fluidity:

To correlate the effect of polyQ on cholesterol depletion and modulation of the cell plasma membrane fluidity, cholesterol was depleted by methyl-beta-cyclodextrin (MβCD) extracts

(Supplemental Figure B8 and Figure B9). Cells were treated with 10 mM of MβCD that is well characterized to deplete cholesterol in the membrane[137]. The previous study indicates a decrease of up to 70% of cellular cholesterol when cells were treated with 10 mM of MβCD for 10 min[138]. Following the treatment with MβCD, we characterized the LAURDAN stained HEK293 and PC12 cells by spectral time-lapse imaging for 45 min. Similar to the shift we observed with 97Q, the shift in membrane fluidity was observed as early as 4 min in HEK293 cells and 2 min in PC12 cells indicated by a shift from a membrane fluidity index of ~70 to~15. Figure B8 and B9 summarize the results obtained here in terms of a shift in the fluidity histogram's center of mass analysis.

3.5. DISCUSSION:

While numerous studies indicate a reduction of cholesterol and biosynthesis of fatty acid in HD[37-39], other researchers show the interaction of mutant huntingtin with Cav-1, a major cholesterol transporter protein, which results in accumulation of cholesterol in neurons [40, 41]. Rising evidence also suggests the role of Huntingtin as a trafficking protein[139-141]. This suggests that there is a problem with the lipid homeostasis in HD. In this paper, we aimed to investigate possible modulation of cell membrane fluidity in HD. For this purpose, we used hyperspectral fluorescent microscopy together with the spectral phasor analysis. Two distinct fluorescent dyes (LAURDAN and NR) were used to characterize changes in the fluidity of plasma membrane of the cells affected by the expanded polyglutamine protein. LAURDAN, in particular, has been well characterized in the literature and shown to be sensitive to the lipid order phases due to the lipid composition and the amount of cholesterol present in the membranes[142, 143]. The shift we observed in membrane fluidity measured in the HD cells when expanded polyQ was expressed may reflect depletion of the cholesterol on the

membrane[144, 145]. We have further verified this by depleting the cholesterol in cells using MβCD. The results show a sharp shift in emission spectra of LAURDAN towards a longer wavelength. This suggests that there may be a possible correlation between the aggregated state of expanded polyQ and its lipid interaction at the membrane. Further studies in this area will need to be done to elucidate the role of the expanded huntingtin protein and cholesterol regulation.

Our results show a clear shift in membrane fluidity of HD cells from a highly packed membrane, liquid-ordered, to the loosely packed membrane, liquid disordered phase. This shift in fluidity may be implicated in HD pathogenesis, and can also be reconciled with following observations: First, research indicates morphological and mechanical changes in the synthetic lipid membrane due to the interaction of huntingtin aggregates with the membrane [146]. This implies that that physical interaction of huntingtin aggregates can contribute to the membrane fluidity of the cells. Second, the cytotoxic entities of polyQ aggregates that are not eliminated from the cell can influence the cell membrane. It has been shown that dysregulation of fatty acids disrupts autophagy in the cell, the lysosomal degradation pathway essential for cell survival [147]. This is important as autophagic failure is the hallmark of HD and other neurodegenerative diseases [148]. Failure to induce autophagosome in HD allows for the accumulation of the polyQ aggregate forming many toxic small aggregates and large insoluble inclusions that can affect cell membrane. Finally, modulation of fatty acid can directly modify the structure of the lipid membrane and alter micro-domain structure and organization that can be the origin of altered cell signaling [149]. Not surprisingly, alteration of endocannabinoids (eCBS), a powerful regulator of synaptic function signaling has been reported in Huntington disease and other similar neurodegenerative diseases, and it is also believed that this altered eCBs signaling is due to

changes in the cell membrane environment with research focused on therapeutic drugs to modulate the eCBs activity [150, 151]. Together, our measurements on the fluidity properties of membranes in HD cells shows for the first time that expanded polyQ results in an increased membrane fluidity which can influence other membrane properties such as lipid domain sequestering, ion transport, receptor dynamics, cell to cell contact, and membrane trafficking[152-154].

The methodologies described in this paper can be used as a platform for better understating of HD and similar neurodegenerative disorders. It also provides a powerful mean to characterize small changes in the membrane microenvironment. This study demonstrates that changes in membrane fluidity can be used as a biomarker for Huntingtin Disease. In addition, the spectral phasors presented in this article, can also rapidly and non-invasively screen for the efficacy of lipid membrane therapies.

3.6. CONCLUSION:

Cell membrane degradation and defects in membrane trafficking is the hallmark of many neurodegenerative diseases. Here, we have characterized the fluidity in the cell plasma membrane of the HD cells using two distinct membrane probes: LAURDAN and NR in conjunction with spectral phasor analysis. Our investigations indicate an alteration in plasma membrane homeostasis that is relevant as it can play a role in cell death, and also can affect control mechanism of ions and molecular transport. We observed a sharp shift using spectral phasor analysis in LAURDAN emission toward longer wavelength indicating increased fluid membrane in HD in both HEK 293 cells and differentiated PC12 cells. As previously discussed, increased membrane fluidity observed here can be related to the observation due to alteration of

biosynthesis of fatty acid or disruption of the transport mechanism of lipid in HD. In addition, mHTT toxicity through physical or biochemical means can also result in the cell membrane defects reported here. Such alternation in membrane fluidity can be used as an HD biomarker and also for future drug discovery.

CHAPTER 4: CLINICAL RELEVANCE

HD IS TRANSMISSIBLE VIA HTT INCLUSIONS PROPAGATION IN MAMMALIAN CELLS

4.1 INTRODUCTION

Huntington disease and other similar neurodegenerative diseases like Parkinson, Alzheimer etc. are characterized by misfolding of protein to its not native conformation which leads to aggregations. In the case of Huntington disease PolyQ aggregation is the hallmark of the disease, and one of the neurophysiological symptoms of such pathology.

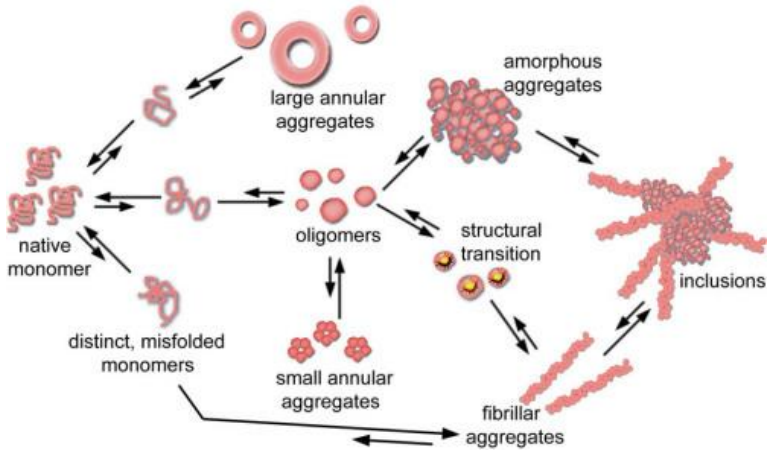

Figure 20: PolyQ aggregations process.

Here the schematic shows how native monomer get to the larger aggregates and form oligomers and other amorphous aggregates and finally form solid structure inclusions [155]

Protein aggregation process progress from misfolded monomer to oligomeric and finally mature fibril like inclusion as it is depicted in Fig.20. While some studies found and argue that the aggregate are toxic to the cell others argue the opposite. In particular soluble form of oligomer have reported as a proteotoxic [156].Yang et al also reported that aggregated polyQ delivered to the nucleus are considered toxic[157].In addition formation of aggregates into IB, inclusions

bodies can trigger other effects: example includes transcriptional dysregulation[158], disruption of normal synaptic transition, and proteasome, a protein complex in charge of clearance mechanism in the cells, impairment[159]that can all affect cell survival. However, other studies argue that the formation of IB reduces the level of toxic diffuse polyQ mutant Htt and thus the risk of neuronal death. So in that sense, IB formation is considered as a new adaptive state of the cells [18, 22].Interestingly, the study also found that when IBs form, there is also smaller fiber like aggregates species presents(example shown in Fig. 21)[160].

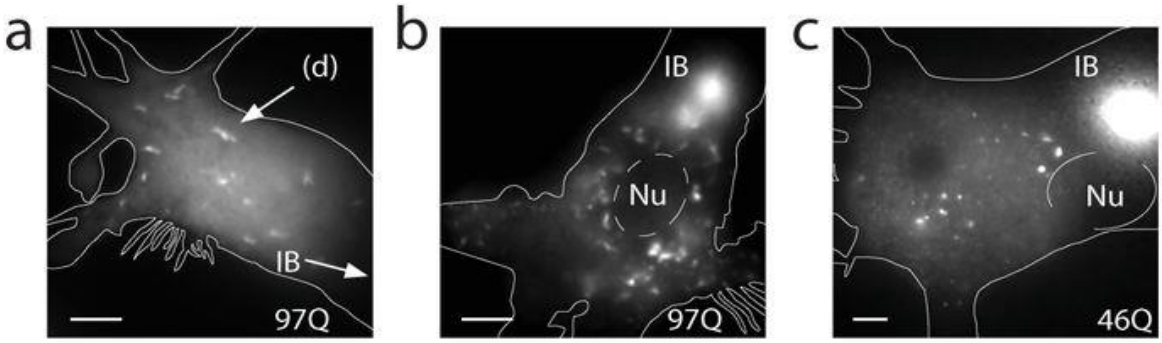

Figure 21: 16 hours post-transfection shows the spread of aggregates thought the cell bodies for 46Q and 97Q.

These images were obtained using super-resolution microscopy and after photobleaching the IB to reduce the brightness that makes the smaller aggregates evident. Adapted based on Sahl et al[160].

So based on the earlier studies, it turns out that there is an early stage of aggregations in which soluble aggregates are cytotoxic to the cells and can affect the cell survival directly and later with the formation of the IBs, smaller fiber like aggregates might be reduced which can affect the cell toxicity; however, these inclusions can disrupt cell normal function leading to the cell death. Recently, it was also found that both forms of aggregation can lead to the cell death. The only difference is that the soluble mutant aggregate trigger apoptosis while the mature inclusions will lead to delayed necrosis[161].

Based on these new understating, now the burning question is that how does the disease propagate. For this purpose, a better understanding of the transfer of these aggregates at the single cell level is crucial. The goal of this chapter is to first speculate the transmissibility of HD at the cellular level. And if such confirmed, determine if this can be done in a passive versus active manner.

4.2. BACKGROUND:

Tunneling nanotube (TNT) has been the focus of many studies in the past decade and became apparent as a fundamental mechanism of the cell to cell communication [162, 163]. This thin tubular structure shows to facilities selective transfer of membrane vesicles and organelles between cells[164]. As an example report indicates that for TNT is essential for the regulation of osteoclastogeneist[165](Fig 22).

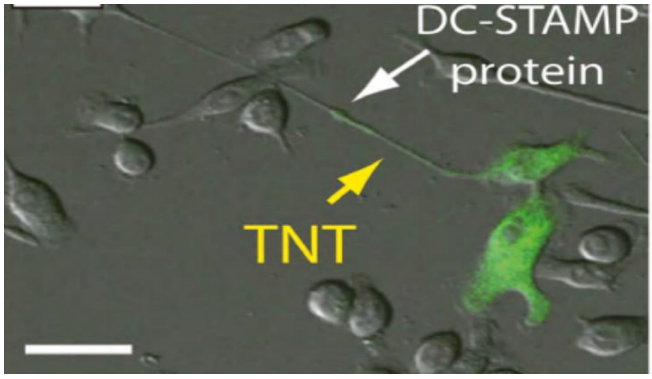

Figure 22: Confocal micrographs showing DC-STAMP along lipid tubes.

This is a key protein which is associated with osteoclastogenesis (bone resorption) that are migrating along a TNT(a tunneling nanotube). Scale 20 µm[165].

A recent study also suggests the possibility of aggregates relocation via TNT. Nanotube has been demonstrated to be involved in prion spreading[166]. Other studies also suggest the spread of pathology from host tissue to the graft in Parkinson's disease (PD)[167, 168].

These emerging evidence suggest the role of TNT in addition to the classically known intrinsic characteristics of neurons like gene expression profile, in the determination of the vulnerability to degeneration in these disorders.

Recently, there is a growing debate about the possible transfer of aggregations/inclusions and whether it can propagate via the passive or active mechanism. Ren et al. following by Yang et al showed that synthetic polyQ can be uptaken by mammalian cells[157, 169]. However, cell to cell transmission of polyQ showed to be in inefficient in non- neuronal cells[169]. This study suggests that the aggregates are released in a passive manner from dead cells that can be uptaken by healthy cells. In a newer study, however, Costanzo et al. argue that they did not detect any dead cell 48 hrs post transfection indicating that the aggregate transfer is active and can occur efficiently between intact cell at an early stage post transfection[170].And contradictory to the previous research, when supernatant of normal cells was replaced with infected cells, no aggregates were found on normal cells. And thus it was concluded that the direct cell to cell contact is required for transfer of aggregate and secretion is not the main transfer mechanism.

Here we sought to clarify the current debate and further determine if A) transfer of HTT large inclusion is possible and can occur through cell- cell contact (ex. through TNT), active transfer B) if secretion in the culture media in both synthetic and natural inclusions can be taken up by different compartment of the cells (i.e nucleolus and cytoplasm), passive transfer and c) to gain better understating if HD inclusions can be transferred between neuronal and non-neuronal cells and to gain better knowledge of normal and infected cell interactions.

4.3. METHOD AND DESIGN:

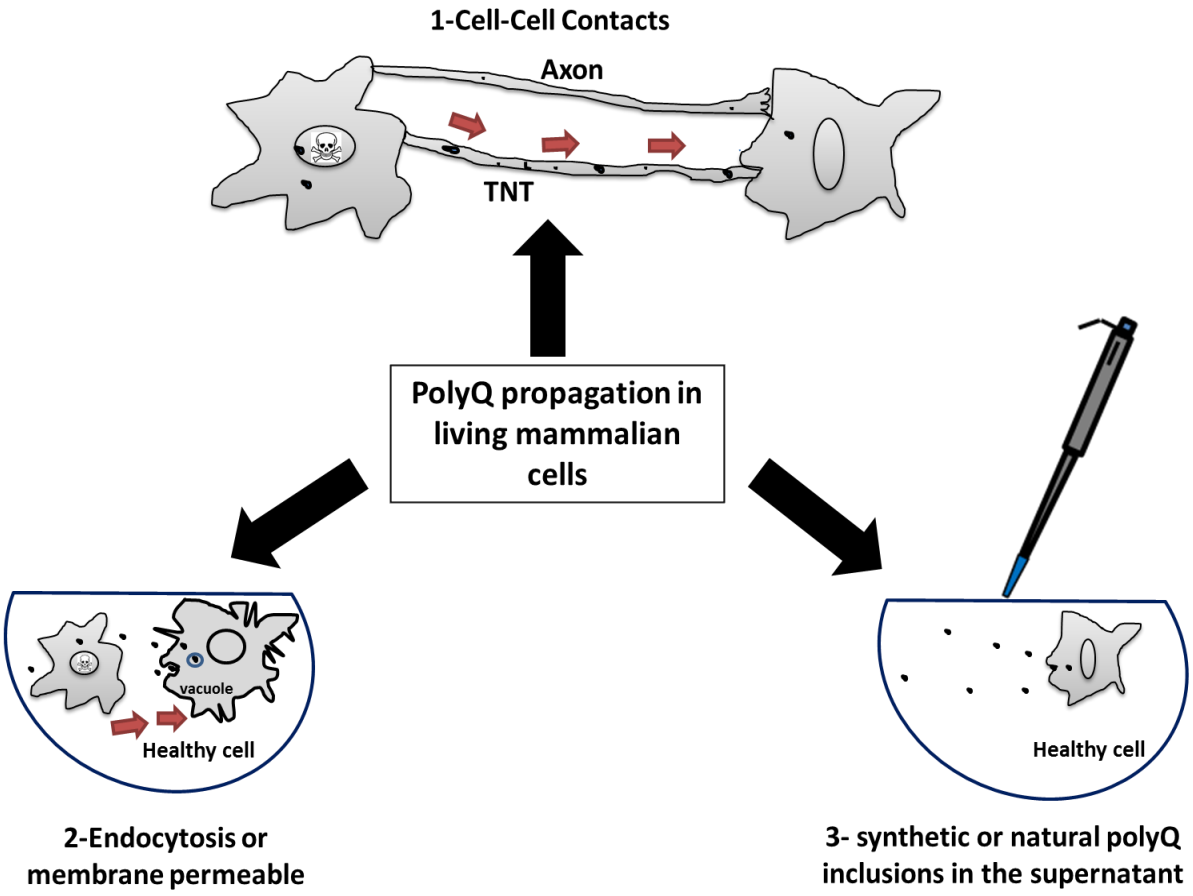

Figure 23: Hypothesized images of polyQ aggregations in living mammalian cells

Here we have tested the transfer of polyglutamine aggregates via three main possible methods (Fig. 23): transfer via lipid tube /axon in live mammalian cells (A), in addition we have further confirmed the penetration of both synthetic and natural polyQ aggregates by cells uptake (B) and finally we have characterized the propagation of polyQ homopolymer from infected cells to normal cells by cell to cell contacts(C).

Aggregates preparation:

Synthetic polyglutamine homopolymers (Q40 tagged Cyan) was obtained as a generous gift from Charles G. Glabe lab- UC Irvine. 4 ul of the synthetic homopolymer solution was added to 1.5 ml of cell media. Cells that were plated for imaging and treated with synthetic homopolymer were incubated overnight at 37 ℃.

To obtained natural aggregates, inducible Htt14A2.6 PC12 cells were first treated with 5 μM ponasterone A (PA) to induce the expression of with 97Q-GFP. Following the expression of 97Q-GFP, the supernatant was aspirated. To ensure that there are no viable cells in the media, the supernatant was centrifuged for 10 min with G= 45000 rpm to lyse any possible cells.

Co-culture study:

HEK293 cells were cultured on 6 well plate to 70 % confluency. Cells were transfected overnight using Lipofectamine 2000 (Invitrogen, Carlsbad, CA) and according to manufacturer's protocol. Transfection was performed with Httex1p 97Q-EGFP , Httex1p25Q-mRuby, Httex1p25Q-EGFP for 5- 20 hours. We found 5 hours to be efficient for polyQ expression in the cells. Cells of interested then were washed with PBS and trypsinized and planted together on 35mm glass bottom dish (MatTek, Ashland, MA) that was previously coated with 3ug/ml fibronectin and co-culture for 4-16 hours. Time-lapse imaging was then followed to track the inclusions transfer and uptake in live mammalian cells. Figure 24 shows the generic schematic of the co-culture study.

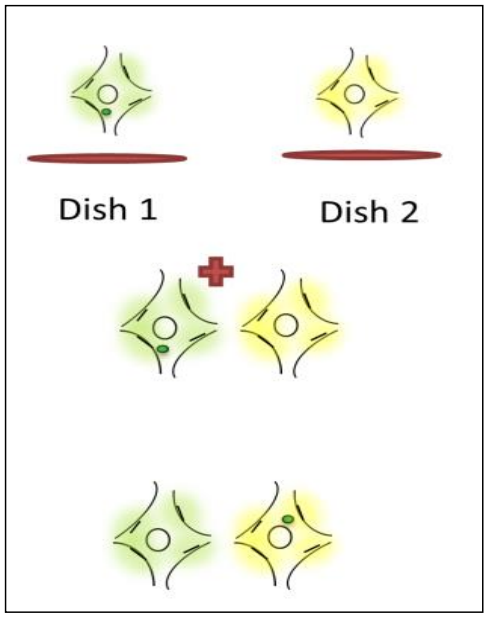

Figure 24: Hypothesized schematic showing translocation of inclusions between co-cultured cells

Microscopy:

Mammalian cells were imaged using confocal microscopy Zeiss LSM 710 confocal microscope (Carl Zeiss, Jena, Germany). The sample was excited with 488nm for EGFP and 561 nm for mRuby excitation. The GFP emission was then collected in 500nm-550nm channel while the emission of mRuby was assigned to 607nm-683 nm channel. Using laser scanning confocal microscope, the fluorophore of the entire specimen was acquired. Images are acquired using 63x oil objective.

4.4. RESULTS:

Transfer via TNT/ axon:

We observed the active transfer of polyQ natural inclusions via TNT and axon in primary rat hippocampal neurons. Figure 25 shows an example of 4 different images obtained from primary neurons transfected with 97Q-EGFP. As it is shown here inclusion is transferred in both axon and tunneling nanotubes.

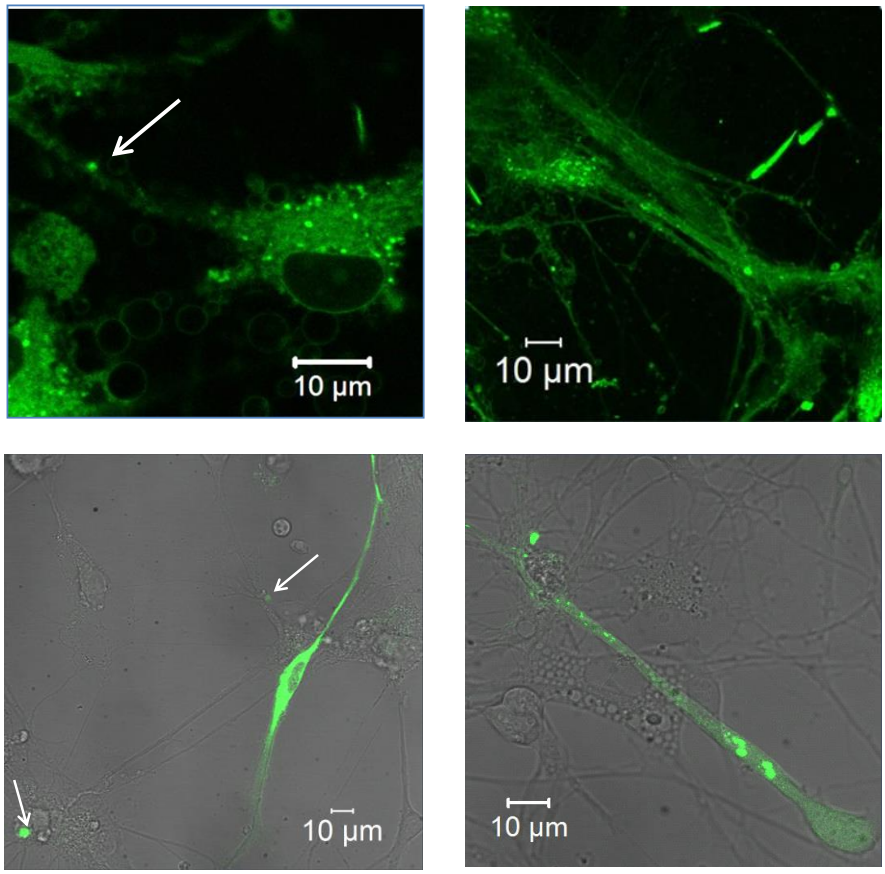

Figure 25:
Live primary neuron imaging indicates Transfer of polyQ inclusions between Rat primary hippocampal neurons expressing 97Q-EGFP

Top two images in figure 25 show the FITC and the locations of inclusions and active transfer through axon. On the bottom images, FITC and bright field are merged to better depict axon and nanotubes. As it is shown in the bottom left corner images inclusion are transferring through

TNT while the bottom right image shows a lot of inclusions transferring via axon. We observed that 71 percent of neurons after transfection with 97QEGP are expressed with some aggregates in the cells. In addition, our results show that about 37 percent of these cells can actively transfer these aggregates between cells as it is shown in figure 25. The graph shown in figure 26 summarizes these results.

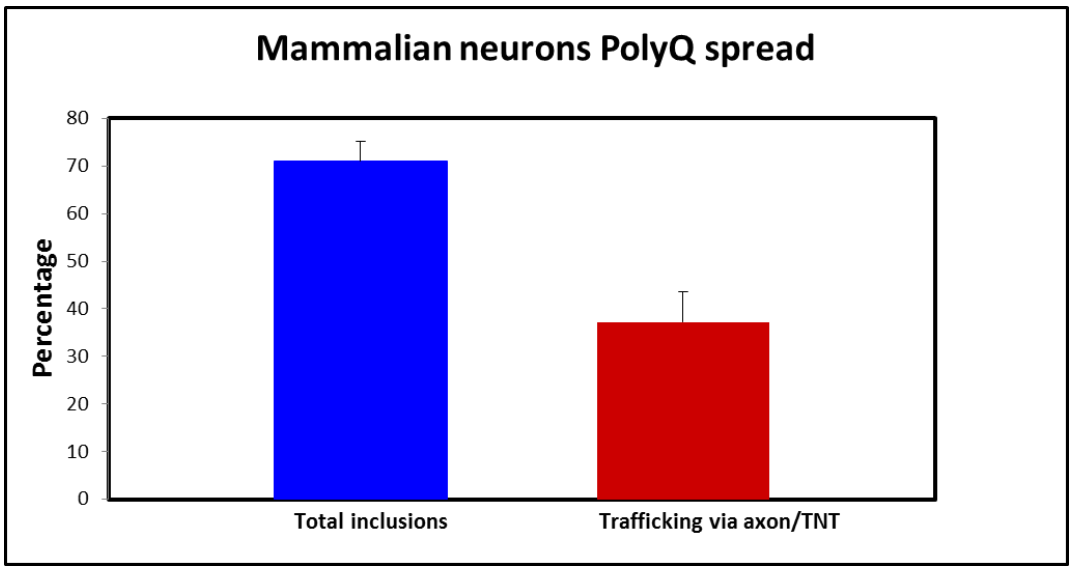

Figure 26: Mammalian neurons PolyQ transfer bar graph.

The graph here shows the percent aggregations in rat hippocampal neurons expressed with 97Q-EGFP as well as the ability of the neurons to actively transfer these aggregates via TNT/Axonal connections(N=38).

Here we have shown that in contrast to the study done by Ren et al[169] which relies on the dead cells(lysed cells) to release aggregates to be taken up by neighboring cells, we believe mammalian cells can actively transfer the aggregates and inclusions between cells. And thus this process doesn't necessarily require the cells to die to release these aggregates.

In addition, similar to neurons, we observed transfer between inducible differentiated PC12 cells expressing 97Q-mRuby. As it is shown in figure 27, polyQ homopolymers are actively transferring through axon between differentiated PC12 cells that are expressed with 97QmRuby.

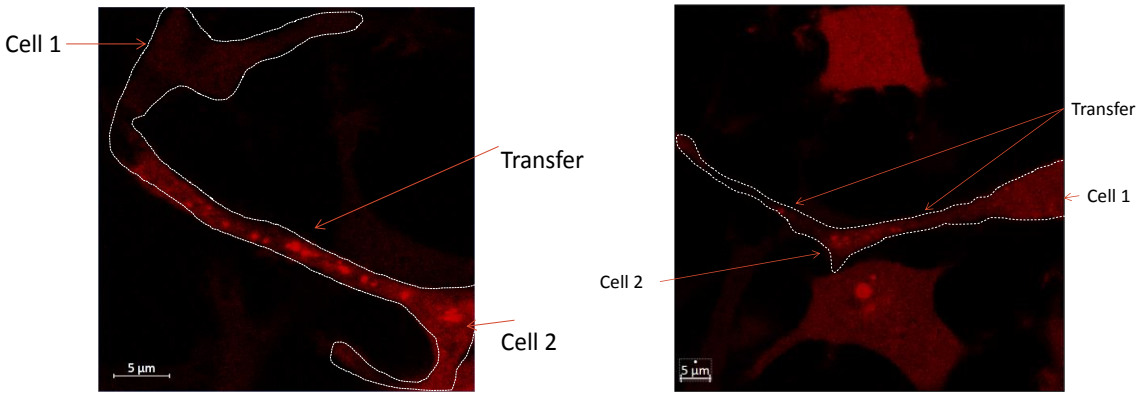

Figure 27: Live cell imaging of differentiated PC12 cells expressing 97Q-mRuby.

Images indicate the cell-cell trafficking of polyQ inclusions between differentiated PC12 cells.

Cellular uptake of Inclusions:

In this section, we have focused on the ability of the cellular uptake of both synthetic and natural polyQ. Our results in both HEK293 (Fig. 28) cells and primary rat neurons (Fig 29) indicates that cells are able to uptake Synthetic polyglutamine homopolymers (Q40 tagged Cyan) when it was presented in their medium.

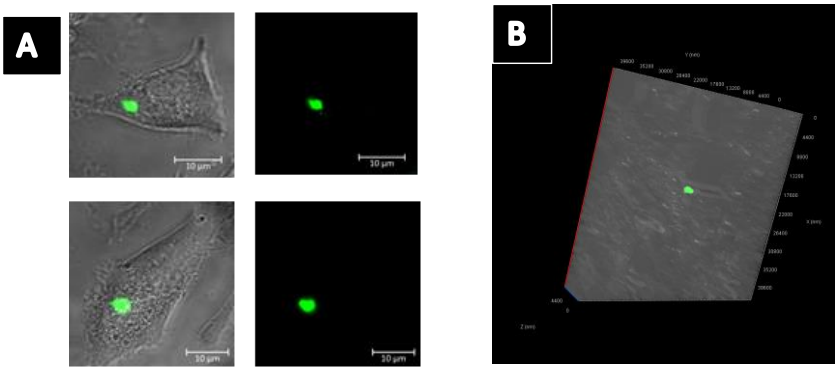

Figure 28: Uptake of Cy3Q40 seeds by HEK293 cells.

A) 2D images of HEK 293 cells with cy3q40 homopolymer shown in green. B) 3D of HEK293 cells further confirmed the uptake of synthetic inclusions.

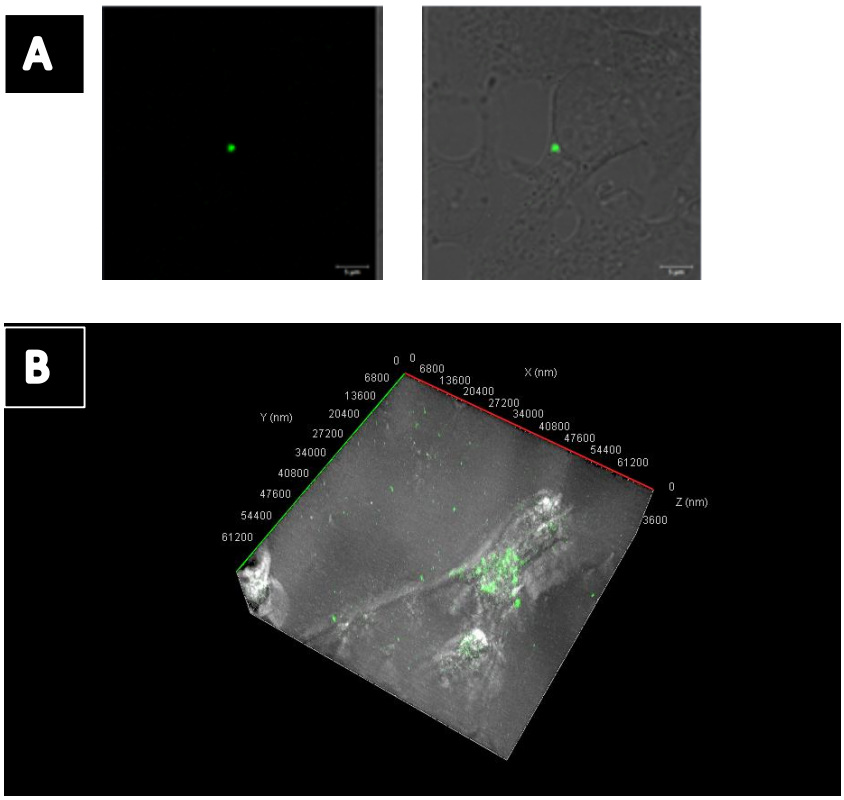

Figure 29: Uptake of synthetic Cy3Q40 seeds by hippocampal neurons.

A) 2D images of hippocampal neurons with cy3q40 homopolymer shown in green. B) 3D images hippocampal neurons further confirmed the uptake of synthetic inclusions

Next, we evaluated the cellular ability of inclusion uptake when natural inclusions were presented in the supernatant. For this purpose after expression of 97Qgfp on PC12 cells, the cell supernatant was aspirated and further process to ensure there are no living cells. After evaluating the supernatant of infected 97QGFP cells and processing it as it is explained in the method section, the medium of healthy HEK293 cells was exchanged with the infected supernatant. Our result here, show that cells are capable of up taking the natural inclusions even without any contacts with infected cells and just by the contact with infected supernatant (Fig 30).

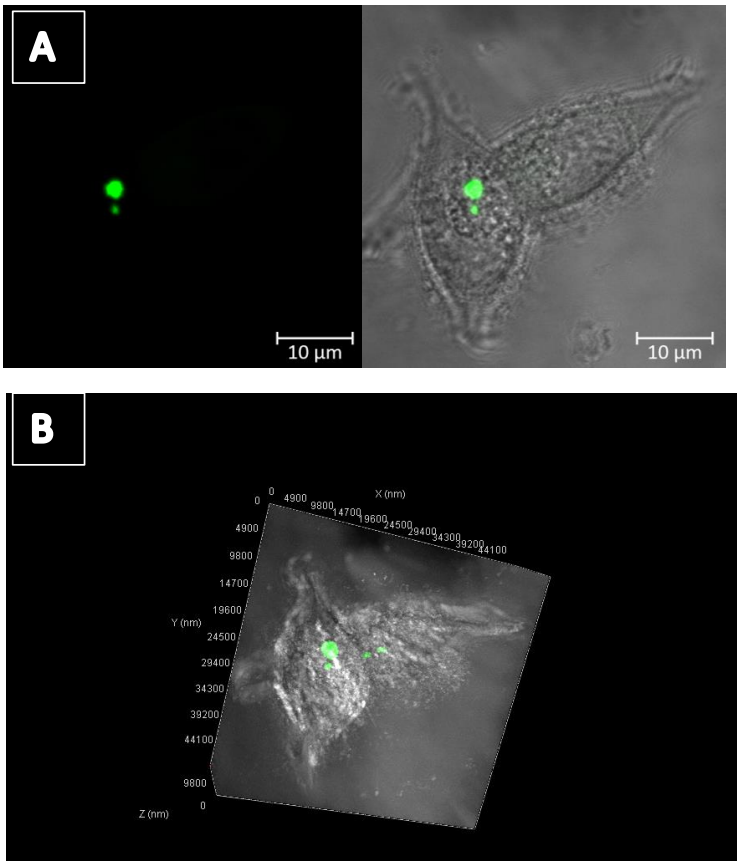

Figure 30: Cellular uptake of natural inclusion.

Example showing the uptake of natural polyQ inclusion when Healthy HEK293 cells were in contact with infected supernatant of pc 12 expressing 97Q- GFP

We have also evaluated cell-cell contacts and possible propagation of polyQ inclusion in healthy mammalians cells. For this purpose, we co-cultured HEK293 cells with Rat hippocampal cells. In this experiment, neurons were stained with Nile Red (Red) to further distinguish them from other cells. Our results indicate that HEK293 cells expressing 97Q-EGFP were able to release their inclusions to the medium that were uptaken by rat neurons. Figure 31 shows an example of the polyQ homopolymer transfer between neuronal and non-neuronal co-cultured mammalian cells.

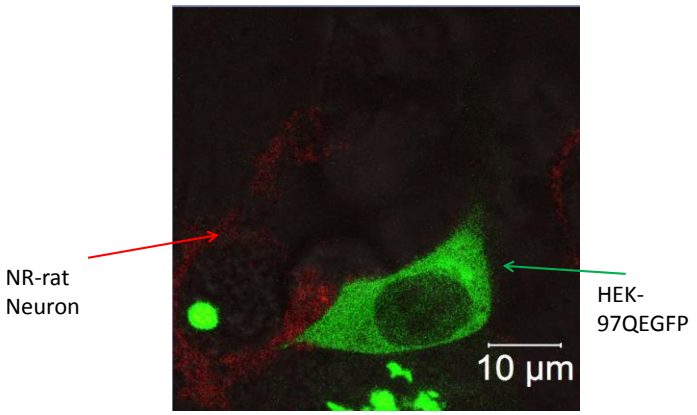

Figure 31: Live mammalian cells imaging shows the transfer of polyQ between HEK 293 and Rat hippocampal neurons.

Mammalian cells are co-cultured together. As it is shown here the Rat neuron stained with Nile Red has up taken a large inclusion from HEK 293-97QEGFP cell.

In addition and beside the transfer of inclusions we observed that 97QEGFP cells can penetrate through neurons by making protrusion as it is shown in figure 32.

So based our studies, the cells infected with extended polyQ(i.e 97Q) can not only release their inclusions that can be uptaken by other normal cells, they are also capable of making protrusion in the normal cells. This is particularity important when studying the pathogenesis of neurodegenerative diseases like Huntington disease as the infected cells can translocate their inclusions and protrude the uninfected neighboring cells.

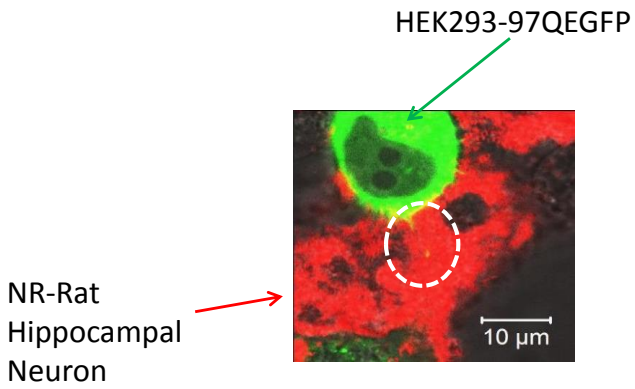

Figure 32: HEK293 cells infected with 97Q-EGFP invading the uninfected rat hippocampal neurons by making protrusion.

The dotted white circle shows the location of the protrusion inserted by HEK cell into a neuron.

The summary graph shown in Figure 33 shows the percentage of aggregation in infected non-neuronal cells as well as translocation of aggregate to uninfected neuronal cells in the co-cultured study.

To further investigate the aggregations and propagation of polyQ aggregates from infected to uninfected cells that are potentially relevant to pathogenies of neurodegenerative diseases we have further evaluated the co-culture live mammalian cells in a time-lapse series imaging. Figure 34 shows an example of HEK293 cells expressed with 25Q mCherry co-cultured with HEK293 cells expressed with 97Q-EGFP. Here cells were followed for about 4 hours and images were acquired for every 10 minutes interval.

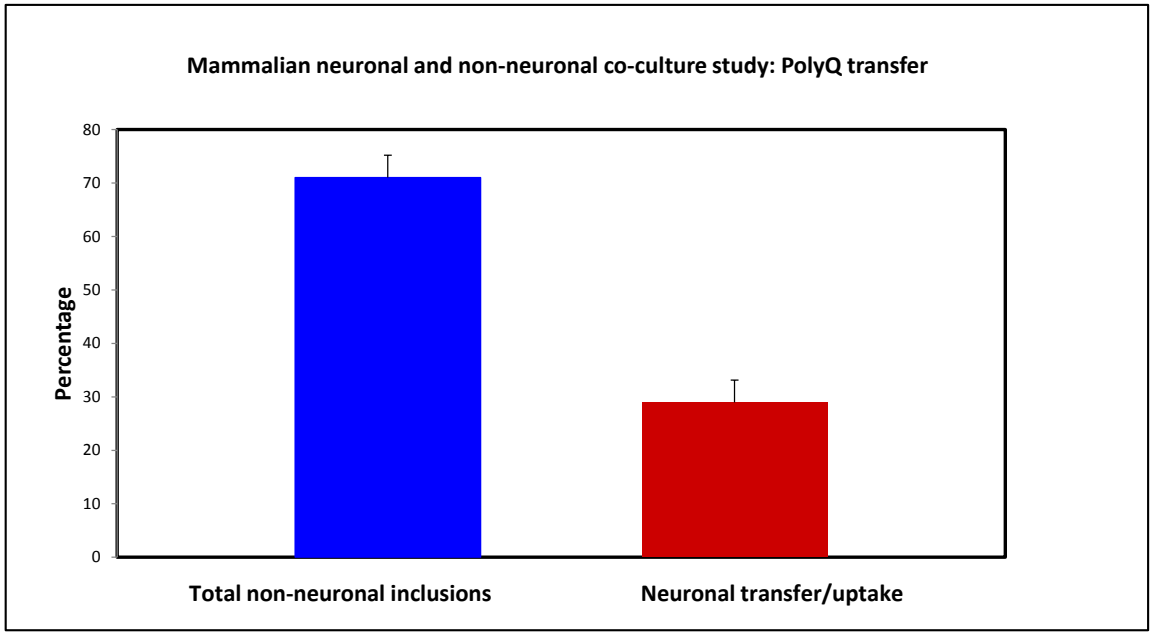

Figure 33: A summary graph showing the percent inclusions formation in non-neuronal cells infected with 97Q-EGFP and the propagation of polyQ inclusions to normal neighboring neuronal cells (N= 17 transfected cells & N=15 normal cells).

Two interesting phenomena is happening in this case. First, the uninfected cell is interacting with the invading infected cell that is completely pushed away during our imaging window. Second, the normal cell is taking up inclusions that are completely internalized during our imaging period as it shown in figure 34 and during about 3 hours imaging.

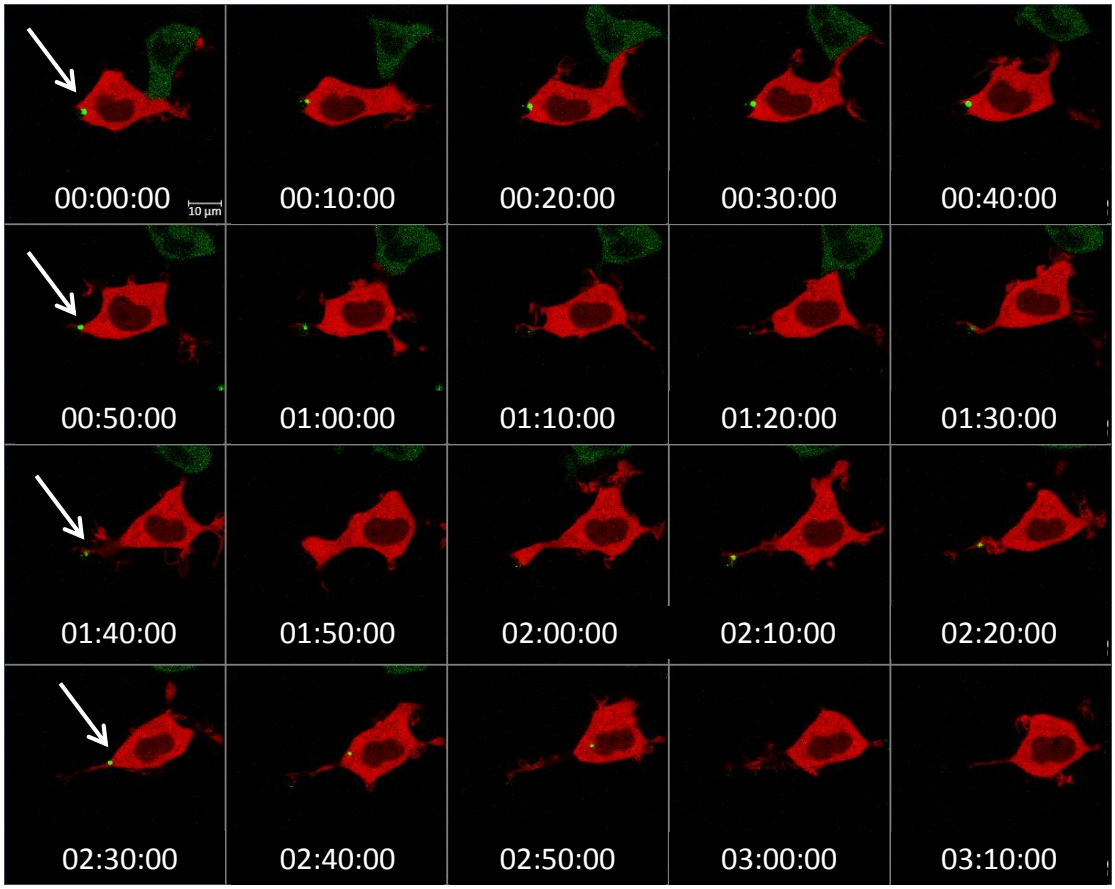

Figure 34: Time-lapse imaging of co-cultured mammalian cells shows the propagation of inclusions to uninfected cells.

As it is shown here the green polyQ inclusions are taken up by normal cells expressing 25Qmcherry and completely internalized by the end of our imaging period. White arrow shows the green inclusion that is taken by the cell. In addition, as it is shown here the normal cell (25Qmcherry) is also interacting with the invading cell (97Q-EGP). The infected cell is completely gone by the end of the imaging window

Figure 35 also shows a condition where the infected cell is interacting with the uninfected cells and pushing them away. In this case, the time-lapse imaging was performed for 9 hours and 30 min for every 30 minutes interval. During this experiment, we observed in this time-lapse imaging that not only infected mammalian cells can propagate their inclusions that can be taken up by other normal cells; in addition, they are capable of directly attacking and invading the normal cells.

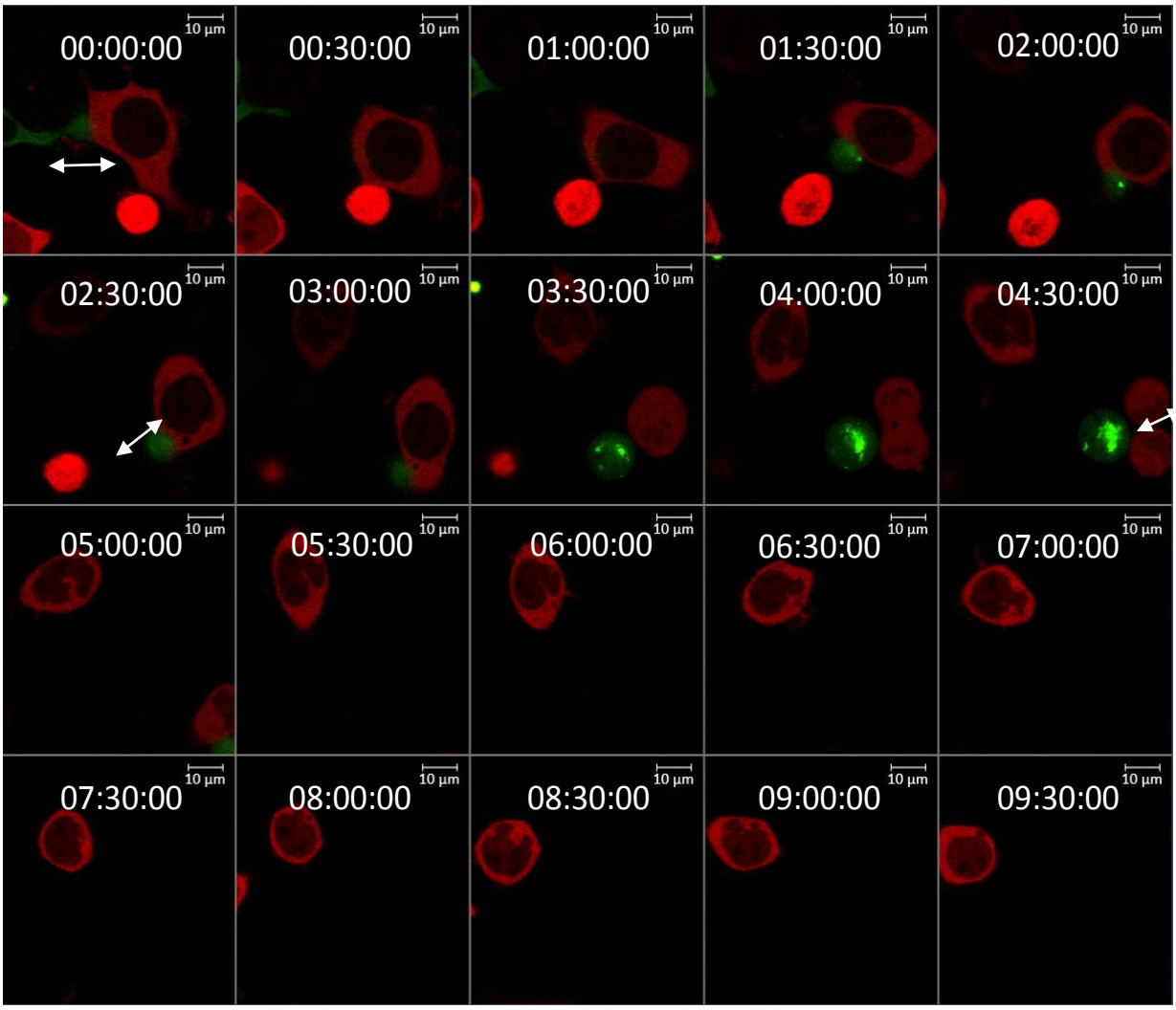

Figure 35: Time-lapse imaging of mammalian cells shows the infected cell interaction with normal cell and how it is pushing it away during our 9 hours and 30 min imaging window. white arrows also show the interactions between the infected and normal cell.

But also more interestingly, as it is depicted in figure 36 and 37 uninfected cells (HEK293 cells expressing 25Qmcherry) can also attack the infected cells(HEK293 cells expressing 97Q-EGFP). In these examples, we can also see the evolution of the inclusions. The images were acquired for 9 hours and 30 minutes window with 30 minutes interval.

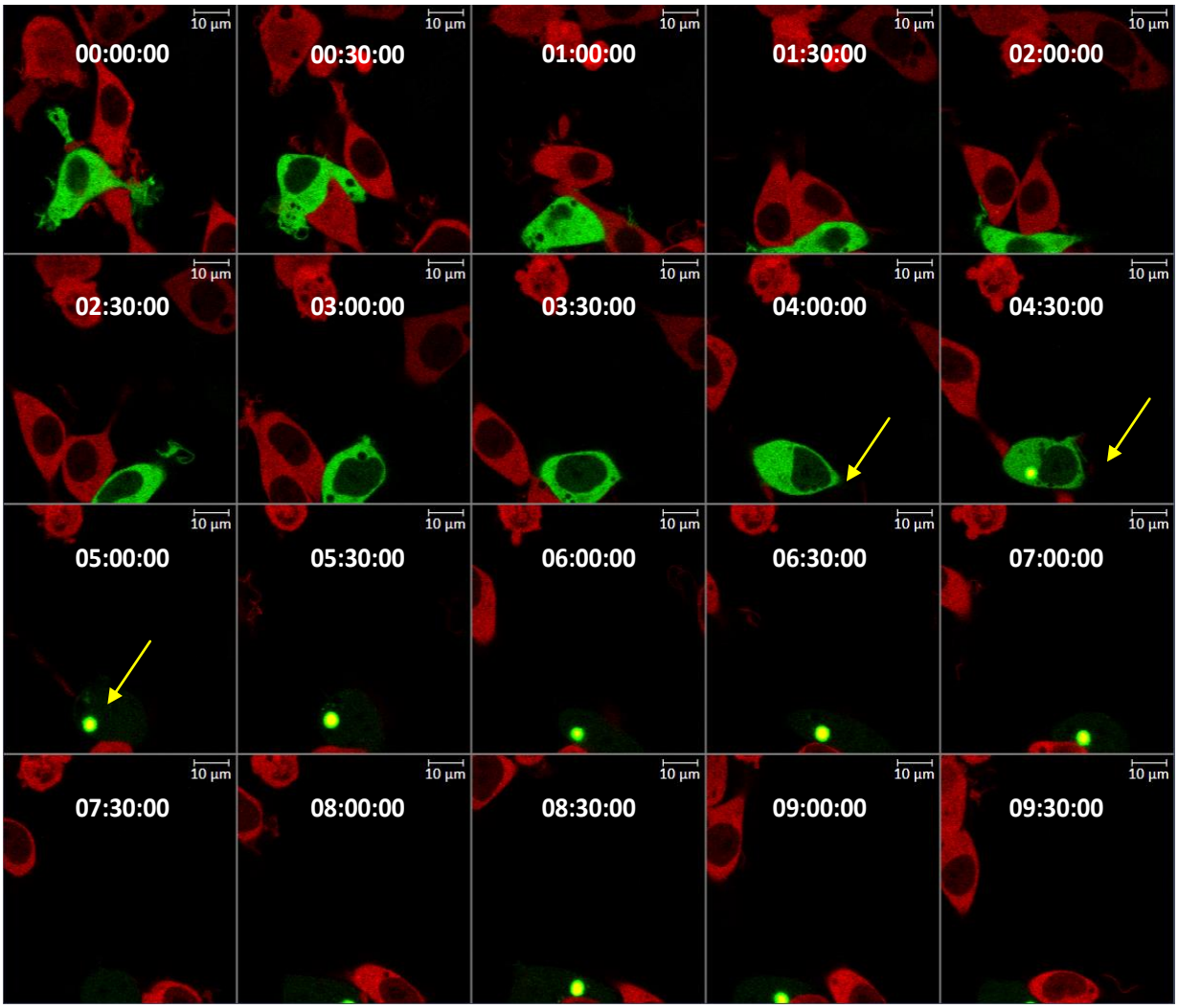

Figure 36: Time-lapse imaging of mammalian cells shows the situation when the uninfected cell (25qmcherry expressed) is interacting with the infected cells (97Q-EGFP). In this figure, we can also see how inclusion is evolving during about 10 hours imaging window. Yellow arrow shows the evolution of the inclusion. As it is seen by 5 hours imaging the inclusions become very bright so that the rest of the cell becomes invisible relative to the brightness of the inclusion.

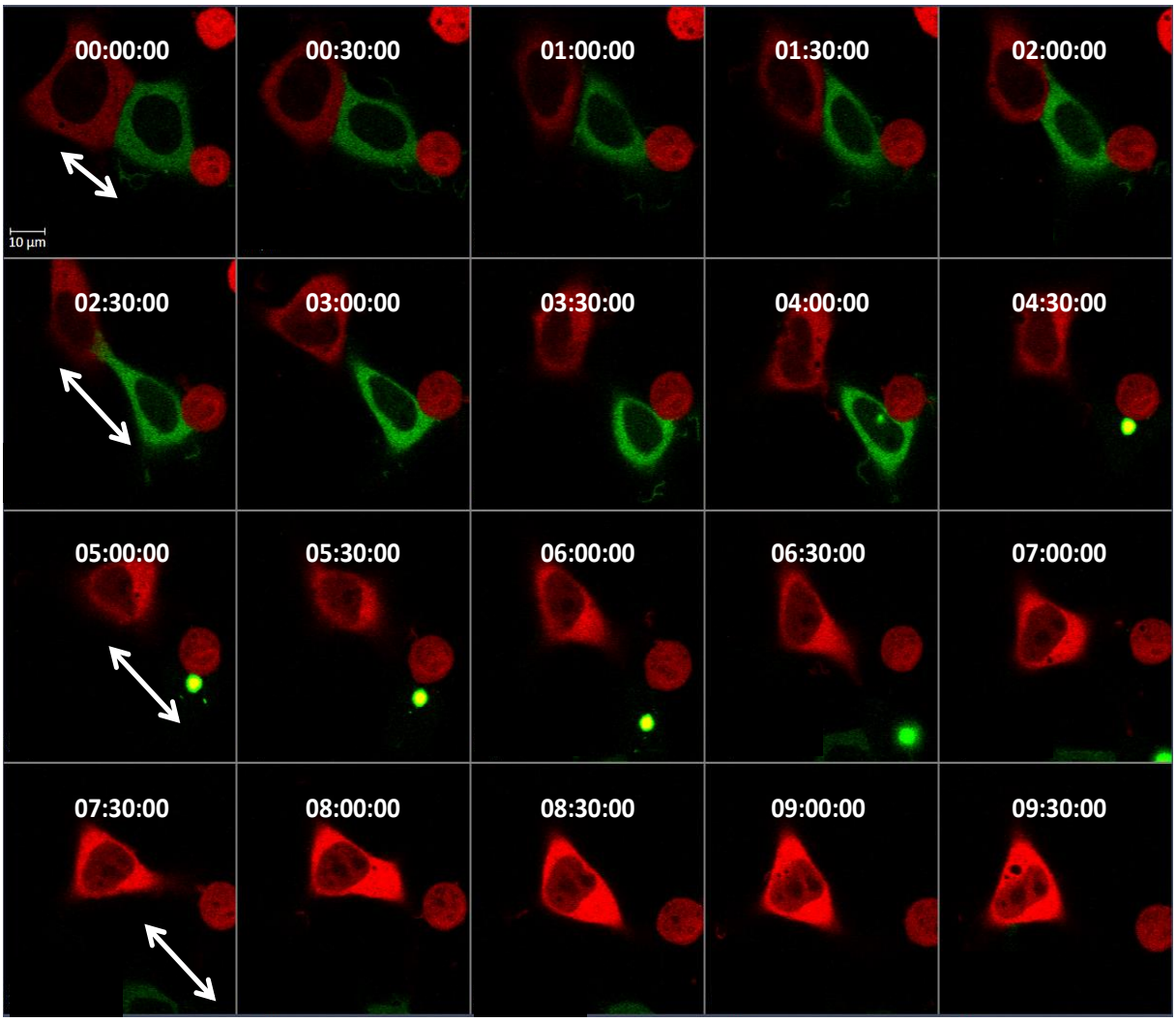

Figure 37: Normal cells interaction with infected cells.

Similar to figure 36 normal cell (25Qmcherry) is interacting with the infected cell (97QGFP) and pushing it away. White arrow shows the two cells that are interacting at different points (the normal and infected cells).

One of the challenges for this study was that as inclusions are forming and as they get larger it is harder to detect the entire cell. Sometimes the smaller inclusions, as well as the cell body, become invisible as these large inclusions are very bright relative to the cell body and smaller inclusions.

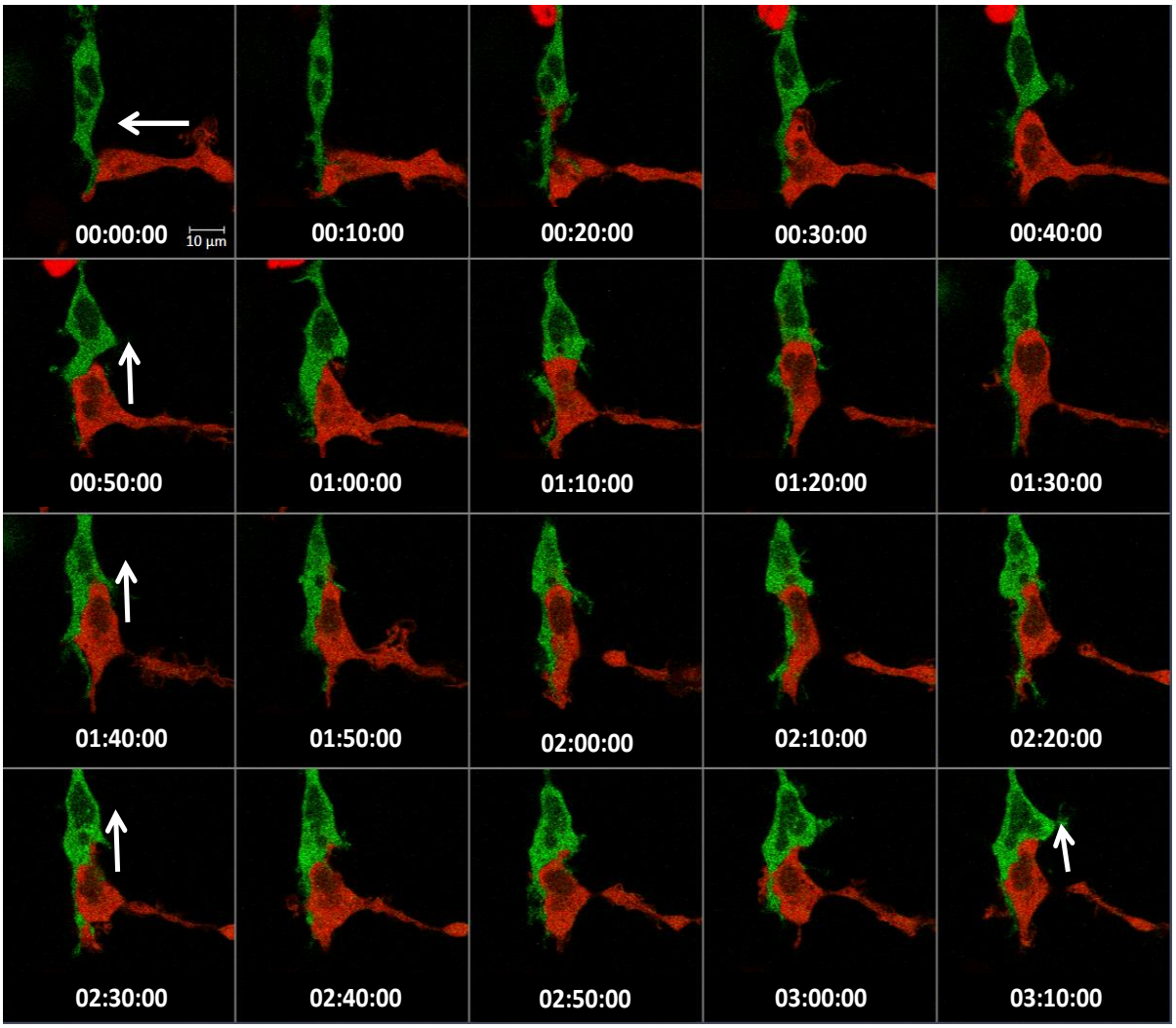

Figure 38: Uninfected cells expressing 25Qmcherry is squishing the neighboring infected cell expressing 97QGFP but with no visible inclusions.

Images were acquired for about 3 hours window with a 10-minute interval. White arrow shows the interactions of two cells (25Q mcherry and 97Q GFP) Scale bar is 10 um.

Figure 38 shows an example in which infected cells with no appeared and visible inclusions, but also, in this case, we can see how normal cell is attacking the neighboring infected cells. Here we image for four hours window for every 10 minutes.

We have also performed co-culture study with HEK293 cells transfected with 25Q mCherry and another group with 25QEGFP as our control (figure 39). Images were acquired for 7 hours for

every 30 minutes interval. In this case, cells retained a diffused cytoplasmic expression of fluorescence. Also, we imaged cells that have some cell-cell contact but we didn't find any protrusion or invasion toward neighboring cells in our control group as it was seen before.

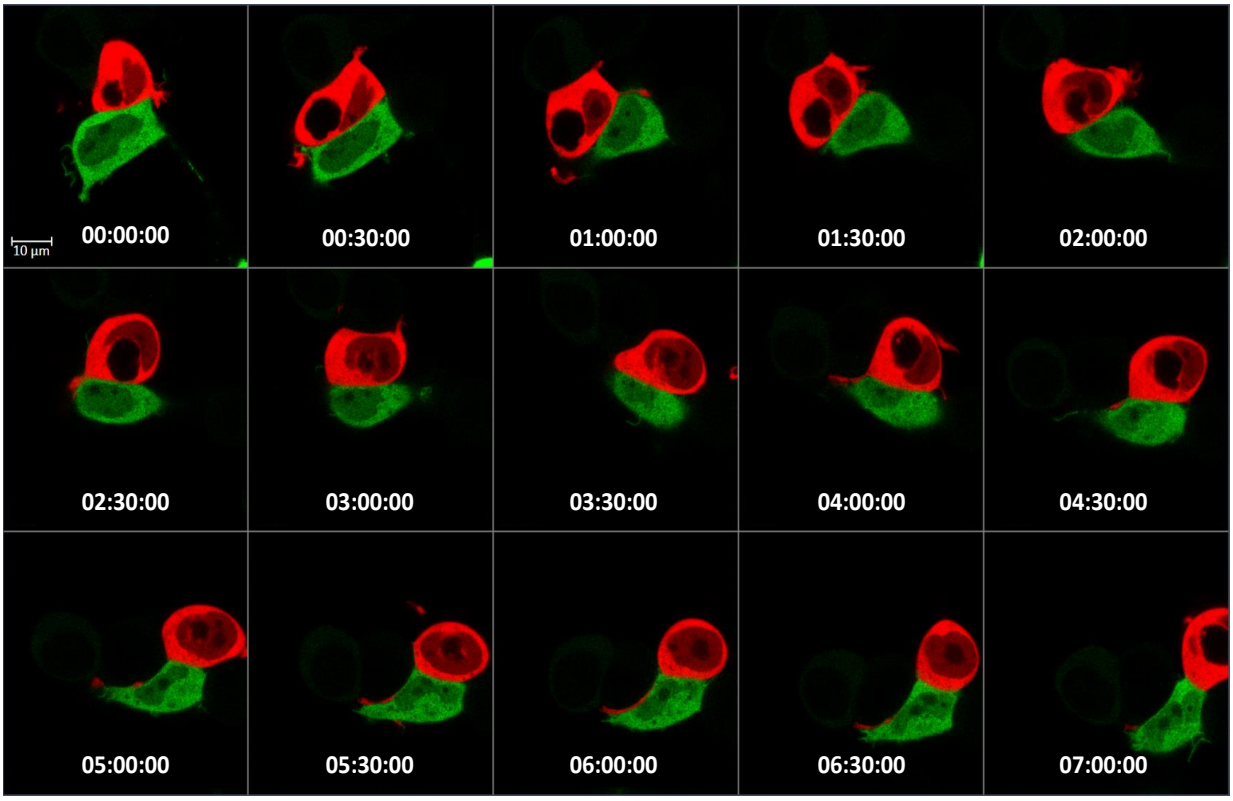

Figure 39: Control condition showing HEK293 cells transfected with 25Qmcherry and co-cultured with HEK293 cells transfected with 25Q-EGFP. No deformation or squashing shown in this control experiments and the interactions appear to be more mutual between the 25Q mcherry and 25Q EGFP. There is also no formation of inclusions in this 7 hours period and GFP expression is more homogenous in this case.

To further confirm the uptake of natural inclusion in a co-culture setting and to analyze if infected cells can propagate their inclusions, we also taken Z-stack of the image 21 hours post-transfection. Cells were co-cultured for 16 hours prior to the imaging. Figure 40 shows three different examples in which normal cells were able to uptake the inclusions from infected cells.

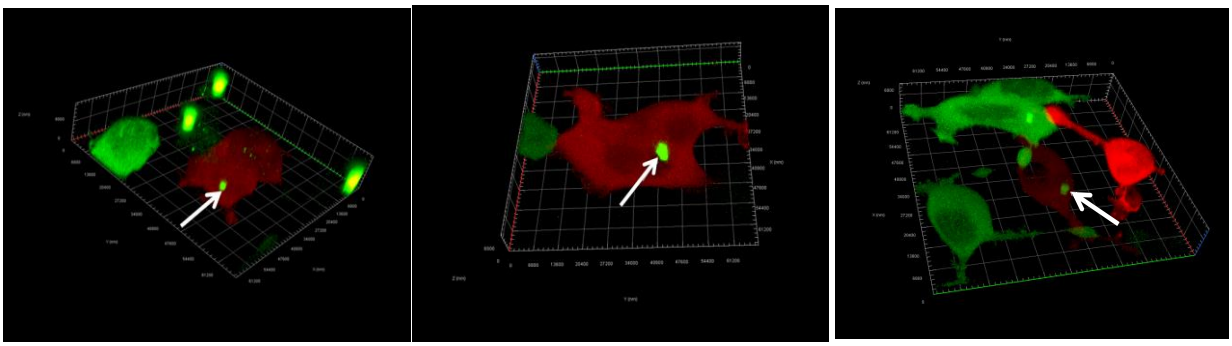

Figure 40: Z-Stack of the mammalian cells showing the uptake of the natural inclusions by normal cells. Cells were expressed with 97QEGFP and 25Qmcherry.

And finally, the graph shown in figure 41 summarizes the results obtained in time-lapse imaging for HEK293 co-culture study. As it is shown in this graph about 68.2 percent of the cells expressed inclusions and among those about 11.8 percent of PolyQ inclusions were transferred and taken up by healthy cells.

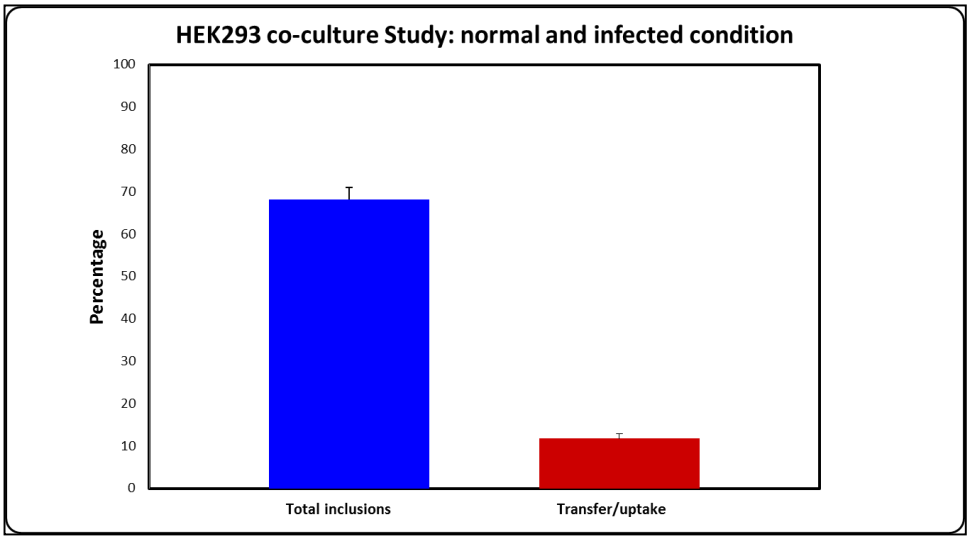

Figure 41: HEK293 co-culture time-lapse imaging bar graph.

As it is depicted in the graph about 12 percent of the inclusions formed in infected cells are propagated to the normal cells.

Icy inclusion analysis:

For characterization of inclusions, we have used the quantitative image analysis software, Icy which is a platform for bio imaging informatics. Using the protocol devolved in Icy software,

polyQ inclusions were characterized. Figure 42 shows the steps for isolation of the inclusion from the original figure. 42.A shows the original image in FITC and bright-field channel. In 42.B the bright filed channel was first deleted and using the FITC channel, inclusions were selected based on their intensity and brightness. And finally, in 42.C, the mask of the inclusions was generated. Based on this automated masks, further information from inclusions was obtained and characterization was performed. The table shown in figure 43 summarizes the results obtained from polyQ inclusions formed in mammalian cells.

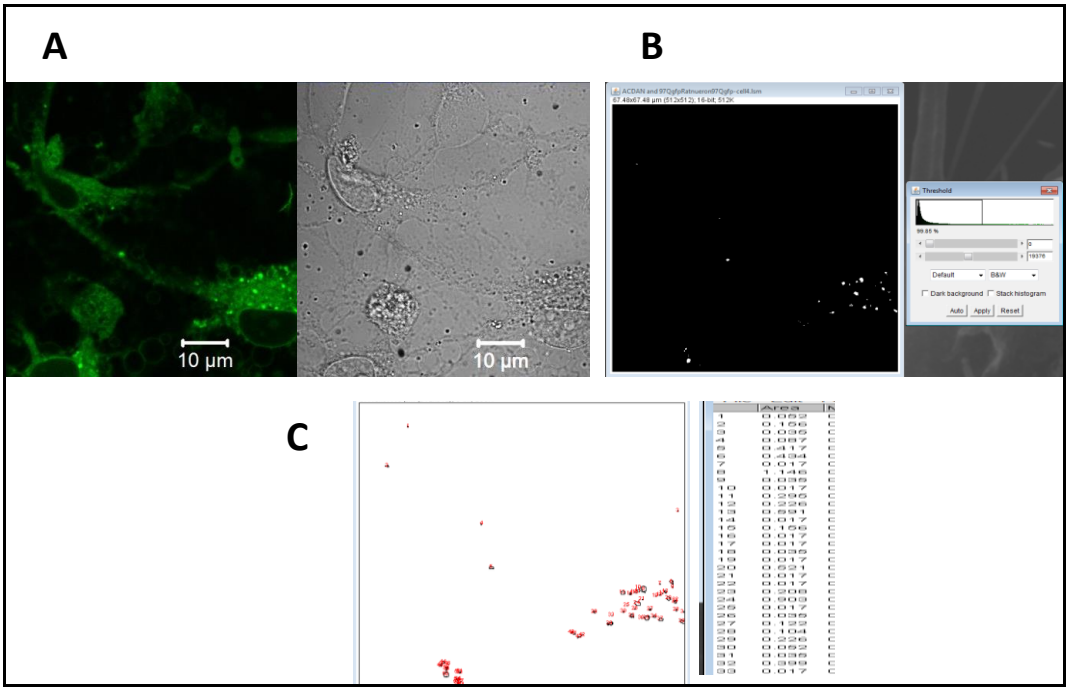

Figure 42: PolyQ inclusions characterization using Icy software shown in primary hippocampal rat neuron.

A. Shows the FITC and brightfield images of primary neurons expressing 97Q GFP.B inclusion selection process based on the intensity. In C. automated mask of the inclusions that are generated are shown with corresponding to size measurement for each inclusion.

Inclusion analysis chart	Rat hippocampal Neuron	HEK 293 cell
The average area of all inclusions ($\mu m^{2)}$	0.38	14.21
Standard deviation	0.99	13.46
Max (μm^2)	10.29	50.71
Min (μm^2)	0.02	0.17
Total counts(N)	375	233

Figure 43: Table summary of polyQ inclusions characterization in mammalian cells.

Inclusions formed in neuronal versus non-neuronal cells expressing 97Q GFP are compared here. As it is shown here based N= 608 inclusions measurements, the inclusions formed in neuronal cells are significantly different and smaller in size compared with the one formed in non-neuronal cells.

4.5. SUMMARY:

Our findings establish for the first time to the best of our knowledge that expanded polyQ expressing mammalian cells invade and attack the normal cells; in addition, polyQ inclusions translocate between cells and can propagate to uninfected cells. But more interestingly, our results indicate that normal cells can also attack the invading cells.

In the study that we have performed, we observed transfer between rat neurons, PC12 cells, and HEK 293 cells. In this study, we confirmed that the HTT polyQ inclusions transfer can occur in both passive and active manner. Mammalian cells were also able to readily uptake the synthetic inclusions (cyn40Q). In addition, we observed that cells can also uptake natural inclusions from different cell types. In specific, we observed that stable line PC12 expressing 97QGFP were able to expel inclusions in their media and normal HEK 293 cells were able to uptake these formed inclusions. Furthermore, our time-lapse imaging on co-culture cell line of HEK 293(25Qmcherry co-culture with 97QGFP) indicates that natural inclusion uptake can also occur in non-neuronal cells. Besides, we observed active transfer as another mechanism of exchange on the axons of both rat neurons and PC12 cells, and via lipid tubes on HEK293 cells. Beside the propagation of inclusions, we also observed the cell-cell interactions both from healthy cells toward infected cells and vice versa as a possible defense mechanism.

Based on our study, we believe that the inclusions are therefore an important biomarker of the HD and have a key role for the propagation of the infections at the single cells level. Importantly, this spread and transfer can occur with/out cell contacts as inclusions can be spell out of the cells and pass to the normal cells.

CHAPTER 5: CONCLUSIONS & FUTURE PERSPECTIVE

5.1. SUMMARY AND DISCUSSIONS

The underlying mechanism undergoing the genetic and progressive neurodegeneration in HD is still not fully understood. At the early stage, HD pathology causes only a minor alteration in the brain. And since HD manifest in midlife, many patients don't have any symptoms and bear children before knowing they have HD and that they can pass their genes to their offspring. Recently, there is a growing community of researchers directing their effort to find a treatment to slow down the progression of the disease or even to delay the onset. However, finding effective therapeutic or even preventive drugs requires accurate ability and sensitive measure of the clinical signs of the HD[171]. And based on the recent publication in the human genome, it appears that the there is a desire for a paradigm shift from treatment to prediction and prevention of the disease in healthy appearing pre-manifest HD[172].Yet, at the moment, there is no proven biomarker that enables the screening of the disease progression and can help assess the efficacy of new drugs. And thus, it is critical to examine and explore possible new biomarkers, early indicators, of Huntington disease during what is known as " prodrome" that is a pre-HD stage. This will provide distinct and valuable information about true nature and progression of the disease on the individual that appear healthy but have about 99% confidence to develop this fatal brain disorder [172].

In this study, I was able to identify multiple biomarkers and establish new assays that can be used to screen HD and to evaluate the efficacy of the treatments. First and foremost, as I have discussed in chapter 2, using phasor-FLIM imaging and by analyzing mammalian cells and examining the tissue in an animal model of the HD, I have discovered a new biomarker in HD.

Based on the results, the cells/tissue that was expressed with extended polyQ showed the elevated level of the free/bound ratio of NADH compared to control. Here for the first time using FLIM measurements, I was able to resolve glycolysis vs. OXPHOS pathway. As it was discussed in chapter 1, current exciting techniques like fMRI or PET imaging are not able to characterize how glucose is being processed in distinct tissue regions. In addition, the bulk measurements provided by means of these techniques are not very sensitive and also difficult to assess for the specific section due to the fact that the metabolites are in constant flux and leave the regions of interests multiple times. However, using the FLIM we can get the metabolic pixel map of the tissue. In this study, besides understanding the specific metabolic pathway that is affected in HD, the great advantage of this label-free method that I have developed is that it can be done in a native tissue sample of HD which can be used for screening progression of the disease or the effect of therapeutic.

In chapter 3 of this study, we are moving from phasor approach in fluorescent lifetime imaging discovery to the hyperspectral imaging. Here I have characterized the fluorescent emission of each pixel in spectral phasor analysis. First, I have developed an elegant and original method to separate fluorescently tagged protein signals from Laurdan in the living cells using the fit-free spectral phasor analysis. The traditional method like well-studied radiometric method known as Generalized Polarization, GP, is usually used on unlabeled cells. On the other hand, the method that I have established here using hyperspectral imaging technique can detect the contribution of multi-components emissions that were not able to resolve using GP approach.

Second, using the developed method, I was able to characterize the membrane fluidity affected in HD and identify another novel biomarker using spectral phasor analysis and employing solvatochromic dyes.

Earlier studies indicate that there are some abnormalities in cholesterol homeostasis that is associated with neurodegenerative disorders like Huntington, Alzheimer, and etc[173].These research indicate that the biosynthesis of cholesterol and fatty acids are impaired in both in vitro studies in cells as well as animal studied in vivo in Huntington disease[37]. In fact, it has also been shown that total level of the cholesterol is also reduced in the central nervous systems of mice model of HD as well as in human cell expressing mutant huntingtin. Research also indicates that the total serum cholesterol concentrations in HD patients are approximately 40 mg/dl lower than normal[174]. This is important as cholesterol is the main compartment of the peripheral membrane as well as it is essential and is highly enriched in the brain[173]. In contradictions to these lines of research, there are other literatures that discuss the abnormality in trafficking rather than biogenesis of the cholesterol. In particular, the study indicates that cholesterol trafficking was impaired in striatal neurons of HD mouse model[41].Whether the impairment of cholesterol and fatty acid is due to their biogenesis or its trafficking, it is still not fully understood how such impairments can have a pathological impact and influences the cell plasma membrane structure.

And thus using the hyperspectral imaging coupled with fluorescent probes that detect changes in the membrane phases, I have studied and characterized the membrane fluidity of the cells affected by HD. The results were astonishing and indicated that mammalian cells expressed with expanded polyQ show an increase in the fluidity of plasma membrane compared to control. This

can have an impact on the cell to cell contact, membrane trafficking, ion transports as well as propagation of the polyQ inclusions to the neighboring normal cells.

To further characterize the HD pathology and its influence on normal cells and to see how and if the polyQ inclusions can be transported across cells, I have also designed a separate study that has been discussed in chapter 4 of this work. Our analysis in this section is divided into two parts. In the first part, I have characterized the uptake of the synthetic inclusions (Cy3 tagged-40Q) by mammalian cells. Here we have confirmed that cells were able to uptake the synthetic inclusions. Beside this passive mechanism, our time-lapse imaging shows that inclusions can be transferred actively between cells via axon/microtubes and can be pass to the neighboring uninfected cells. In addition, we have also shown that cell medium of the HD cells was enough to pass the polyQ inclusions to uninfected cells. Together with our results strongly suggest that the polyQ inclusion can freely pass from infected cells to uninfected cells. Normal cells can either get contaminated via the supernatant obtained from diseased cells or directly from the cell to cell contact. In addition, for the first time, we have also shown that normal cells also attack and make protrusion to the HD cells.

Future studies need to be done to show how such transfer and propagation of inclusions to uninfected cells also affect the normal cells. This has a great impact on the fundamental understanding of the pathology of the HD and also can enlighten the path for future cell/ tissue transplantation therapy.

5.2. FUTURE PERSPECTIVE:

Having developed novel methodology and biomarkers to look into the progression and screening of Huntington disease, the future works would be to look into the therapeutic effect using in vitro

and *in vivo* Study. The future prospect of this study is to look into an intervention mechanism that can slow down or stop the propagation of the disease. And so the sections below are designed based on some of my hypothesis and as potential future works for this study.

Can Hypothermia protect from neurodegeneration?

As early as 1987, hypothermia has shown in an animal study to reduce neuronal death after brain injury [175]. In addition, it has been shown that cooling may influence protein overexpression that can potentially benefit neurodegenerative diseases [176]. Also based on some of our preliminary data (not shown here) mild hypothermia were able to reduce the aggregates formation in synthetic polyQ. Since the neuroprotective effect of hypothermia is not still well studied, the future work should focus on understating how hypothermia may affect Huntington disease. The study can focus on:

A) Effect of mild hypothermia on metabolism and based on the developed biomarker in this work

B) Influence of therapeutic hypothermia on cell structure and plasma membrane fluidity

C) Effect of mild hypothermia on aggregation process and inclusions transfer mechanism

Figure 44 depicts the hypothesized image showing the influence of hypothermia and hyperthermia on both synthetic and natural aggregations formations and process based on our earlier preliminary data(not shown here).

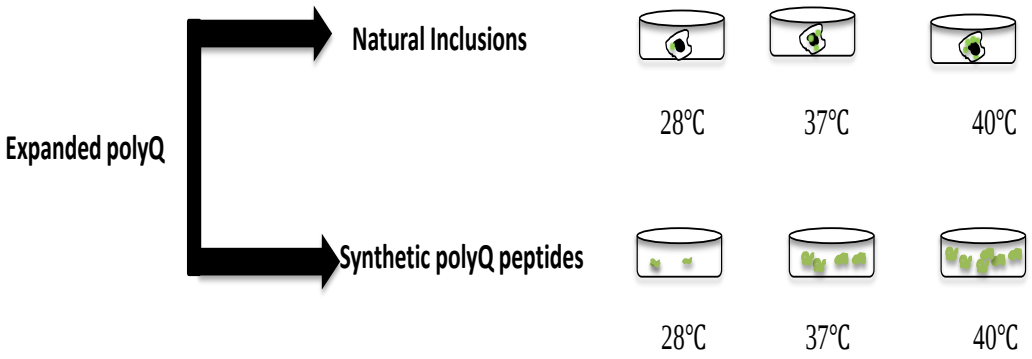

Figure 44: Hypothesized figure showing the effect of therapeutic hypothermia on aggregations

Peptide-based therapeutic approach to fight HD: P42

It has been shown that the onset and progression of the Huntington disease are based on the ratio of normal and mutant Huntingtin. Recent literature indicates that the addition of normal huntingtin may improve the disease defects[177]. A 23 aa peptide, P42, is part of endogenous Huntingtin protein located within the proteolytic rich region.P42 has shown to play a critical role in HD pathogenesis. An earlier study indicated that P42 may have a therapeutic effect and reduces the aggregation process[178].

For this purpose using the developed assay and methodology, the therapeutic power of P42 can be evaluated in live mammalian cells. The future work should focus on analyzing the effect of P42 on aggregations process, transport, and propagation of the inclusions.

After confirming the effect of P42 on possible reduction of aggregating formations, the following experiments should focus on analyzing the mammalian cells to see how that would possibly influence the cell metabolism that we have discussed in chapter 2. In addition, research should follow to see if the increased in membrane fluidity that we have shown earlier in HD cell plasma

membrane is reversible using a treatment such as P42 therapy based on the biomarker that was identified and discussed on chapter 3 of this work.

APPENDIX. A

The phasor-FLIM fingerprints reveal shifts from OXPHOS to enhanced glycolysis in Huntington Disease

Sara Sameni[1], Adeela Syed[2], J. Lawrence Marsh[2], and Michelle A. Digman[1,2,3]

[1]Laboratory for Fluorescence Dynamics, Department of Biomedical Engineering, [2]Department of Developmental and Cell Biology,
[3]Department of Chemical Engineering and Material Sciences, University of California Irvine

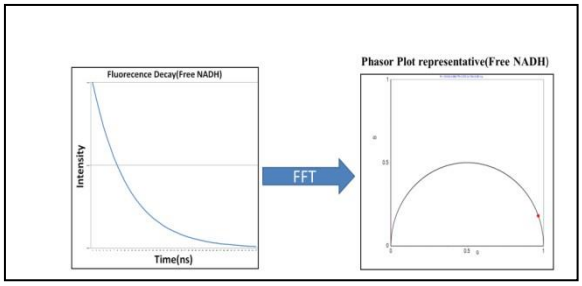

$$g_{i,j}(\omega) = \frac{\int_0^\infty I_{i,j}(t)\cos(\omega t)dt}{\int_0^\infty I_{i,j}(t)dt},$$
$$s_{i,j}(\omega) = \frac{\int_0^\infty I_{i,j}(t)\sin(\omega t)dt}{\int_0^\infty I_{i,j}(t)dt},$$

Figure A1: The process of Phasor transformation is depicted here. Coordinates g and s were obtained using the formulas in the right panel. ω is the angular modulation frequency obtained as $\omega=2\pi f$ where f is 80 MHz for our laser system

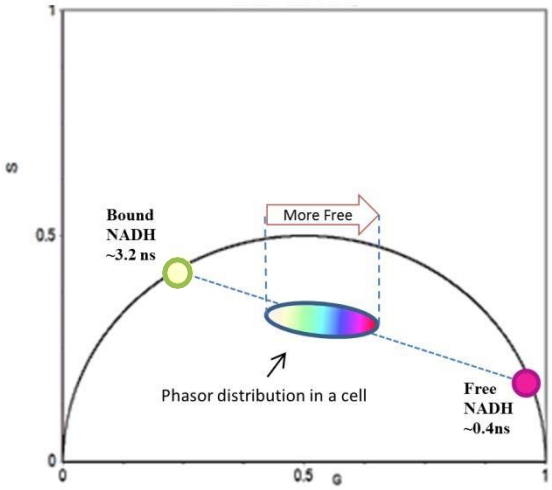

Figure A2: Phasor plot is obtained by calculating the cosine and sine transform of the fluorescence decay at each pixel of an image (Digman et al, 2008). And thus the measured fluorescent decay is transformed to single points in the 2D phasor with g and s coordinates(x and y-axis corresponding to cosine and sine components. The pure NADH is shown in a pink circle with a lifetime of 0.4ns The NADH phasors shifts towards the longer lifetime (3.2ns) when free NADH is incubated with lactate dehydrogenase (LDH) depicted by the green/white circle. The dotted blue line connecting Free (pink circle) to the bound NADH (green/white circle) is the total possible range. Due to the linearity rule of phasor coordinate, the cluster of data shown as a mixture of free and bound NADH lays on the straight (blue line) line connecting the pure free to bound NADH

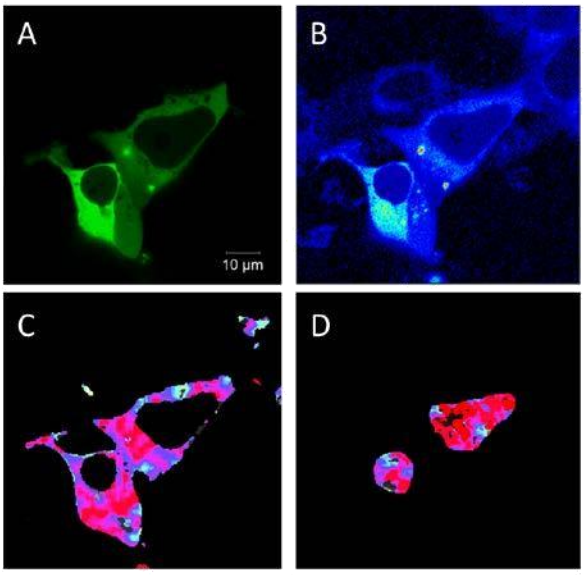

Figure A3: A shows confocal images of 97Q-EGFP using 488 nm. B is the intensity FLIM map obtained with two-photon excitation at 740 nm. C&D shows the segmented image that isolates cytoplasmic portion(C) from the nuclear compartment (D).

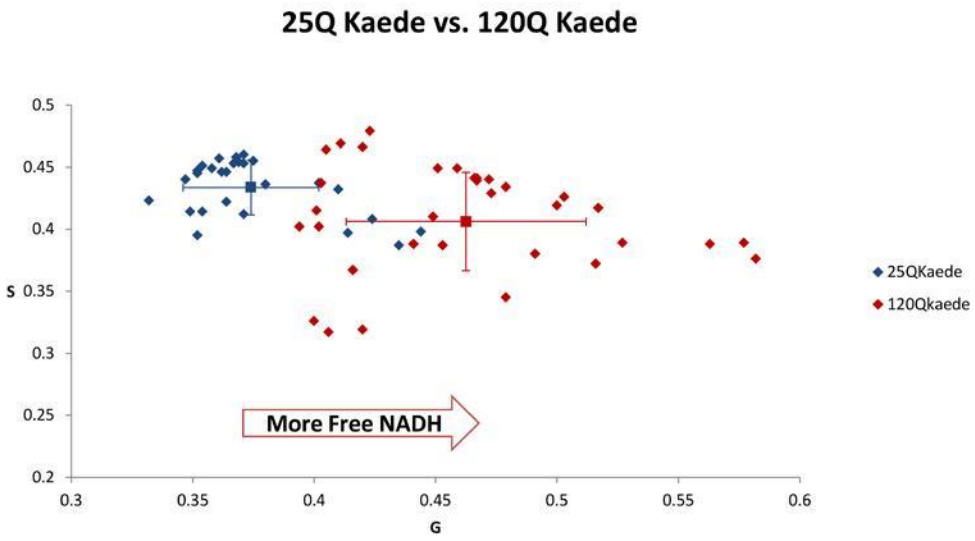

Figure A4: NADH phasor FLIM scatter plot of 25QKaede vs. 120Q Kaede showing average g and s phasor values for each animal eye disc ROI for a total of 15 animals and 66 ROI measurements. The blue diamond refers to 25Q Kaede(N=27), and expanded expression 120QKaede (N=39, in red diamond) that indicates shortening of the lifetime towards the glycolytic state, shifted to the right similar to the other Drosophila experiments that we reported here.

APPENDIX. B

Alteration in Fluidity of Cell Plasma Membrane in Huntington Disease Revealed by Spectral Phasor Analysis

Sara Sameni[1,2], Leonel Malacrida[1,2,3], Zhiqun Tan[4], and Michelle A. Digman[1,2*]

[1]Laboratory for Fluorescence Dynamics, UC Irvine, CA,USA, [2]Department of Biomedical Engineering, UC Irvine, CA,USA, [3]Departamento de Fisiopatología, Hospital de Clinicas, Facultad de Medicina, Universidad de la República. Montevideo, Uruguay, [4] Institute for Memory Impairments and Neurological Disorders, University of California, Irvine.

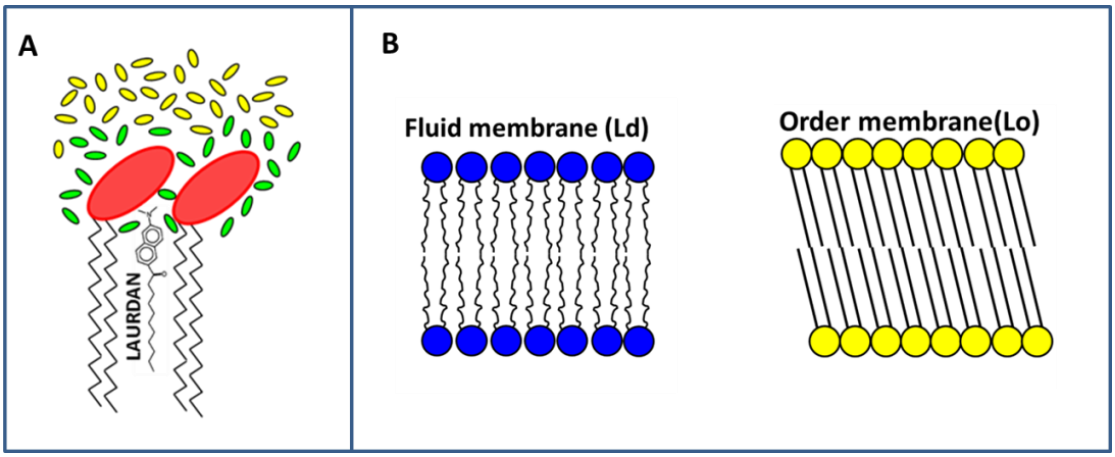

Figure B1: Schematic of LARUDAN in the membrane. A) schematic figure of plasma membrane is depicted with fluorescent membrane probe LAURDAN with the emission sensitive to the polarity of the membrane B) schematic of cell membrane fluidity ; fluid membrane (Ld) is depicted in blue compared to ordered membrane(Lo) depicted in yellow.

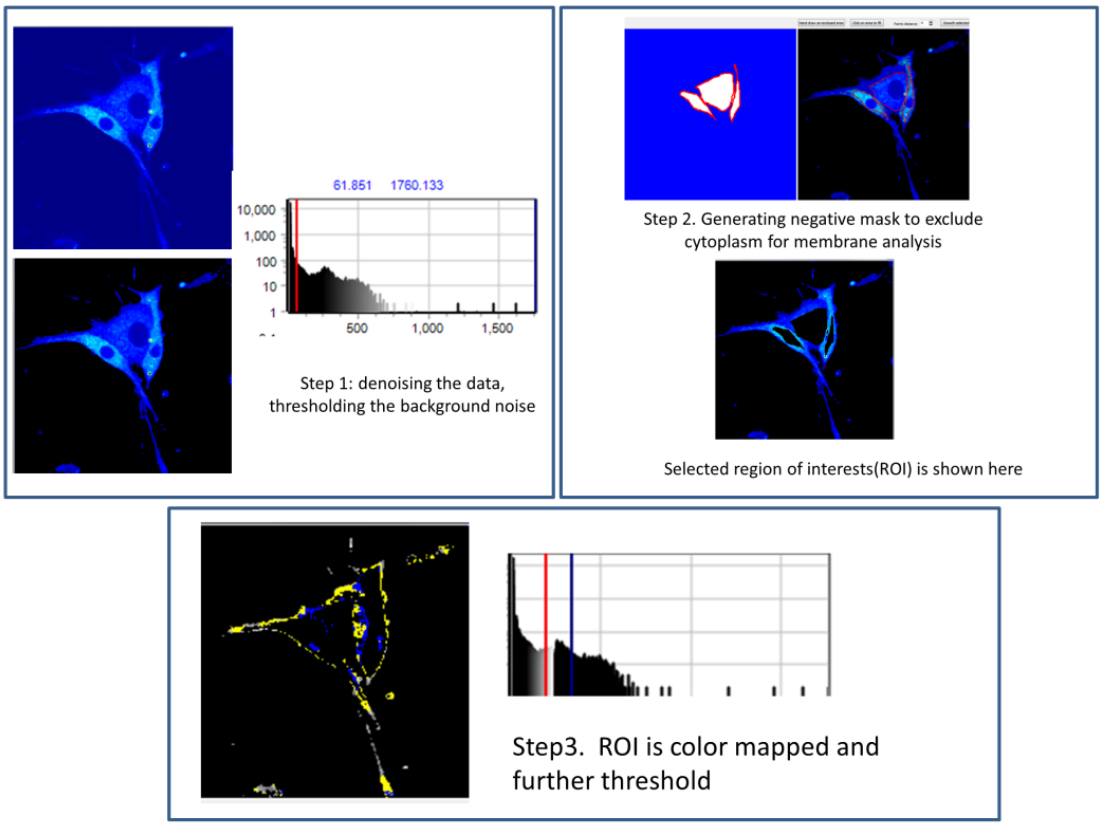

Figure B2: The process of generating membrane masks. First image is threshold to remove the background, and then negative masks are made by excluding the cytosolic region to isolate the membrane. Selected ROI are then color coded on spectral phasor and then further threshold to generate the optimum masks.

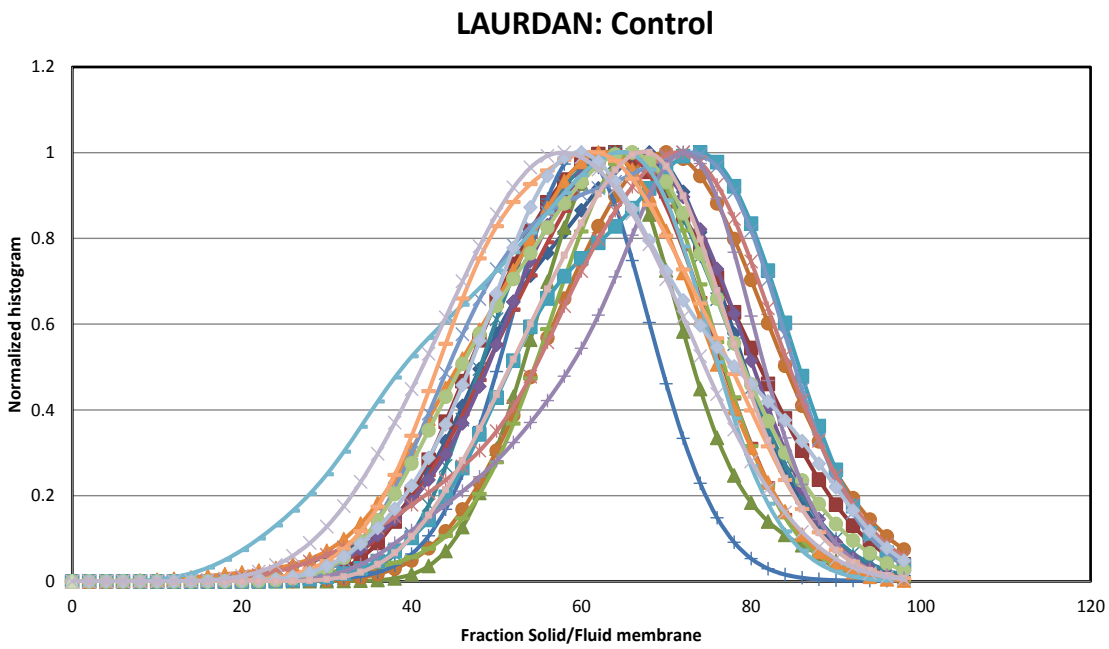

Figure B3: Normalized histogram of the fraction of solid to fluid contribution with LAURDAN in the masked membrane (differentiated PC12 cells without PA). The histogram shows the position along the green/blue trajectory in the membrane as a fluidity fraction which indicates a shift toward blue trajectory (Lo phase).

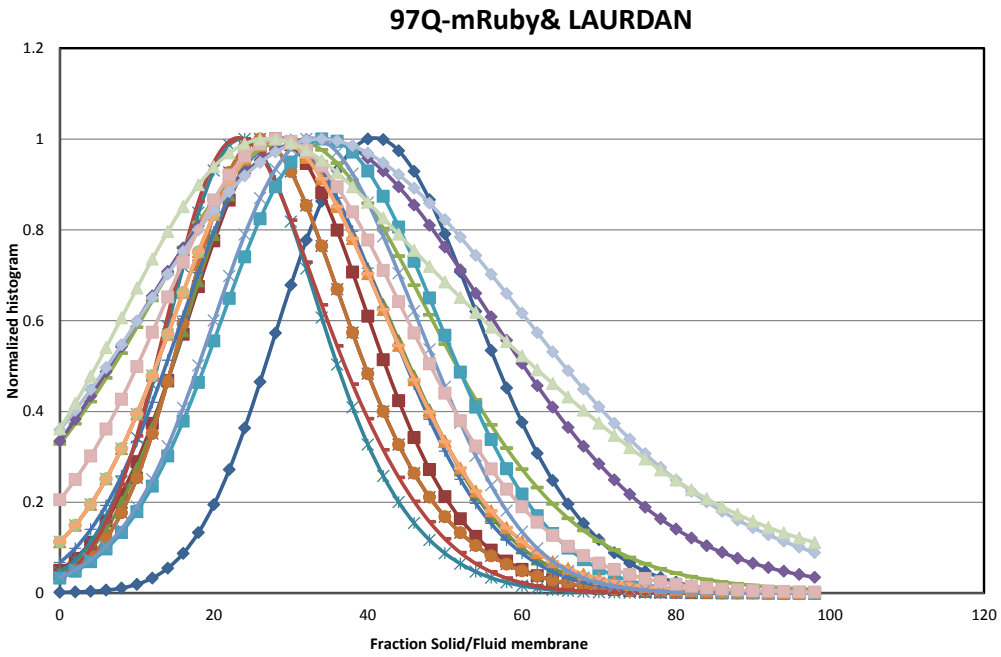

Figure B4: Normalized histogram of the fraction of solid to fluid contribution of cells expressing 97Q-mRuby stained with LAURDAN in the masked membrane (expanded PolyQ). The histogram shows the position along the green/blue trajectory as a fluidity fraction which shows the shift towered green trajectory (Ld phase).

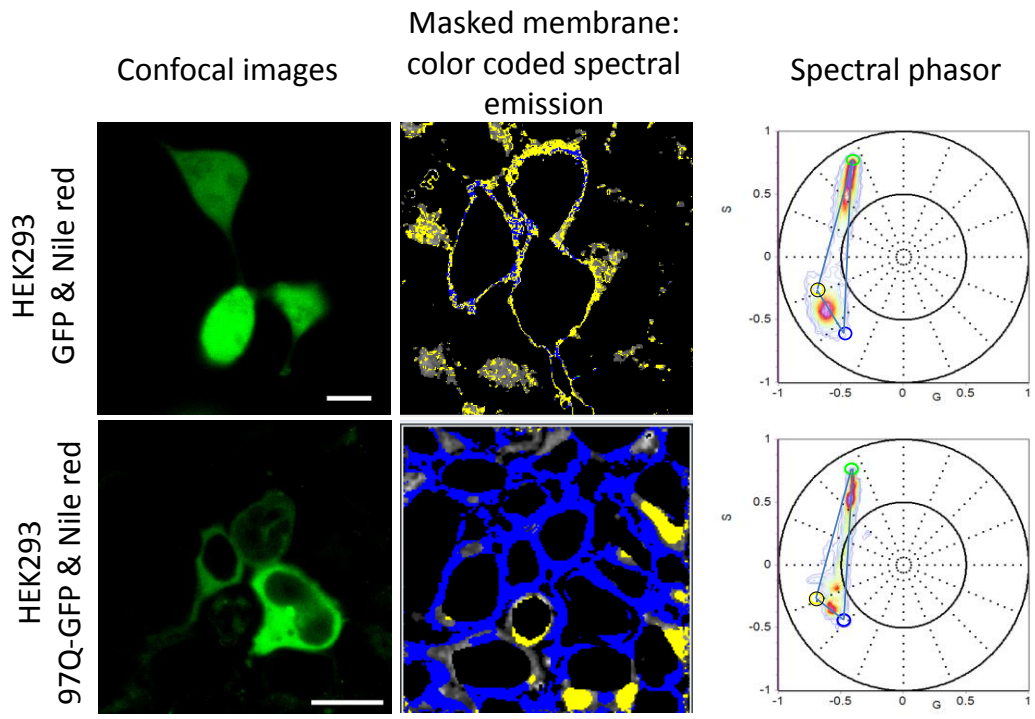

Figure B5: Nile Red and HEK 293 cells. HEK 293 cells expressing 97Q-GFP(bottom panel) and GFP(top panel) that are stained with Nile red are depicted here with the corresponding cell masks generated and color coded with blue and yellow with a black outline as it is shown in the phasor plot on the right. The triangle on the graph shows the linear combination rules. As it is presented here 97QGFP is shifted toward longer wavelength indicating increased polarity in NR and increased in the fluidity of the membrane (Ld). Scale bar is 20μm.

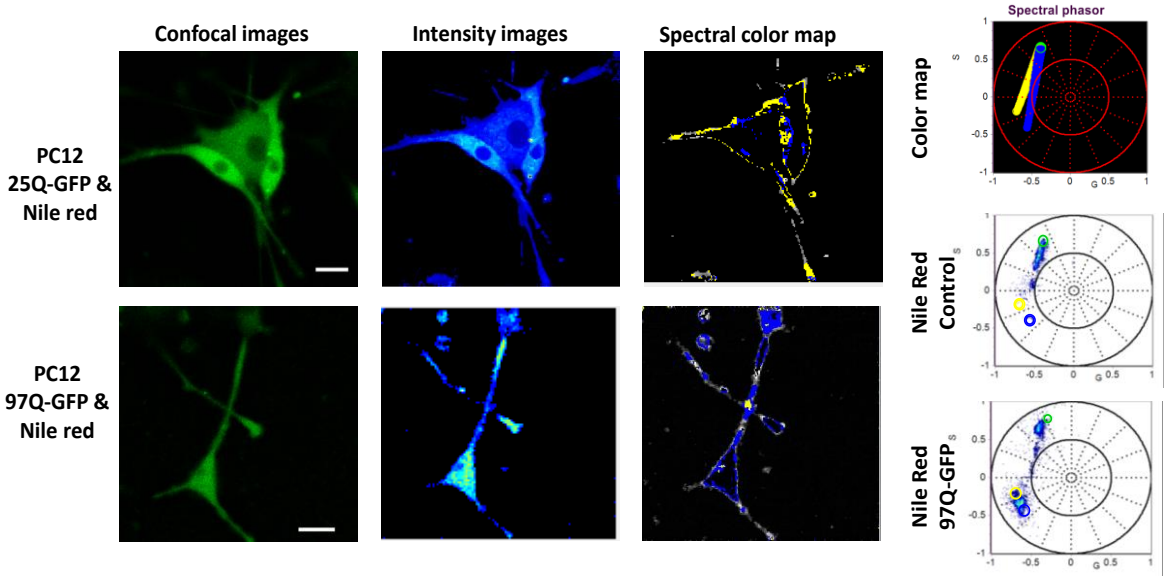

Figure B6: Differentiated PC12 cells expressing 25Q-GFP (control) and 97QGFP are shown here. Color-coded membrane masks are depicted next to intensity images. The corresponding spectral phasor plots are shown on the right-hand side. The first plot shows how cells are color coded. As it is shown here, there is a shift toward higher polarity for NR in 97Q-GFP indicating fluid membrane. Scale bar is 20μm.

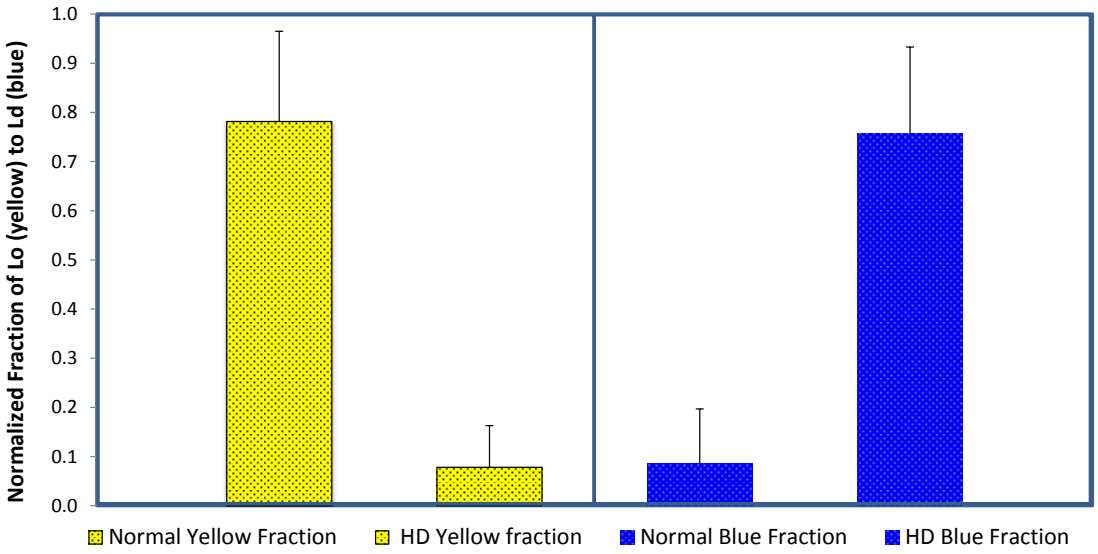

Figure B7: The results obtained using fluorescent probe NR is summarized on the bar graph and by calculating the fraction of color contribution. Yellow bars (pseudo-color) designates fraction of Lo compared to blue bars(pseudo color) fraction of Ld phase in the membrane for N=20 HD (n=10 for HEK293 97Q GFP and n=10 differentiated PC12 97Q GFP) stained with NR and N=21 control cells(n=11 HEK293-GFP,n=10 differentiated PC12 25Q GFP) stained with NR . The graphs indicate shift to high fluidity in the membrane of 97q-GFP cells((Ld phase) compared to control.

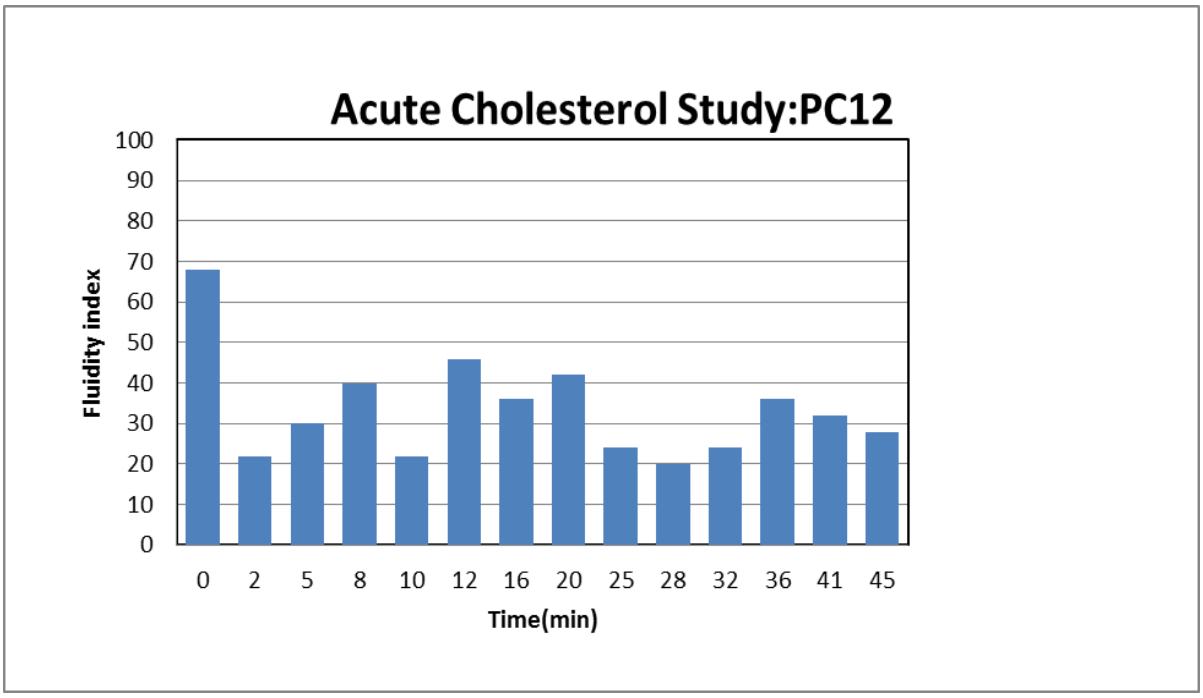

Figure B8 PC12 cells treated with MβCD are shown with smaller fluidity index that indicates increased in membrane fluidity.

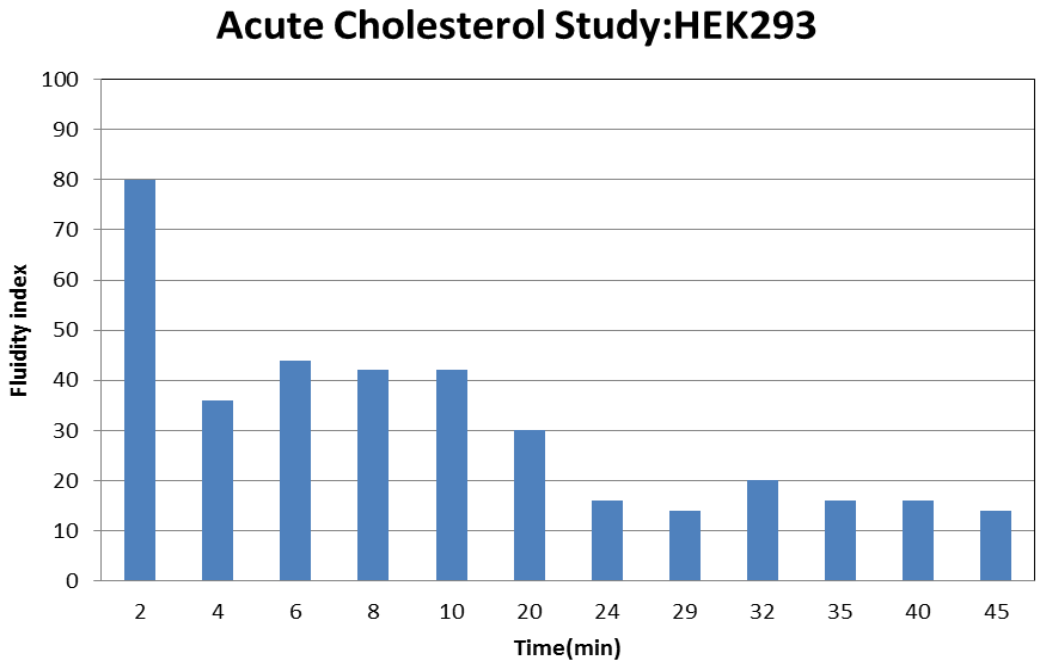

Figure B9: Similar to PC12 cells, HEK293 cells with depleted cholesterol in the membrane shows smaller fluidity index correlated with increased fluidity in the membrane

REFERENCES

1. Buxton , R. *center for functional MRI*. Available from: http://fmri.ucsd.edu/Research/whatisfmri.html.

2. Francesco, C., S. Anya, and G. Enrico, *Spectral phasor approach for fingerprinting of photo-activatable fluorescent proteins Dronpa, Kaede and KikGR.* Methods and Applications in Fluorescence, 2013. **1**(3): p. 035001.

3. Warby, S.C., et al., *CAG Expansion in the Huntington Disease Gene Is Associated with a Specific and Targetable Predisposing Haplogroup.* American Journal of Human Genetics, 2009. **84**(3): p. 351-366.

4. Myers, R.H., *Huntington's Disease Genetics.* NeuroRx, 2004. **1**(2): p. 255-262.

5. Kopito, R.R. and D. Ron, *Conformational disease.* Nature cell biology, 2000. **2**: p. E207.

6. Bates, G.P., *The molecular genetics of Huntington disease — a history.* Nature Reviews Genetics, 2005. **6**: p. 766.

7. Quarrell, O.W.J., et al., *Managing juvenile Huntington's disease.* Neurodegenerative disease management, 2013. **3**(3): p. 10.2217/nmt.13.18.

8. McFarland, K.N. and J.-H.J. Cha, *Chapter 3 - Molecular biology of Huntington's disease*, in *Handbook of Clinical Neurology*, W.J. Weiner and E. Tolosa, Editors. 2011, Elsevier. p. 25-81.

9. Nasir J, et al., *Targeted disruption of the Huntington's disease gene results in embryonic lethality and behavioral and morphological changes in heterozygotes.* Cell. **81**(5): p. 811-823.

10. Hilditch-Maguire P, et al., *Huntingtin: an iron-regulated protein essential for normal nuclear and perinuclear organelles. .* Hum Mol Genet, 2000. **9**(19): p. 2789–2797.

11. Dragatsis I, Levine MS, and Z. S., *Inactivation of Hdh in the brain and testis results in progressive neurodegeneration and sterility in mice.* Nat Genet., 2000. **26**(3): p. 300-306.

12. Mochel, F. and R.G. Haller, *Energy deficit in Huntington disease: why it matters.* J Clin Invest, 2011. **121**(2): p. 493-499.

13. Koopman, et al., *OXPHOS mutations and neurodegeneration.* The EMBO Journal, 2013. **32**(1): p. 9-29.

14. Ayala-Peña, S., *Role of oxidative DNA damage in mitochondrial dysfunction and Huntington's disease pathogenesis.* Free Radical Biology and Medicine, 2013. **62**: p. 102-110.

15. Z. Xun, et al., *Targeting of XJB-5-131 to mitochondria suppresses oxidative DNA damage and motor decline in a mouse model of Huntington's disease.* Cell Rep., 2012: p. 1137–1142.

16. Heikal, A.A., *Intracellular coenzymes as natural biomarkers for metabolic activities and mitochondrial anomalies.* Biomarkers in medicine, 2010. **4**(2): p. 241-263.

17. GP, B., *Huntingtin aggregation and toxicity in Huntington's disease.* Lancet, 2003. **361**(93696): p. 1642-4.

18. Arrasate M, et al., *Inclusion body formation reduces levels of mutant huntingtin and the risk of neuronal death.* Nature., 2004. **431**: p. 805–810.

19. Doi H, et al., *p62/SQSTM1 differentially removes the toxic mutant androgen receptor via autophagy and inclusion formation in a spinal and bulbar muscular atrophy mouse model. .* J Neurosci., 2013. **33**: p. 7710–7727.

20. Saudou F, F.S., Devys D, Greenberg ME., *Huntingtin acts in the nucleus to induce apoptosis but death does not correlate with the formation of intranuclear inclusions.* Cell., 1998. **95**: p. 55-66.

21. K, T. and Y. S, *Induction of pluripotent stem cells from mouse embryonic and adult fibroblast cultures by defined factors.* Cell, 2006. **126**(4): p. 663-76.

22. Miller J, A.M., Brooks E, Libeu CP, Legleiter J, Hatters D, Curtis J, Cheung K, Krishnan P, Mitra S, et al., *Identifying polyglutamine protein species in situ that best predict neurodegeneration. .* Nat Chem Biol., 2011. **7**: p. 925–934.

23. Nagai Y, I.T., Popiel HA, Fujikake N, Hasegawa K, Urade Y, Goto Y, Naiki H, Toda T. , *A toxic monomeric conformer of the polyglutamine protein. 2007.* Nat Struct Mol Biol., 2007. **14**: p. 332-340.

24. Belinda, B., E.M. Meg, and P. Alison, *Effectiveness of Physiotherapy, Occupational Therapy, and Speech Pathology for People with Huntington's Disease: A Systematic Review.* Neurorehabilitation and Neural Repair, 2003. **17**(1): p. 12-24.

25. Ross, C.A., et al., *Huntington disease: natural history, biomarkers and prospects for therapeutics.* Nat Rev Neurol, 2014. **10**(4): p. 204-216.

26. Wild, E., M. Björkqvist, and S.J. Tabrizi, *Immune markers for Huntington's disease?* Expert Review of Neurotherapeutics, 2008. **8**(12): p. 1779-1781.

27. van der Burg, J.M.M., M. Björkqvist, and P. Brundin, *Beyond the brain: widespread pathology in Huntington's disease.* The lancet Neurology, 2009. **8**(8): p. 765-774.

28. Hoogeveen, A.T., et al., *Characterization and localization of the Huntington disease gene product.* Human Molecular Genetics, 1993. **2**(12): p. 2069-2073.

29. Li, S.H., et al., *Huntington's disease gene (IT15) is widely expressed in human and rat tissues.* Neuron, 1993. **11**(5): p. 985-993.

30. Trottier, Y., et al., *Cellular localization of the Huntington disease protein and discrimination of the normal and mutated form.* Nature Genetics, 1995. **10**: p. 104.

31. Cattaneo, E., C. Zuccato, and M. Tartari, *Normal huntingtin function: an alternative approach to Huntington's disease.* Nature Reviews Neuroscience, 2005. **6**: p. 919.

32. Almeida, S., et al., *Evidence of apoptosis and mitochondrial abnormalities in peripheral blood cells of Huntington's disease patients.* Biochemical and Biophysical Research Communications, 2008. **374**(4): p. 599-603.

33. Panov, A.V., S. Lund, and J.T. Greenamyre, *Ca2+-induced permeability transition in human lymphoblastoid cell mitochondria from normal and Huntington's disease individuals.* Molecular and Cellular Biochemistry, 2005. **269**(1): p. 143-152.

34. Pattison, J.S., et al., *Cardiomyocyte Expression of a Polyglutamine Preamyloid Oligomer Causes Heart Failure.* Circulation, 2008. **117**(21): p. 2743-2751.

35. Markianos, M., et al., *Plasma testosterone in male patients with Huntington's disease: Relations to severity of illness and dementia.* Annals of Neurology, 2005. **57**(4): p. 520-525.

36. Panov, A.V., et al., *Early mitochondrial calcium defects in Huntington disease are a direct effect of polyglutamines.* Nature neuroscience, 2002. **5**: p. 731.

37. Valenza, M., et al., *Dysfunction of the Cholesterol Biosynthetic Pathway in Huntington's Disease.* The Journal of Neuroscience, 2005. **25**(43): p. 9932-9939.

38. Valenza, M., et al., *Progressive dysfunction of the cholesterol biosynthesis pathway in the R6/2 mouse model of Huntington's disease.* Neurobiology of Disease, 2007. **28**(1): p. 133-142.

39. Ritch, J.J., et al., *Multiple phenotypes in Huntington disease mouse neural stem cells.* Molecular and Cellular Neuroscience, 2012. **50**(1): p. 70-81.

40. Trushina, E., et al., *Loss of caveolin-1 expression in knock-in mouse model of Huntington's disease suppresses pathophysiology in vivo.* Human Molecular Genetics, 2014. **23**(1): p. 129-144.

41. Trushina, E., et al., *Mutant huntingtin inhibits clathrin-independent endocytosis and causes accumulation of cholesterol in vitro and in vivo.* Human Molecular Genetics, 2006. **15**(24): p. 3578-3591.

42. Kagan, B.L., et al., *The channel hypothesis of Huntington's disease.* Brain Research Bulletin, 2001. **56**(3): p. 281-284.

43. Huppert, T.J., et al., *Sensitivity of neural-hemodynamic coupling to alterations in cerebral blood flow during hypercapnia.* Journal of Biomedical Optics, 2009. **14**(4): p. 044038-044038.

44. Bandettini, P.A., *Functional MRI Limitations and Aspirations*, in *Neural Correlates of Thinking*, E. Kraft, B. Gulyás, and E. Pöppel, Editors. 2009, Springer Berlin Heidelberg: Berlin, Heidelberg. p. 15-38.

45. Parievsky, A., C. Cepeda, and M.S. Levine, *Evidence from the R6/2 Mouse Model of Huntington's Disease for Using Abnormal Brain Metabolism as a Biomarker for Evaluating Therapeutic Approaches for Treatment.* Future neurology, 2012. **7**(5): p. 527-530.

46. Holland, J.P., P. Cumming, and N. Vasdev, *PET radiopharmaceuticals for probing enzymes in the brain.* American Journal of Nuclear Medicine and Molecular Imaging, 2013. **3**(3): p. 194-216.

47. Teune, L.K., A.L. Bartels, and K.L. Leenders, *FDG- PET Imaging in Neurodegenerative Brain Diseases.* InTech, 2013.

48. Lepron, E., et al., *A PET study of word generation in Huntington's disease: Effects of lexical competition and verb/noun category.* Brain and Language, 2009. **110**(2): p. 49-60.

49. Gouarné, C., et al., *Early Deficits in Glycolysis Are Specific to Striatal Neurons from a Rat Model of Huntington Disease.* PLoS ONE, 2013. **8**(11): p. e81528.

50. Nambron, R., et al., *A Metabolic Study of Huntington's Disease.* PLoS ONE, 2016. **11**(1): p. e0146480.

51. Peter, M., and S. M. Ameer-Beg. , *Imaging molecular interactions by multiphoton FLIM. .* Biol. Cell., 2004. **96**(3): p. 231–236.

52. Becker, W., *Fluorescence lifetime imaging – techniques and applications.* Journal of Microscopy, 2012. **247**(2): p. 119-136.

53. Stringari, C., et al., *Phasor Fluorescence Lifetime Microscopy of Free and Protein-Bound NADH Reveals Neural Stem Cell Differentiation Potential.* PLoS ONE, 2012. **7**(11).

54. Zheng, W., D. Li, and J.Y. Qu, *Monitoring changes of cellular metabolism and microviscosity in vitro based on time-resolved endogenous fluorescence and its anisotropy decay dynamics.* Journal of Biomedical Optics, 2010. **15**(3).

55. Jorge Vergen, et al., *Metabolic imaging using two-photon excited NADH intensity and fluorescence lifetime imaging.* Microscopy and Microanalysis : The Official Journal of Microscopy Society of America, Microbeam Analysis Society, Microscopical Society of Canada, 2012. **18**(4).

56. H. Lodish, et al., *Molecular Cell Biology*2003, New York: W. H. Freeman and Co.

57. B. Alberts, et al., *Molecular Biology of the Cell*2007, New York: Garland Science.

58. StudyDroid. *Studying Chem 351*. Available from: <http://www.studydroid.com/index.php?page=viewPack&packId=128877>.

59. Mayevsky A and R. GG., *Mitochondrial function in vivo evaluated by NADH fluorescence: From animal models to human studies. .* Am J Physiol Cell Physiol, 2007. **292**: p. 615-640.

60. CHANCE B, et al., *Intracellular oxidation-reduction states in vivo.* Science., 1962. **137**(3529): p. 499-508.

61. Formoso, E., et al., *Aluminum and its effect in the equilibrium between folded/unfolded conformation of NADH.* Journal of Inorganic Biochemistry, 2015. **152**: p. 139-146.

62. Bird DK, Y.L., Vrotsos KM, Eliceiri KW, Vaughan EM, Keely PJ, White JG, Ramanujam N., *Metabolic mapping of MCF10A human breast cells via multiphoton fluorescence lifetime imaging of the coenzyme NADH.* Cancer Res, 2005. **65**(19): p. 8766-73.

63. Wouters, F.S., P. J. Verveer, and P. I.Bastiaens., *Imaging biochemistry inside cells.* Trends Cell Biol., 2001. **11**(5): p. 203–211.

64. Becker, W., A. Bergmann, M. A. Hink, K. Konig, K. Benndorf, and C. Biskup., *Fluorescence lifetime imaging by time-correlated single-photon counting.* Microsc. Res. Tech, 2004. **63**: p. 58–66.

65. Gerritsen, H.C., M. A. Asselbergs, A. V. Agronskaia, and W. G. Van Sark., *Fluorescence lifetime imaging in scanning microscopes: acquisition speed, photon economy and lifetime resolution.* J. Microsc., 2002. **206**: p. 218–224.

66. Weber, G., *Resolution of the fluorescence lifetimes in a heterogeneous system by phase and modulation measurements.* J. Phys. Chem., 1981. **85**: p. 949–953.

67. Jameson, D.M., E. Gratton, and R. Hall., *The measurement and analysis of heterogeneous emissions by multifrequency phase and modulation fluorometry.* Appl. Spectrosc. Rev., 1984. **20**: p. 55–106.

68. Suhling, K., J., et al., *Imaging the environment of green fluorescent protein. .* Biophys. J. , 2002. **83**: p. 3589–3595.

69. Verveer, P.J., A. Squire, and P.I. Bastiaens., *Global analysis of fluorescence lifetime imaging microscopy data.* Biophys. J., 2000(78): p. 2127–2137.

70. Pelet, S., M. J. Previte, L. H. Laiho, and P. T. So., *A fast global fitting algorithm for fluorescence lifetime imaging microscopy based on image segmentation. .* Biophys J, 2004. **87**: p. 2807–2817.

71. Podolsky, S., N. Leopold, and D. Sax, *Increased frequency of diabetes mellitus in patients with Huntington's chorea.* The Lancet, 1972. **299**(7765): p. 1356-1359.

72. Hurlbert, M.S., et al., *Mice transgenic for an expanded CAG repeat in the Huntington's disease gene develop diabetes.* DIABETES, 1999. **48**(3): p. 649-651.

73. Oláh, J., et al., *Increased glucose metabolism and ATP level in brain tissue of Huntington's disease transgenic mice.* FEBS Journal, 2008. **275**(19): p. 4740-4755.

74. Browne, S.E., *Mitochondria and Huntington's Disease Pathogenesis.* Annals of the New York Academy of Sciences, 2008. **1147**(1): p. 358-382.

75. Wright, B.K., et al., *NADH Distribution in Live Progenitor Stem Cells by Phasor-Fluorescence Lifetime Image Microscopy.* Biophysical Journal, 2012. **103**(1): p. 7-9.

76. Stringari, C., et al., *In Vivo Single-Cell Detection of Metabolic Oscillations in Stem Cells.* 2015. **10**(1): p. 1-7.

77. Plotegher, N., et al., *NADH fluorescence lifetime is an endogenous reporter of α-synuclein aggregation in live cells.* FASEB Journal, 2015. **29**.

78. Skala, M.C.e.a., *In vivo Multiphoton Fluorescence Lifetime Imaging of Protein-bound and Free NADH in Normal and Pre-cancerous Epithelia.* Journal of biomedical optics, 2007. **12**(2).

79. J. Lawrence Marsh1, J.P., and Leslie M. Thompson, *Fly models of Huntington's disease.* Hum. Mol. Genet., 2003. **2**(2): p. 187-193.

80. Cagan, R.L. and D.F. Ready, *The emergence of order in the Drosophila pupal retina.* Dev. Biol., 1998. **136**: p. 346-362.

81. Roberts, D.B., *Drosophila: A Practical Approach*. IRL Press1986, Oxford, UK.

82. Zhang, Q., D.W. Piston, and R.H. Goodman, *Regulation of Corepressor Function by Nuclear NADH.* Science, 2002. **295**(5561): p. 1895-1897.

83. Chinnadurai, G., *CtBP family protiens*2007, New York,U.S.A: Springer.

84. Chance, B. and H. Baltscheffsky, *Respiratory enzymes in oxidative phosphorylation. VII. binding of intramitochondrial reduced pyridine nucleotide.* J Biol Chem, 1958. **233**: p. 736–739.

85. Chance, B., et al., *Basic principles of tissue oxygen determination from mitochondrial signals.* Adv Exp Med Biol, 1973: p. 277–292.

86. Chance, B. and M. Lieberman, *Intrinsic fluorescence emission from the cornea at low temperatures: Evidence of mitochondrial signals and their differing redox states in epithelial and endothelial sides.* Exp Eye Res., 1978. **26**: p. 111-117.

87. Obi-Tabot, E.T., et al., *Changes in hepatocyte NADH fluorescence during prolonged hypoxia.* J Surg Res, 1993. **55**(6): p. 573-80.

88. Foster, K.A., C.J. Beaver, and D.A. Turner, *Interaction between tissue oxygen tension and NADH imaging during synaptic stimulation and hypoxia in rat hippocampal slices.* Neuroscience, 2005. **132**(3): p. 645-57.

89. Scholz, R., R.G. Thurman, and T. Bücher, *Flavin and pyridine nucleotide oxidation-reduction changes in perfused rat liver. I. Anoxia and subcellular localization of fluorescent flavoproteins.* J. Biol. Chem. , 1969: p. 2317–2324.

90. Ji, S., et al., *Periportal and pericentral pyridine-nucleotide fluorescence from the surface of the perfused liver: evaluation of the hypothesis that chronic treatment with ethanol produces pericentral hypoxia.* Proc. Natl. Acad. Sci USA, 1982. **79**(17): p. 5415–5419.

91. Stringari, C., et al., *Metabolic trajectory of cellular differentiation in small intestine by Phasor Fluorescence Lifetime Microscopy of NADH.* Scientific reports, 2012. **2**(568).

92. Stringari, C., et al., *Phasor approach to fluorescence lifetime microscopy distinguishes different metabolic states of germ cells in a live tissue.* Proc Natl Acad Sci U S A, 2011. **108**(33).

93. Marsh, J.L., J. Pallos, and L.M. Thompson, *Fly models of Huntington's disease.* Hum. Mol. Genet. , 2003. **2**(2): p. 187-193.

94. Osterwalder, T., et al., *A conditional tissue-specific transgene expression system using inducible GAL4.* Proceedings of the National Academy of Sciences of the United States of America, 2001. **98**(22): p. 12596-12601.

95. Brody, T.B. *The Interactive Fly:Genes involved in tissue and organ development*. 1996.

96. Barbaro, B.A., et al., *Comparative study of naturally occurring huntingtin fragments in Drosophila points to exon 1 as the most pathogenic species in Huntington's disease.* Hum Mol Genet, 2014.

97. Stringari, C., et al., *Phasor approach to fluorescence lifetime microscopy distinguishes different metabolic states of germ cells in a live tissue.* Proc Natl Acad Sci U S A, 2011. **108**(33).

98. Lee, S.J., et al., *Apparent Relative Hypermetabolism of Selective Brain Areas in Huntington Disease and Importance of Reference Region for Analysis.* Clinical Nuclear Medicine, 2012. **37**(7): p. 663-668.

99. Herskovits, A.Z. and L. Guarente, *Sirtuin deacetylases in neurodegenerative diseases of aging.* Cell Research, 2013. **23**: p. 746-758.

100. Lüesse, H.G., et al., *Evaluation of R6/2 HD transgenic mice for therapeutic studies in Huntington's disease: behavioral testing and impact of diabetes mellitus.* Behavioural Brain Research, 2001. **126**(1–2): p. 185-195.

101. Shin, H., et al., *Decreased Metabolism in the Cerebral Cortex in Early-Stage Huntington's Disease: A Possible Biomarker of Disease Progression?* Journal of Clinical Neurology (Seoul, Korea), 2013. **9**(1): p. 21-25.

102. Ciarmiello, A., et al., *18F-FDG PET uptake in the pre-Huntington disease caudate affects the time-to-onset independently of CAG expansion size.* European Journal of Nuclear Medicine and Molecular Imaging, 2012. **39**(6): p. 1030-1036.

103. Valencia, A., et al., *Elevated NADPH oxidase activity contributes to oxidative stress and cell death in Huntington's disease.* Human Molecular Genetics, 2013. **22**(6): p. 1112-1131.

104. Chakraborty, S., et al., *Quantification of the Metabolic State in Cell-Model of Parkinson's Disease by Fluorescence Lifetime Imaging Microscopy.* Scientific reports, 2016. **6**: p. 19145.

105. Jentsch, S., et al., *Retinal fluorescence lifetime imaging ophthalmoscopy measures depend on the severity of Alzheimer's disease.* Acta Ophthalmologica, 2015. **93**(4): p. e241-e247.

106. Digman, M.A., et al., *The Phasor Approach to Fluorescence Lifetime Imaging Analysis.* Biophys J, 2008. **94**(2).

107. Chiti, F. and C.M. Dobson, *Protein Misfolding, Functional Amyloid, and Human Disease.* Annual Review of Biochemistry, 2006. **75**(1): p. 333-366.

108. Davies, S.W., et al., *Formation of Neuronal Intranuclear Inclusions Underlies the Neurological Dysfunction in Mice Transgenic for the HD Mutation.* Cell, 1997. **90**(3): p. 537-548.

109. Sameni, S., et al., *The phasor-FLIM fingerprints reveal shifts from OXPHOS to enhanced glycolysis in Huntington Disease.* Nature scientific reports, 2016.

110. Block, R.C., et al., *Altered Cholesterol and Fatty Acid Metabolism in Huntington Disease.* Journal of clinical lipidology, 2010. **4**(1): p. 17-23.

111. Cheng, D., et al., *Lipid Pathway Alterations in Parkinson's Disease Primary Visual Cortex.* PLoS ONE, 2011. **6**(2): p. e17299.

112. Conquer, J.A., et al., *Fatty acid analysis of blood plasma of patients with alzheimer's disease, other types of dementia, and cognitive impairment.* Lipids, 2000. **35**(12): p. 1305-1312.

113. Kosicek, M. and S. Hecimovic, *Phospholipids and Alzheimer's Disease: Alterations, Mechanisms and Potential Biomarkers.* International Journal of Molecular Sciences, 2013. **14**(1): p. 1310-1322.

114. Walter, J. and G. van Echten-Deckert, *Cross-talk of membrane lipids and Alzheimer-related proteins.* Molecular Neurodegeneration, 2013. **8**(1): p. 34.

115. Brown, M.S. and J.L. Goldstein, *The SREBP Pathway: Regulation of Cholesterol Metabolism by Proteolysis of a Membrane-Bound Transcription Factor.* Cell, 1997. **89**(3): p. 331-340.

116. Malacrida, L., et al., *Spectral phasor analysis of LAURDAN fluorescence in live A549 lung cells to study the hydration and time evolution of intracellular lamellar body-like structures.* Biochimica et Biophysica Acta (BBA) - Biomembranes, 2016. **1858**(11): p. 2625-2635.

117. Matsumura, Y., et al., *ABCA3-mediated choline-phospholipids uptake into intracellular vesicles in A549 cells.* Federation of European Biochemical Societies Letters, 2007. **581**(17): p. 3139-3144.

118. Rumin, J., et al., *The use of fluorescent Nile red and BODIPY for lipid measurement in microalgae.* Biotechnology for Biofuels, 2015. **8**: p. 42.

119. Golfetto, O., E. Hinde, and E. Gratton, *Laurdan Fluorescence Lifetime Discriminates Cholesterol Content from Changes in Fluidity in Living Cell Membranes.* Biophysical Journal, 2013. **104**(6): p. 1238-1247.

120. Malacrida, L., E. Gratton, and D.M. Jameson, *Model-free methods to study membrane environmental probes: a comparison of the spectral phasor and generalized polarization approaches.* Methods and Applications in Fluorescence, 2015. **3**(4): p. 047001.

121. Weber, G. and F.J. Farris, *Synthesis and spectral properties of a hydrophobic fluorescent probe: 6-propionyl-2-(dimethylamino)naphthalene.* Biochemistry, 1979. **18**(14): p. 3075-3078.

122. Sanchez S.A., Tricerri M.A., and G. E., *Laurdan generalized polarization: from cuvette to microscope.* Modern Research and Educational Topics in Microscopy, 2007: p. 1007–101.

123. Simons, K. and W.L.C. Vaz, *Model Systems, Lipid Rafts, and Cell Membranes.* Annual Review of Biophysics and Biomolecular Structure, 2004. **33**(1): p. 269-295.

124. Greenspan , P., E. Mayer, and S. Fowler, *Nile red: a selective fluorescent stain for intracellular lipid droplets.* The Journal of Cell Biology, 1985. **100**(3): p. 965-973.

125. Greenspan, P. and S.D. Fowler, *Spectrofluorometric studies of the lipid probe, nile red.* Journal of Lipid Research, 1985. **26**(7): p. 781-9.

126. Kou, Z., et al., *Fluorescent measurement of lipid content in the model organism Chlamydomonas reinhardtii.* Journal of Applied Phycology, 2013. **25**(6): p. 1633-1641.

127. Ira and G. Krishnamoorthy, *Probing the Link between Proton Transport and Water Content in Lipid Membranes.* The Journal of Physical Chemistry B, 2001. **105**(7): p. 1484-1488.

128. Kucherak, O.A., et al., *Switchable Nile Red-Based Probe for Cholesterol and Lipid Order at the Outer Leaflet of Biomembranes.* Journal of the American Chemical Society, 2010. **132**(13): p. 4907-4916.

129. Mukherjee, S., H. Raghuraman, and A. Chattopadhyay, *Membrane localization and dynamics of Nile Red: Effect of cholesterol.* Biochimica et Biophysica Acta (BBA) - Biomembranes, 2007. **1768**(1): p. 59-66.

130. Golini, C.M., B.W. Williams, and J.B. Foresman, *Further Solvatochromic, Thermochromic, and Theoretical Studies on Nile Red.* Journal of Fluorescence, 1998. **8**(4): p. 395-404.

131. Parasassi, T., et al., *Phase fluctuation in phospholipid membranes revealed by Laurdan fluorescence.* Biophysical Journal, 1990. **57**(6): p. 1179-1186.

132. Wheeler, G. and K.M. Tyler, *Widefield microscopy for live imaging of lipid domains and membrane dynamics.* Biochimica et Biophysica Acta, 2011. **1808**(3): p. 634-641.

133. Parasassi, T., et al., *Two-photon fluorescence microscopy of laurdan generalized polarization domains in model and natural membranes.* Biophysical Journal, 1997. **72**(6): p. 2413-2429.

134. Apostol, B.L., et al., *A cell-based assay for aggregation inhibitors as therapeutics of polyglutamine-repeat disease and validation in Drosophila.* Proceedings of the National Academy of Sciences of the United States of America, 2003. **100**(10): p. 5950-5955.

135. Tan, Z., et al., *Huntington's disease cerebrospinal fluid seeds aggregation of mutant huntingtin.* Molecular Psychiatry, 2015. **20**(11): p. 1286-1293.

136. Angelova, M.I., et al., *Preparation of giant vesicles by external AC electric fields. Kinetics and applications*, in *Trends in Colloid and Interface Science VI*, C. Helm, M. Lösche, and H. Möhwald, Editors. 1992, Steinkopff: Darmstadt. p. 127-131.

137. Neufeld, E.B., et al., *Intracellular Trafficking of Cholesterol Monitored with a Cyclodextrin.* Journal of Biological Chemistry, 1996. **271**(35): p. 21604-21613.

138. Sun, Z.-X., Q.-H. Zhou, and S.-F. Sui, *Cholesterol depletion inhibits the degradation of amyloid β-peptide in rat pheochromocytoma (PC12) cells.* Neuroscience Letters, 2005. **391**(1): p. 71-75.

139. Trushina, E., et al., *Mutant Huntingtin Impairs Axonal Trafficking in Mammalian Neurons In Vivo and In Vitro.* Molecular and Cellular Biology, 2004. **24**(18): p. 8195-8209.

140. Gunawardena, S., et al., *Disruption of Axonal Transport by Loss of Huntingtin or Expression of Pathogenic PolyQ Proteins in Drosophila.* Neuron, 2003. **40**(1): p. 25-40.

141. Szebenyi, G., et al., *Neuropathogenic Forms of Huntingtin and Androgen Receptor Inhibit Fast Axonal Transport.* Neuron, 2003. **40**(1): p. 41-52.

142. Golfetto, O., E. Hinde, and E. Gratton, *The Laurdan Spectral Phasor Method to Explore Membrane Micro-heterogeneity and Lipid Domains in Live Cells*, in *Methods in Membrane Lipids*, D.M. Owen, Editor 2015, Springer New York: New York, NY. p. 273-290.

143. Aguilar, L.F., et al., *Differential Dynamic and Structural Behavior of Lipid-Cholesterol Domains in Model Membranes.* PLoS ONE, 2012. **7**(6): p. e40254.

144. Hung, W.-C., et al., *The Condensing Effect of Cholesterol in Lipid Bilayers.* Biophysical Journal, 2007. **92**(11): p. 3960-3967.

145. Mukherjee, S. and A. Chattopadhyay, *Monitoring the organization and dynamics of bovine hippocampal membranes utilizing Laurdan generalized polarization.* Biochimica et Biophysica Acta (BBA) - Biomembranes, 2005. **1714**(1): p. 43-55.

146. Gao, X., et al., *Cholesterol Modifies Huntingtin Binding to, Disruption of, and Aggregation on Lipid Membranes.* Biochemistry, 2016. **55**(1): p. 92-102.

147. Wang, J. and D. Nie, *Modulation of Autophagy by Free Fatty Acids*, ed. D.T. Ntuli2015: InTech.

148. Wong, E. and A.M. Cuervo, *Autophagy gone awry in neurodegenerative diseases.* Nature neuroscience, 2010. **13**(7): p. 805-811.

149. Ibarguren, M., D.J. López, and P.V. Escribá, *The effect of natural and synthetic fatty acids on membrane structure, microdomain organization, cellular functions and human health.* Biochimica et Biophysica Acta (BBA) - Biomembranes, 2014. **1838**(6): p. 1518-1528.

150. Maccarrone, M., N. Battista, and D. Centonze, *The endocannabinoid pathway in Huntington's disease: A comparison with other neurodegenerative diseases.* Progress in Neurobiology, 2007. **81**(5–6): p. 349-379.

151. Castillo, P.E., et al., *Endocannabinoid signaling and synaptic function.* Neuron, 2012. **76**(1): p. 70-81.

152. Donner, M., S. Muller, and J.F. Stoltz, *[Importance of membrane fluidity determination].* JOURNAL DES MALADIES VASCULAIRES, 1990. **15**(4): p. 353-8.

153. Grecco, Hernán E., M. Schmick, and Philippe I.H. Bastiaens, *Signaling from the Living Plasma Membrane.* Cell, 2011. **144**(6): p. 897-909.

154. Shaikh, S.R. and M. Edidin, *Polyunsaturated fatty acids, membrane organization, T cells, and antigen presentation.* American Society for Clinical Nutrition, 2006. **84**(6): p. 1277-89.

155. Legleiter, J., et al., *Mutant Huntingtin Fragments Form Oligomers in a Polyglutamine Length-dependent Manner in Vitro and in Vivo.* The Journal of Biological Chemistry, 2010. **285**(19): p. 14777-14790.

156. Takahashi, T., et al., *Soluble polyglutamine oligomers formed prior to inclusion body formation are cytotoxic*. Vol. 17. 2008. 345-56.

157. Yang W, et al., *Aggregated polyglutamine peptides delivered to nuclei are toxic to mammalian cells.* Hum Mol Genet, 2002. **11**(23): p. 2905-17.

158. Steffan, J.S., et al., *The Huntington's disease protein interacts with p53 and CREB-binding protein and represses transcription.* Proceedings of the National Academy of Sciences of the United States of America, 2000. **97**(12): p. 6763-6768.

159. Donaldson, K.M., et al., *Ubiquitin-mediated sequestration of normal cellular proteins into polyglutamine aggregates.* Proceedings of the National Academy of Sciences of the United States of America, 2003. **100**(15): p. 8892-8897.

160. Sahl, S.J., et al., *Cellular Inclusion Bodies of Mutant Huntingtin Exon 1 Obscure Small Fibrillar Aggregate Species.* Scientific reports, 2012. **2**: p. 895.

161. Ramdzan, Y.M., et al., *Huntingtin Inclusions Trigger Cellular Quiescence, Deactivate Apoptosis, and Lead to Delayed Necrosis.* Cell Reports. **19**(5): p. 919-927.

162. Marzo, L., K. Gousset, and C. Zurzolo, *Multifaceted Roles of Tunneling Nanotubes in Intercellular Communication.* Frontiers in Physiology, 2012. **3**: p. 72.

163. Hurtig, J., D.T. Chiu, and B. Önfelt, *Intercellular nanotubes: insights from imaging studies and beyond.* Wiley Interdisciplinary Reviews: Nanomedicine and Nanobiotechnology, 2010. **2**(3): p. 260-276.

164. Davis, D.M. and S. Sowinski, *Membrane nanotubes: dynamic long-distance connections between animal cells.* Nat Rev Mol Cell Biol, 2008. **9**(6): p. 431-436.

165. Gözen, I. and A. Jesorka, *Lipid nanotube networks: Biomimetic Cell-to-Cell Communication and Soft-Matter Technology*, in *Nanofabrication*2015.

166. Gousset, K., et al., *Prions hijack tunnelling nanotubes for intercellular spread.* Nat Cell Biol, 2009. **11**(3): p. 328-336.

167. Kordower, J.H., et al., *Lewy body-like pathology in long-term embryonic nigral transplants in Parkinson's disease.* Nat Med, 2008. **14**(5): p. 504-506.

168. Li, J.-Y., et al., *Lewy bodies in grafted neurons in subjects with Parkinson's disease suggest host-to-graft disease propagation.* Nat Med, 2008. **14**(5): p. 501-503.

169. Ren, P.-H., et al., *Cytoplasmic penetration and persistent infection of mammalian cells by polyglutamine aggregates.* Nature cell biology, 2009. **11**(2): p. 219-225.

170. Costanzo, M., et al., *Transfer of polyglutamine aggregates in neuronal cells occurs in tunneling nanotubes.* Journal of Cell Science, 2013. **126**(16): p. 3678.

171. Stout, J.C., et al., *Neurocognitive Signs in Prodromal Huntington Disease.* Neuropsychology, 2011. **25**(1): p. 1-14.

172. Paulsen, J.S., *Early Detection of Huntington Disease.* Future neurology, 2010. **5**(1): p. 10.2217/fnl.09.78.

173. Valenza, M. and E. Cattaneo, *Cholesterol dysfunction in neurodegenerative diseases: Is Huntington's disease in the list?* Progress in Neurobiology, 2006. **80**(4): p. 165-176.

174. Lütjohann, D., et al., *Cholesterol homeostasis in human brain: evidence for an age-dependent flux of 24S-hydroxycholesterol from the brain into the circulation.* Proceedings of the National Academy of Sciences of the United States of America, 1996. **93**(18): p. 9799-9804.

175. Raul, B., et al., *Small Differences in Intraischemic Brain Temperature Critically Determine the Extent of Ischemic Neuronal Injury.* Journal of Cerebral Blood Flow & Metabolism, 1987. **7**(6): p. 729-738.

176. Peretti, D., et al., *RBM3 mediates structural plasticity and protective effects of cooling in neurodegeneration.* Nature, 2015. **518**: p. 236.

177. Arribat, Y., et al., *Systemic delivery of P42 peptide: a new weapon to fight Huntington's disease.* Acta Neuropathologica Communications, 2014. **2**: p. 86.

178. Arribat, Y., et al., *A Huntingtin Peptide Inhibits PolyQ-Huntingtin Associated Defects.* PLoS ONE, 2013. **8**(7): p. e68775.